A FEASIBILITY STUDY FOR PROTECTING TRANSMISSION LINES USING TRAVELING WAVES

A Thesis

Submitted to the College of Graduate Studies and Research

in Partial Fulfillment of the Requirements

for the Degree of

Master of Science

in the

Department of Electrical Engineering

University of Saskatchewan

Saskatoon, Saskatchewan

Canada

By

TAMIJE SELVY MUNIAN

Spring 2003

PERMISSION TO USE

In presenting this thesis in partial fulfilment of the requirements for a Master's degree from the University of Saskatchewan, I agree that the Libraries of this University may make it freely available for inspection. I further agree that permission for copying of this thesis in any manner, in whole or in part, for scholarly purposes may be granted by the professor or professors who supervised my thesis work or, in their absence, by the Head of the Department or the Dean of the College in which my thesis work was done. It is understood that any copying, publication, or use of this thesis or parts thereof for financial gain shall not be allowed without my written permission. It is also understood that due recognition shall be given to me and to the University of Saskatchewan in any scholarly use which may be made of any material in my thesis.

Requests for permission to copy or to make other use of material in this thesis in whole or part should be addressed to:

Head of the Department of Electrical Engineering,
University of Saskatchewan,
Saskatoon, Saskatchewan, Canada S7N 5A9

ABSTRACT

Faults occur in power systems because of the failure of insulation and structures. The faults almost always result in the flow of large quantities of currents. Protective relays are used, therefore, for detecting the faults and isolating the faulted section of the system before the damage spreads. Traditionally, electromechanical and static technologies have been used for designing and manufacturing relays. More recently, advancements in the VLSI technology have resulted in the development of microprocessor-based numerical relays. Several algorithms have been proposed in the past, which are suitable for using in numerical relays for detecting the occurrence of faults. These algorithms convert the samples taken from the waveforms to phasors of the fundamental and harmonic frequencies. The conversion techniques usually take time that is at least one-cycle of the fundamental frequency. This time is 16 ms for a 60 Hz system and 20 ms for a 50 Hz system.

This thesis describes two techniques for designing high-speed numerical relays. The first technique uses sampled voltages and currents from the local terminal of the line. The second technique uses samples of voltages and currents from the local terminal and processed information from the remote terminal of the line. Both techniques are based on the arrival of traveling waves starting by the onset of faults. The first differences are used to detect the instants of the arrival of the voltage and current traveling waves.

The performance of the proposed techniques was investigated by computer-based simulations. Different types of faults on different locations in a sample power system were simulated using the electromagnetic transient program, EMTDC. The impacts of hardware constraints were also evaluated. Some of the cases investigated during this project are reported. The results indicate that the proposed techniques are suitable for protecting a transmission line. Their operating times are less than 4 ms compared to 10 ms or more for the presently available relays.

ACKNOWLEDGEMENTS

The author would like to express her gratitude and appreciation to Dr. M. S. Sachdev for his invaluable guidance and help throughout the course of this research work. The advice and constant encouragement given by Dr. T. S. Sidhu is gratefully acknowledged.

The author is grateful to her husband Mr. Balamourougan for his constant encouragement and moral support. Without him, higher studies would have been only a dream.

The author is thankful to Mr. Amitpal Bimbhra, Dr. David Sebastian, Mr. Sandro Aquiles Perez and Mr. Harjeet Singh Birdi for providing an excellent working environment in the power system protection lab. Their support was invaluable all through this research work.

Special thanks are extended to the author's family for their selfless love and guidance. Special thanks are extended to the author's friends for their moral support.

Financial support provided by the National Sciences and Engineering Research Council (NSERC) of Canada is gratefully acknowledged.

Dedicated To My Family

Mr. Munian

Mrs. Tamilarasy

Mrs. Indirani

Miss. Tamil Vany

Miss. Tamil Malar

TABLE OF CONTENTS

LIST OF TABLES

LIST OF FIGURES

LIST OF ACRONYMNS

EMTDC	Electro Magnetic Transient Direct Current Analysis
PSCAD	Power Systems Computer Aided Design
DAS	Data Acquisition System
CT	Current Transformer
VT	Voltage Transformer
RAM	Random Access Memory
ROM	Read-Only Memory
EEPROM	Electronically Erasable Programmable Read-Only Memory
DFT	Discrete Fourier Transform
LES	Least Error Squares
GPS	Global Positioning System
A/D Converter	Analog to Digital Converter
EHV	Extra High Voltage

Chapter 1

Introduction

1.1 Background

An electric power system is a complex network that spans vast areas and comprises of a large numbers of elements. The chances for the occurrence of faults on the system are, therefore, high. Faults are caused by lightning, high winds, ice and snowstorms, contamination of insulators, aging of insulation, falling trees, human errors and flying objects. The different types of faults are

1. Single-phase to ground faults,
2. Two-phase faults,
3. Two-phase to ground faults,
4. Three-phase faults, and
5. Three-phase to ground faults.

When a fault occurs, the voltages decrease and currents increase. Figures 1.1 and 1.2 show the changes in the voltages and currents when a phase-B to ground fault occurs. The phase B voltage reduces substantially while the voltages in the other phases remain practically unaltered. Also, the current in phase B increases and, due to the imbalance created by this increase, current flows in the neutral.

It can be seen from Figure 1.2 that on the occurrence of the fault, the increase in current is more than ten times the prefault value, and is in the range of kilo amperes. A power system is built to withstand high levels of currents for a very short period of time only. If such high levels of currents were allowed to flow for a long time, they would overheat the conductors, burn insulation or physically damage the lines and the

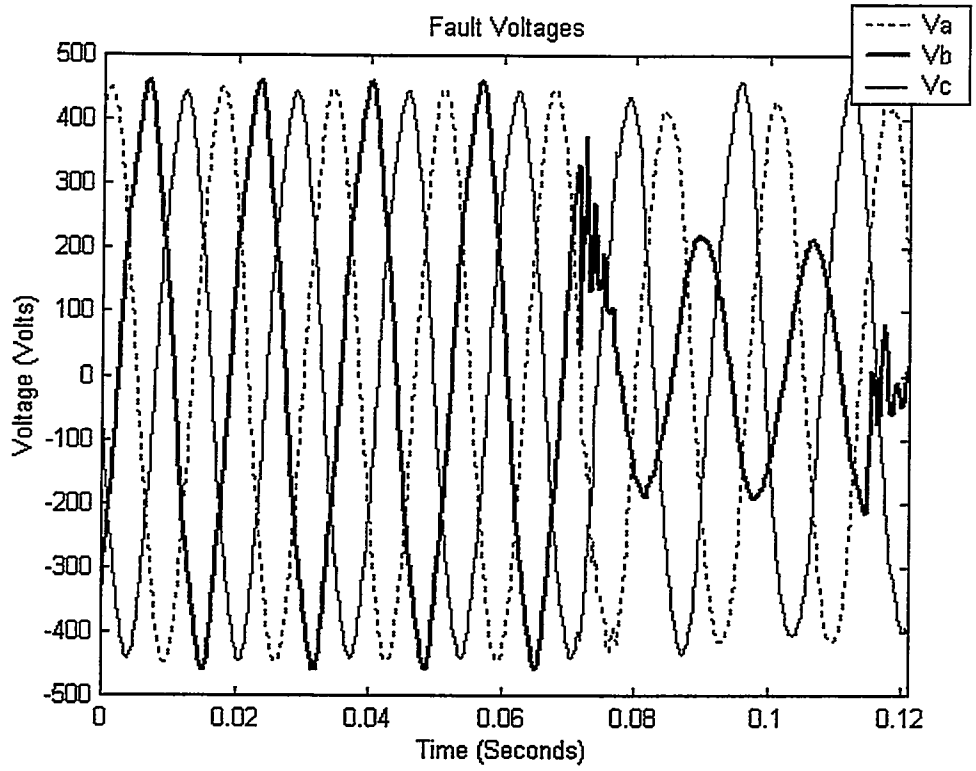

Figure 1.1: Three-phase voltages before, during and after a phase-B to ground fault

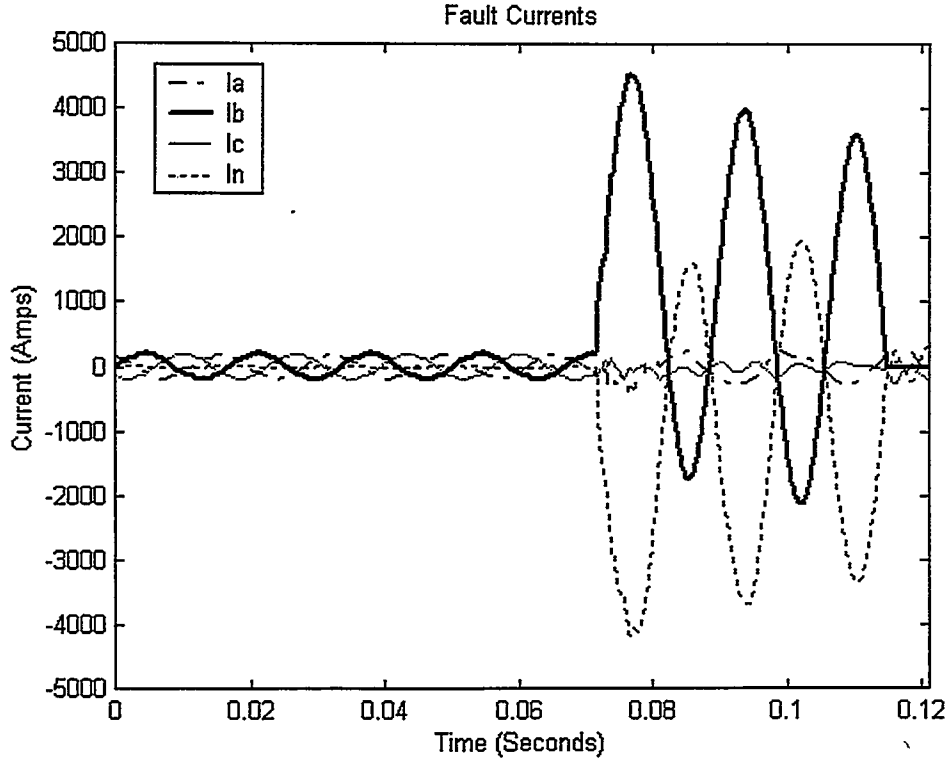

Figure 1.2: Three-phase currents before, during and after a phase-B to ground fault

equipments connected to it. It could also cause stability problems. Figure 1.3 gives a rough idea about the damage caused by a fault that is not cleared. A fault left for 100 ms melts the cables and a fault left for more than 200 ms melts steel. This would cause huge monitory losses. It is, therefore, desirable that the faults be cleared as early as possible.

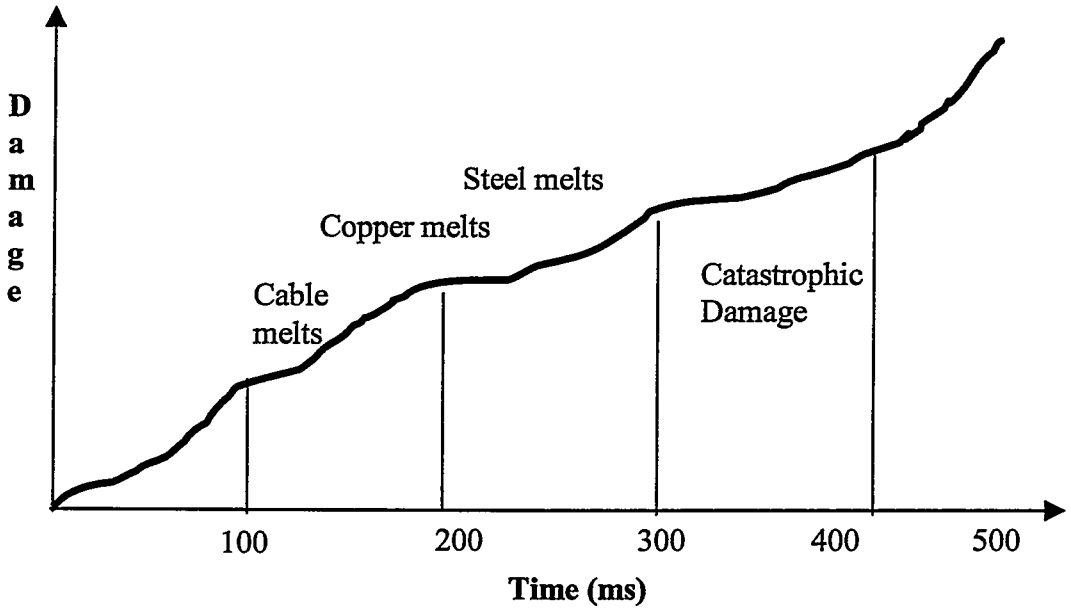

Figure 1.3: Damage caused by fault currents

In a power system there are many factors that indicate the occurrence of a fault. Some of the factors are over current, under voltage, low power factor, low impedance as seen by the relay, change in the direction of power flow and the presence of traveling waves. A protective relay is a device that monitors these conditions and detects the faults. When a fault is detected by the relay it sends trip signals to the circuit breakers.

1.2 Protective Relays

The main function of a protective relay is to sense the onset of a disturbance in the power system and to make trip decisions. A typical arrangement of a relay [8] is shown in Figure 1.4. The current and voltage levels in a power system are very high and cannot be directly applied to the relay. Hence, the currents and voltages are stepped down to lower levels by current transformers and voltage transformers and their outputs are applied to the relay. These signals are analysed in the relay. If necessary, trip

decisions are made and trip signals are sent to the circuit breakers. In some applications, information is passed on to other relays. Different technologies have been used in relays during the previous one hundred years for performing these functions.

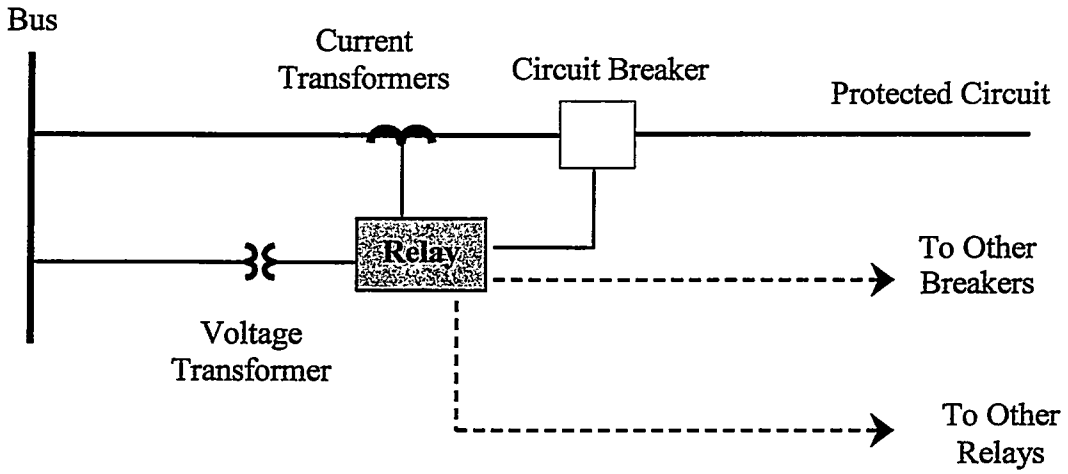

Figure 1.4: Typical arrangement of a relay

In early 1900's, electromechanical and electromagnetic principles were used to manufacture relays. These technologies allowed the operating times of the relays to be controlled. Re-closing of the circuit after the clearing of a fault was possible, which was an advantage over the fuses used in earlier days. Electromechanical relays have no significant drawbacks in performing the protection functions, but the additional features offered by the newer technologies encouraged further evolution in this field.

In early 1950's solid-state relays were developed, which were improved later by using Large-Scale Integrated technology. Among the advances found in solid-state relays were faster operating speeds, absence of moving parts, shorter reset times, lower burdens, and compact size. Simpler and more precise settings as well as reduced maintenance were also among the advantages offered. Many kinds of electromechanical and solid-state relays are used in power systems today.

The advancements in Very Large Scale Integrated technology have resulted in the development of many microprocessors and data acquisition chips, which in turn have led to the development of numerical relays. These numerical relays are described in more detail in Chapter 2.

1.2.1 Application in Power Systems

The power system is divided in to protection zones, each zone consisting of one major element like generator, motor, bus or transmission line. Adjacent zones are made to overlap so that no part of the system is left unprotected. A typical division of protection zones [8] is shown in Figure 1.5. Each zone is protected by a system consisting of a set of protective relays. When a fault occurs, this system detects the on-set of the fault in its zone and isolates the zone from the rest of the power system. These systems are called primary protection systems. There is always a possibility that a primary protection system may fail to perform its intended function. Backup relays are provided to disconnect the faulted components and sometimes a few adjoining components, when the primary protection system fails to operate.

Each protection system performs different functions depending on the element it is designed to protect. For example, some of the functions a generator protection system performs are as follows.

1. Field protection
2. Stator-earth fault protection
3. Negative sequence over-current protection
4. Over-current protection
5. Reverse power protection

A transmission line is protected using a transmission line protection system. This system also performs many functions some of which are listed here.

1. Basic over-current protection
2. Directional over-current protection
3. Distance protection
4. Phase comparison pilot relaying protection scheme
5. Directional comparison pilot relaying protection scheme
6. Combined phase and directional comparison. pilot relaying protection scheme

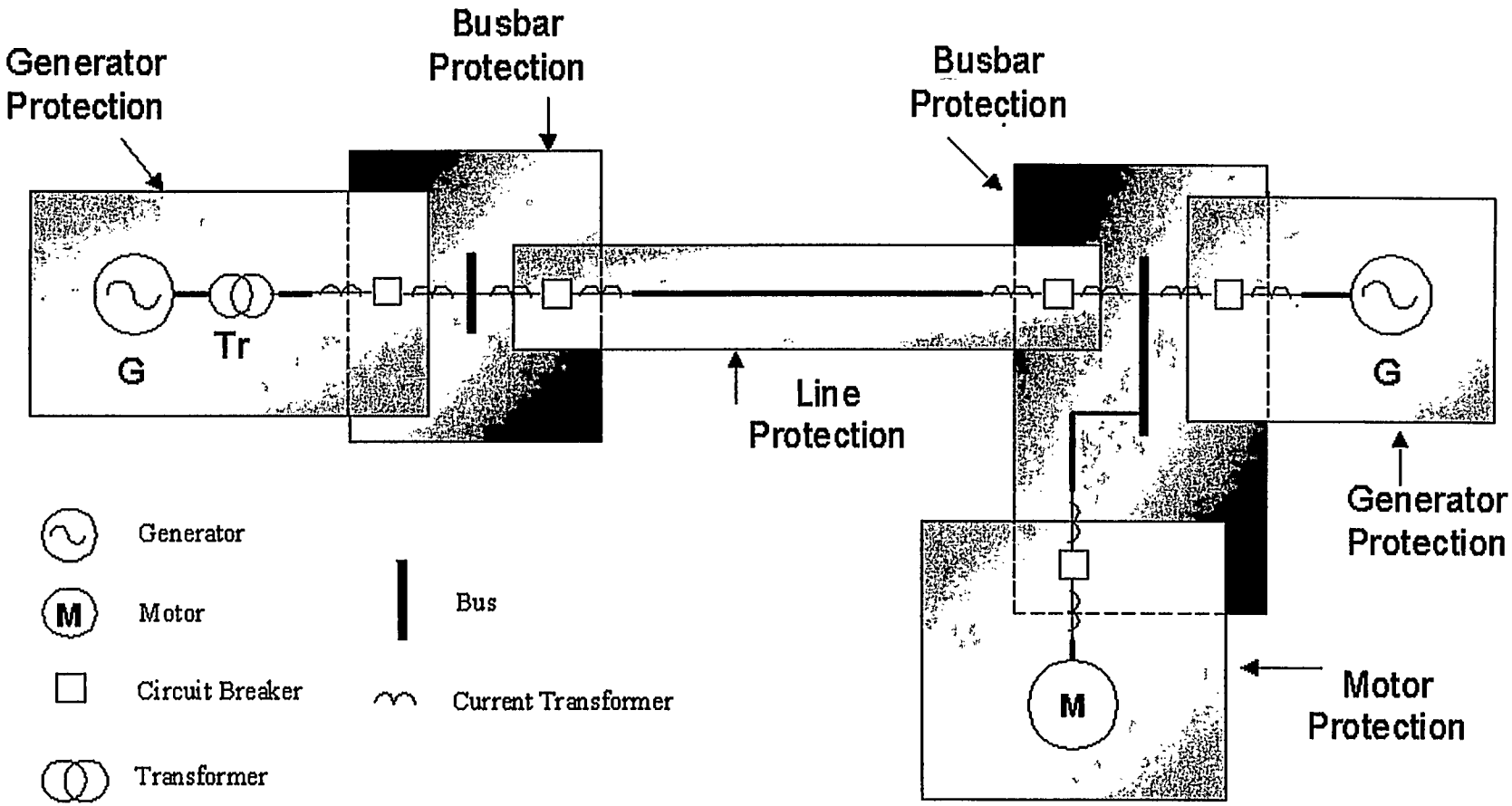

Figure 1.5: Zones of protection

1.2.2 Selectivity and Speed

A protection system must be selective and fast in operation. A fault occurring in a protection zone is an internal fault for the relay protecting that zone. All other faults are external faults. Selectivity is the ability of a protection system to distinguish between internal and external faults.

Consider the system in Figure 1.6. The zone of protection of the relay R_A is line A. The relay should operate for all faults on line A. The relay should not operate for faults on line B or on line C.

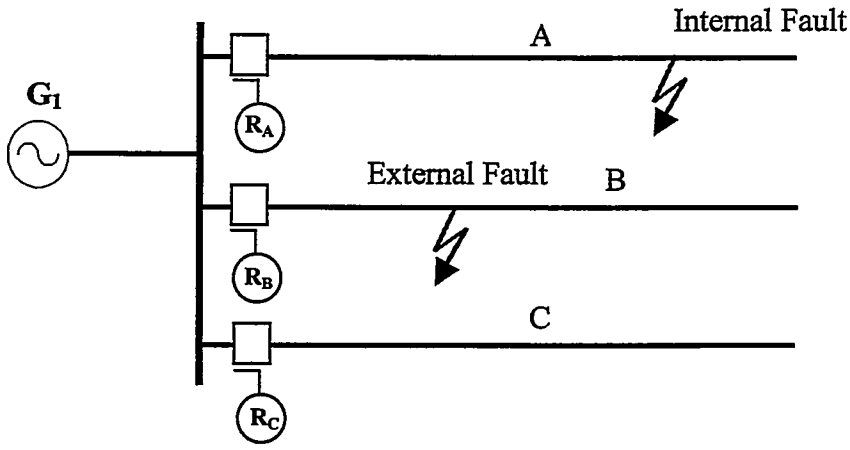

Figure 1.6: Internal and external faults

The second important property of a protection system is the time it takes to respond to a fault. As already discussed, a fault not cleared promptly can cause serious problems to the power system and result in substantial financial losses.

1.3 Objective of the Research

Faults give rise to traveling waves, which are present for only a short period of time after the occurrence of a fault. In about a millisecond, traveling waves develop into fundamental frequency signals. The conventional algorithms use the fundamental frequency components for making relaying decisions; the time taken to make the decisions ranges from 16 to 40 ms.

The objective of this research is to investigate the possibility of using traveling waves for detecting transmission line faults and to design a high-speed numerical traveling wave relay.

1.4 Outline of the Thesis

The thesis is organized in five chapters and five appendices. The first chapter presents the background of protective relays, introduces the subject of the thesis and describes its organization.

An overview of numerical relays, the algorithms used in them and the disadvantages of these conventional algorithms are reviewed in Chapter 2.

The traveling wave theory is introduced in Chapter 3. The behavior of traveling waves, when they encounter discontinuities, is also examined. The previously proposed traveling-wave relays are briefly examined in that chapter, as well.

Two high-speed relaying techniques that use traveling waves and algorithms for the techniques were developed. The proposed high-speed relaying techniques are presented in Chapter 4. The procedural steps involved in implementing of the algorithms are illustrated using flow charts.

The proposed techniques were tested using data generated by simulating a power system using the electromagnetic transient simulation application, EMTDC. Fault data were generated by applying different types of faults at different locations, with different fault inception angles. The impacts of hardware limitations were also included. The proposed algorithms were modeled as well. The modeling and data processing for the proposed techniques are described in Chapter 5. Results obtained from the simulated data are presented and discussed.

An introduction to the EMTDC is given in Appendix A. The parameters of the transmission line and other components of the power system used for generating

simulation data is listed in Appendix B. The parameters of the data acquisition system (DAS) and the processor model coded in the EMTDC are described in Appendix C.

The specific contributions made by this thesis are as follows.

1. Two techniques using traveling waves for a high-speed relay have been proposed.

2. Two digital algorithms based on the proposed techniques are also reported in Chapter 4.

3. Several tests have been done to evaluate the performance of these algorithms.

1.5 Summary

A brief introduction to the concepts of power system protection has been presented in this chapter. The development of protective devices from electromechanical relays to the present day numerical relays has been described. The objective and outline of the thesis have been presented as well.

Chapter 2

Numerical Relays

An introduction to the subject of numerical relays is presented in this chapter. The major functional blocks of a typical numerical relay are described. The features of numerical relays are outlined. Then, the conventional algorithms used in numerical relays are presented. A brief introduction to traveling wave relays is also given.

2.1 Numerical Relays

Numerical relays are microprocessor-based devices that use software to process quantized signals for implementing protection functions. The general purpose of a numerical relay is the same as the purpose of a conventional relay, in the sense that it should accept data representing voltage and current, process the data and execute a control action, like giving a trip signal to the breaker, when it is deemed to be necessary. Because the inputs from a power system are analog in nature, they are converted to digital form for the microprocessors. Numerical relays, therefore require appropriate hardware for analog to digital conversion. A block diagram of a typical numerical relay [1] is shown in Figure 2.1.

A numerical relay receives currents and voltages from a power system through CTs and VTs. The outputs of these transducers are applied to the relay. Each block of a typical relay is briefly explained in the following sections.

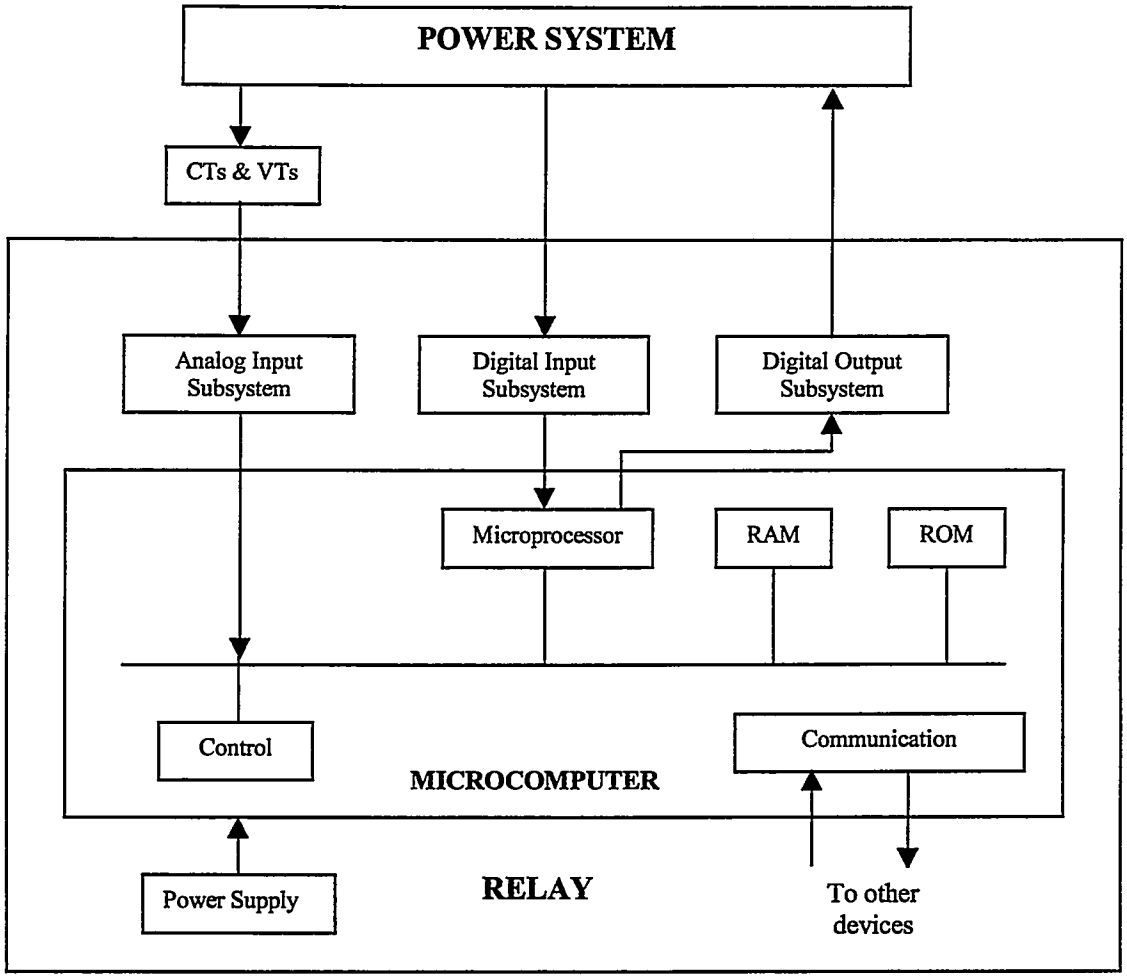

Figure 2.1: Block diagram of a typical numerical relay

2.1.1 Analog Input Subsystem

The analog input subsystem consists of the isolation and scaling system and the data acquisition system. The isolation and scaling system comprises of auxiliary CTs and VTs. This system also includes surge arrestors to block surges from the power system. The data acquisition system consists of the anti-aliasing filters, sample and hold circuits and the analog to digital converters. The analog input subsystem performs the following functions.

- Isolates the relay from the power system using surge arrestors.

- Scales down the input voltage or current using auxiliary CTs and VTs.
- Filters the high frequency components and noise using anti-aliasing filters.
- Samples the scaled down filtered voltage using sample and hold circuits.
- Converts the analog input signal to digital signal using analog to digital converters.

The analog input subsystem is connected to the power system through CTs and VTs. The transducers are generally of the electromagnetic type except for system voltages over 200 kV, capacitive voltage transformers (CVT) are used. These transducers step down the currents and voltages from the power system levels of kilo-amperes and kilo-volts to 5A and 110 V rms nominal values.

These levels of the CT and VT outputs are suitable for use with electromechanical and static relays but are not appropriate for use with the electronic circuits of numerical relays. The voltages are, therefore, stepped down further to the range of ± 10 V peak value. The currents are converted to equivalent voltages. The signals are converted to equivalent numerical representations because microprocessors can handle only numbers. Also, electronic circuits of numerical relays are protected from transients in power systems by surge arrestors.

2.1.2 Digital Input Subsystem

This subsystem receives information like status of breakers (ON/OFF), isolators and relay targets. The number of digital inputs can be twenty or more [1].

2.1.3 Central Processing Unit

The central processing unit processes data from the input subsystems and makes decisions based on the algorithms stored in the memory. It also controls the sample and hold circuits, the multiplexer and the A/D converters. This unit could be a general-purpose microprocessor, a DSP or a micro-controller. Sometimes two processors are used, one for performing calculations and the other for control and communication.

2.1.4 Memory

There are three types of memory. ROM (Read-Only Memory) is used for storing programs. EEPROM (Electronically-Erasable Programmable Read-Only Memory) is used for storing relay settings and other vital information. RAM (Random Access Memory) is used for temporarily storing intermediate numbers and fault data records. The processor communicates with these memory elements through its data, address and control buses. Some times multiple-input RAMs are used. This is useful when more than one processor is to read from and write on the same memory.

2.1.5 Digital Output Subsystem

The output of a numerical relay is provided to the power system through its digital output subsystem. A maximum of five to ten outputs are sufficient for most relaying applications.

2.1.6 Other Components

Communication ports are provided to share information with other devices. Numerical relays are usually powered from the station battery, which is provided with a battery charger. This ensures that the relay continues to perform its intended function during outages of the station ac supply.

2.2 Features of a Numerical Relay

A numerical relay has many special features. Some of the features are listed here.

1. Its ability to perform self-diagnostic tests to detect component failures. This eliminates the need to remove the relay from operation for maintenance; this increases the reliability of the system.
2. Most manufacturers use a common hardware platform for several classes of relays. The function of such a relay can be changed by changing the software.
3. The relay settings can be changed by using communication interface, making adaptive relaying possible.
4. A numerical relay can be programmed to do multiple protection functions with a single unit, thus reducing the cost of protection systems.
5. A digital relay can store fault data, which can be used for diagnostic purposes and system improvements. Fault locations can be calculated from the stored data making it easier for the maintenance staff to carry out repairs.

2.3 Relaying Algorithms

Most research in the area of digital protection relates to the development of algorithms for specific applications. Many relaying algorithms extract fundamental frequency phasors from quantized values of currents and voltages [3]. The phasors are used to make control decisions such as trip or reclose circuit breakers.

2.3.1 Nature Of Signals

A power system is a complex network of linear and non-linear components. The major part, of voltages and currents experienced in power systems are of the fundamental frequency. A voltage may, therefore, be expressed as

$$y(t) = V_P \sin(\omega_0 t + \theta) + e(t) \tag{2.1}$$

where,

ω_0 is the nominal power system frequency,
V_P is the peak value of the voltage,
θ is the phase angle of the voltage phasor, and
$e(t)$ is the error signal.

This error signal e(t), includes the unpredictable contributions from

- transducer (CTs and VTs) errors,
- traveling wave effects,
- fault arc,
- exponentially decaying offsets,
- truncating and rounding by A/D converters,
- transient outputs of anti-aliasing filters, and
- the power system.

The nature of the signals experienced in power systems depends on fault location, fault resistance and the fault incidence angle. The nature of the signals experienced during a disturbance is, therefore, unpredictable. A current could be represented by an equation similar to Equation 2.1.

2.3.2 Extracting Phasors

Consider that the signal $y(t)$ is sampled every ΔT seconds. From these samples, the parameters of the phasors, such as V_P and θ are to be estimated.

Algorithms differ in the ways they estimate the unknown parameters of the phasors from the quantized samples. They also differ in the number of samples they use to obtain an estimate. The number of samples used to obtain an estimate is called the data-window size.

Because the voltages and currents contain components of the fundamental and other frequencies, it would be useful to include the components of other frequencies in formulating the model of a signal. This ensures that the phasor estimates are more accurate. It can be seen that the error e(t) reduces as more components of the signals are included in the model. However, this may require the use of larger data-window for estimating the unknown parameters increasing the delay for obtaining the estimates.

2.4 Classification of Algorithms

The relaying algorithms can be broadly classified by the mathematical principles that are used for estimating phasors. Some of the classifications are as follows.

1. Trigonometric Algorithms,
2. Correlation Algorithms, and
3. Least Error Square Algorithms.

The algorithms, which use a window of less than half-cycle, are called short-window algorithms and the algorithms, which use a window of more than half-cycle, are called long-window algorithms. A phasor estimate is a complex number and, therefore, has a real part and an imaginary part.

$$V = V_P \angle\theta \;\; = \;\; V_{\mathrm{Re}} + \mathrm{j}\, V_{\mathrm{Im}}.$$

The algorithms generally estimate the real and imaginary parts of the phasors separately. The processes are basically digital filters. Depending on the frequency response of the filters some frequencies are passed without attenuation and the others are attenuated or amplified. The peak value and angle of the phasor are calculated from the estimated real and imaginary parts using the following equations.

$$V_P = \sqrt{(V_{\text{Re}}{}^2 + V_{\text{Im}}{}^2)}.$$

$$\theta = \tan^{-1}\left(\frac{V_{\text{Im}}}{V_{\text{Re}}}\right).$$

2.4.1 Trigonometric Algorithms

These algorithms use basic trigonometric identities [1,2] to estimate phasors from quantized samples. Some of the trigonometric algorithms are

1. Mann and Morrison Algorithm,
2. Rockefeller and Udren Algorithm, and
3. Gilbert and Shovlin Algorithm
4. Miki and Makino Algorithm,

The Mann and Morrison algorithm is described to give a brief overview of the procedures involved in trigonometric algorithms. This algorithm uses only three samples.

Consider the following three samples,

V_0 sample taken at time t = 0,

V_{-1} sample taken at time t = - ΔT seconds, and

V_{+1} sample taken at time t = + ΔT seconds.

Consider that a voltage can be described by the equation

$$v = V_P \sin(\omega t + \theta).$$

The sample taken at time t = 0 can be expressed as

$$V_P \sin(\theta) = V_0. \tag{2.2}$$

This is the imaginary part of the phasor.

The sample taken at time t = - ΔT seconds can be expressed as

$$V_{-1} = V_P \sin(-\omega\Delta T + \theta). \tag{2.3}$$

Similarly the sample taken at time t = + ΔT seconds can be expressed as

$$V_{+1} = V_P \sin(\omega\Delta T + \theta). \tag{2.4}$$

The derivative of the voltage signal is

$$\frac{dv}{dt} = \omega V_P \cos(\omega t + \theta).$$

At time t = 0 the above equation becomes

$$\left.\frac{dv}{dt}\right|_{t=0} = \omega V_P \cos(\theta). \tag{2.5}$$

The derivative of the voltage at time t = 0 in terms of the three samples is given by

$$\left.\frac{dv}{dt}\right|_{t=0} \approx \frac{V_{+1} - V_{-1}}{2\Delta T}. \tag{2.6}$$

Equating Equations 2.5 and 2.6 gives

$$\omega V_P \cos(\theta) \approx \frac{V_{+1} - V_{-1}}{2\Delta T}.$$

Rearranging this equation gives

$$V_P \cos(\theta) \approx \frac{[V_{+1} - V_{-1}]}{(2\omega_0 \Delta T)}. \tag{2.7}$$

This is the real part of the filter.

For a nominal frequency of 60 Hz and a sampling frequency of 720 Hz, Equation 2.7 becomes

$$V_P \cos(\theta) \approx 0.955V_{+1} - 0.955V_{-1}.$$

This is an FIR filter with filter coefficients, 0.955, 0 and –0.955. Multiplying the input signal with these filter coefficients provides the real part of the phasor. Similarly the coefficient of the filter, which calculates the imaginary part of the phasor, is 1.

To calculate the frequency response of the two filters, the filter equations are written in terms of z-transform. This process gives

$$Hi(z) = 1z^0$$

$$Hr(z) = 0.955z^{+1} + 0z^0 - 0.955z^{-1}$$
$$= 0.955\left(z^{+1} - z^{-1}\right)$$

Replacing z with $e^{j\omega\Delta T}$ gives,

$$Hi(\omega) = 1$$

$$Hr(\omega) = 0.955\left(e^{j\omega\Delta T} - e^{-j\omega\Delta T}\right)$$
$$= 0.955 \times 2j \times \sin(\omega\Delta T)$$
$$= 1.91j\sin(\omega\Delta T)$$

At 60 Hz the frequency response of the filter that calculates the real part is 0.955. To normalize the output at 60 Hz to 1, the coefficient can be changed to 1 from 0.955.

Figure 2.2 shows the frequency response of the filter that calculates the real part of the phasor.

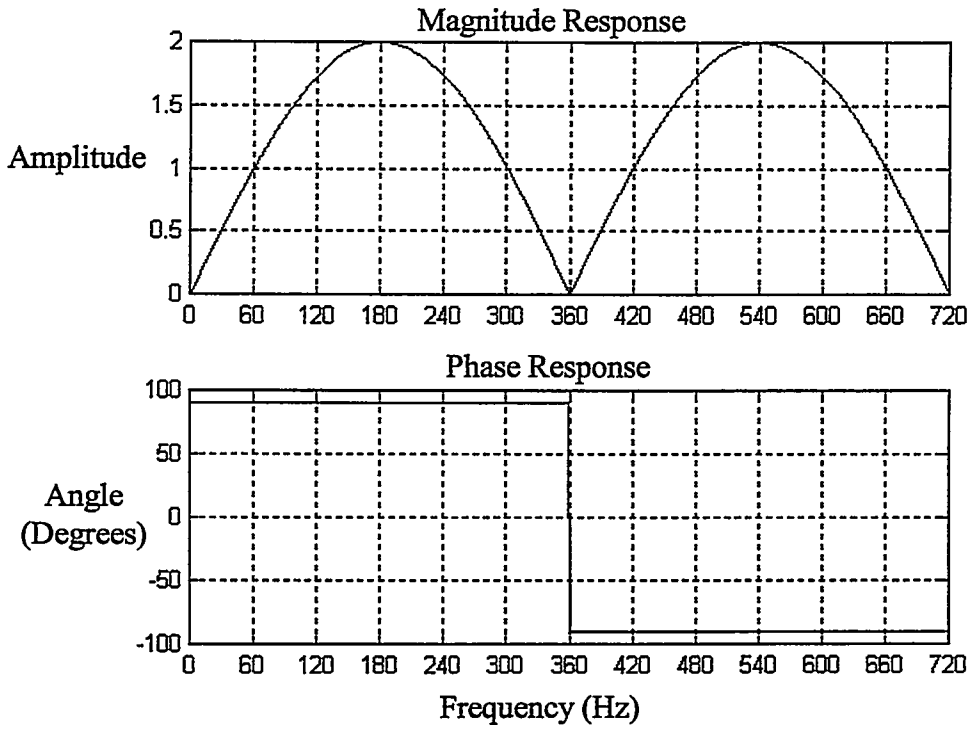

Figure 2.2: Frequency response of a Mann and Morrison real part filter

This figure shows that the procedure for calculating the real part of the phasor

- passes 60Hz component without attenuation,
- removes the non-decaying dc component,
- amplifies the 2nd, 3rd and 4th harmonics, and
- phase shifts all frequencies by 90^0.

Figure 2.3 shows the frequency response of the filter that calculates the imaginary part of the phasor.

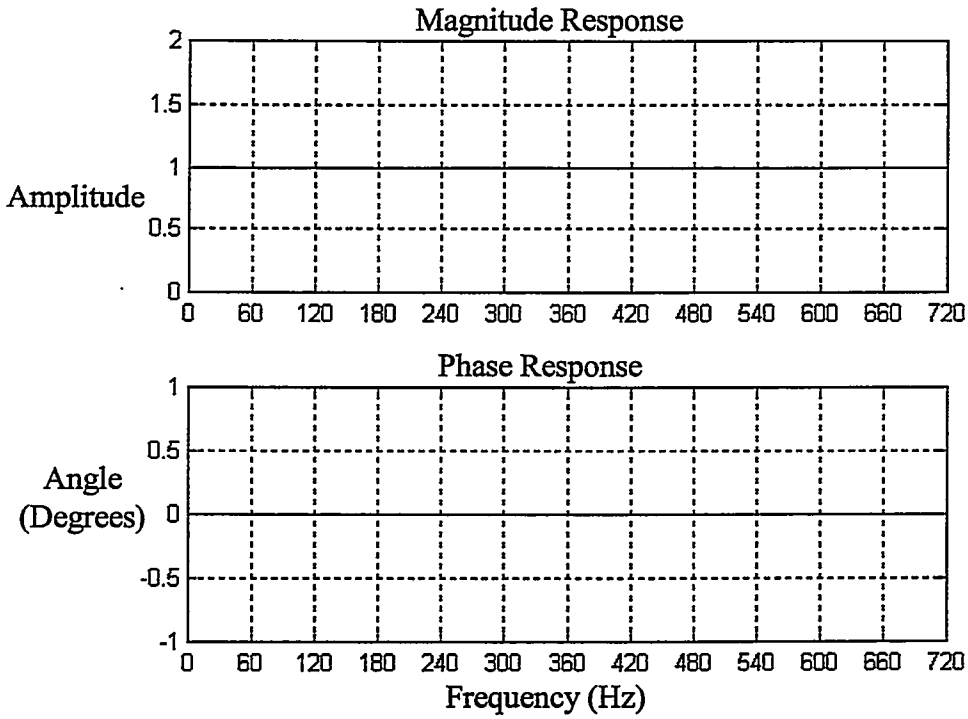

Figure 2.3: Frequency response of a Mann and Morrison imaginary part filter

This figure shows the procedure for calculating the imaginary part of the phasor passes all frequencies without attenuating, amplifying or phase-shifting them.

This algorithm gives accurate results when the input signal is of the nominal frequency only. However, when an input signal contains harmonics or a dc component, the output becomes inaccurate.

The other trigonometric algorithms are also designed with the assumption that the input signal is made up of a waveform of the nominal frequency only. This is, however rarely true in an actual power system.

2.4.2 Correlation Algorithms

These algorithms use two orthogonal functions, which would effectively extract components of the frequency of interest from a given signal [4]. Two functions g(t) and f(t) are orthogonal over a period of time T if,

$$\int_{t=0}^{T} f(\omega t)g(\omega t)dt = 0 \ . \tag{2.8}$$

where,

T is the time period of the function.

The input signal is multiplied with $f(\omega t)$ and $g(\omega t)$ over one time period, T, to get the real and imaginary parts of the phasors of the required frequency. This process is called correlation.

The main steps for developing these algorithms are as follows

1. Find a set of orthogonal functions.
2. Extract the imaginary and real parts of the phasor (of required frequency).
3. Estimate the phasor of the required frequency from the calculated real and imaginary parts.

Some of the correlation algorithms are:

1. Discrete Fourier Transform (DFT) Algorithm.
2. Even and Odd Functions Algorithm.
3. Walsh Functions Algorithm.
4. Half-Cycle DFT Algorithm.
5. Cosine Filters.

The basic difference between these algorithms is the orthogonal functions that are used for performing the correlations.

The DFT algorithm [2] is described to show the procedure used by correlation algorithms. Samples of a full cycle of the nominal frequency are used. For example, when a 60 Hz signal is sampled at 720 Hz there are 12 samples. Therefore, the width of the data window is 12 samples.

The sine and cosine waveforms of the nominal frequency, which are orthogonal functions, are used in this case. The proof that the sine and cosine waveforms are orthogonal is as follows.

$$\int_{\omega t=0}^{T} f(\omega t)g(\omega t)d\omega t = \int_{\omega t=0}^{2\pi} \sin(\omega t)\cos(\omega t)d\omega t$$
$$= \frac{1}{2}\int_{\omega t=0}^{2\pi} \sin(2\omega t)d\omega t$$
$$= -\frac{1}{2}\cdot\frac{1}{2}\cos(2\omega t)\Big|_0^{2\pi}$$
$$= 0\cdot$$

The real and imaginary components of a phasor representing a signal can be obtained by correlating with these orthogonal functions as follows. Consider the signal

$$\begin{aligned} v &= Vp\sin(\omega t+\theta) \\ &= Vp\cos(\theta)\sin(\omega t) + Vp\sin(\theta)\cos(\omega t)\cdot \end{aligned} \tag{2.9}$$

Correlating with $\sin(\omega t)$ provides

$$\int_0^{2\pi} Vp\sin(\omega t+\theta)\sin(\omega t)d(\omega t)$$
$$= \int_0^{2\pi} Vp\cos(\theta)\sin(\omega t)\sin(\omega t)d(\omega t) + \int_0^{2\pi} Vp\sin(\theta)\cos(\omega t)\sin(\omega t)d(\omega t) \tag{2.10}$$
$$= \int_0^{2\pi} Vp\cos(\theta)\sin^2(\omega t)d(\omega t) + \int_0^{2\pi} \frac{Vp\sin(\theta)}{4}\sin(2\omega t)d(2\omega t)\cdot$$

Because the integral of $\sin(2\omega t)$ over one period is zero, this equation becomes,

$$\int_0^{2\pi} Vp\sin(\omega t+\theta)\sin(\omega t)d(\omega t) = \int_0^{2\pi} Vp\cos\theta\sin^2(\omega t)d(\omega t)\cdot$$

Simplifying further, this equation becomes

$$\int_0^{2\pi} Vp\sin(\omega t+\theta)\sin(\omega t)d(\omega t) = \tfrac{1}{4}Vp\cos(\theta)\left(\int_{\omega t=0}^{2\pi} d(2\omega t) - \int_{\omega t=0}^{2\pi}\cos(2\omega t)d(2\omega t)\right). \tag{2.11}$$
$$= \pi\cdot Vp\cos(\theta)$$

Rearranging Equation 2.11 provides

$$Vp\cos(\theta) = \frac{1}{\pi}\int_0^{2\pi} Vp\sin(\omega t+\theta)\sin(\omega t)d(\omega t)\,. \tag{2.12}$$

Similarly,

$$Vp\sin(\theta) = \frac{1}{\pi}\int_0^{2\pi} Vp\sin(\omega t+\theta)\cos(\omega t)d(\omega t) \tag{2.13}$$

Equation 2.12 and 2.13 give the real and imaginary parts of the phasor representing the waveform described by Equation 2.9.

Replacing the integrations in Equations 2.12 and 2.13 by numerical processes provides

$$V_{\mathrm{Re}}(k) = \frac{2}{m}\sum_{n=0}^{m-1} v_{k+n-m+1}\sin(2\pi\cdot n/m) \quad \text{and} \tag{2.14}$$

$$V_{\mathrm{Im}}(k) = \frac{2}{m}\sum_{n=0}^{m-1} v_{k+n-m+1}\cos(2\pi\cdot n/m) \tag{2.15}$$

where,

k is the most recent sample, and
m is the number of samples taken in one cycle of the fundamental frequency.

These equations show that correlating a signal with the cosine waveform provides the imaginary part of the phasor and correlating with the sine waveform provides the real part of the phasor. For a 60 Hz signal, sampled at 720 Hz, Equations 2.14 and 2.15 yield the following coefficients.

For calculating the real part of the phasor the filter is given by the coefficients

{0, 0.5, 0.866, 1.0, 0.866, 0.5, 0, -0.5, -0.866, -1.0, -0.866, -0.5}.

For calculating the imaginary part of the phasor the filter is given by the coefficients

{1.0, 0.866, 0.5, 0, -0.5, -0.866, -1.0, -0.866, -0.5, 0, 0.5, 0.866}

These are 12-point FIR filters. The filter, which gives the real part of the phasor ($Vp\cos\theta$), is called the cosine filter and the filter, which gives the imaginary part of the phasor ($Vp\sin\theta$), is called the sine filter.

Figures 2.4 and 2.5 show the frequency responses of the sine and cosine filters respectively when a sampling frequency of 720 Hz is used to calculate phasors of 60 Hz frequency. These figures show that both the sine and cosine filters

- pass 60Hz component without any attenuation,
- completely remove the non-decaying dc component, and
- remove all harmonics.

The frequency response of the DFT algorithm, which is the most widely used algorithm in relays, is better than the frequency response of the trigonometric algorithms. The transient response of the DFT is slower than the transient response of the trigonometric algorithms because the DFT uses longer data window. The DFT algorithm, however, does not remove the decaying part of the DC component.

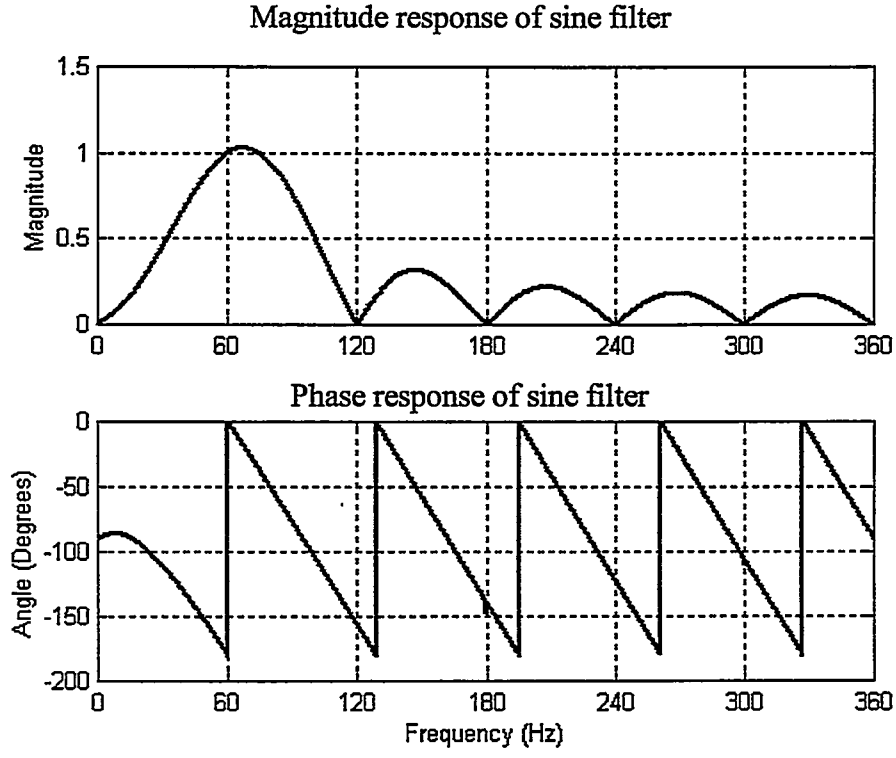

Figure 2.4: Frequency response of a DFT sine filter

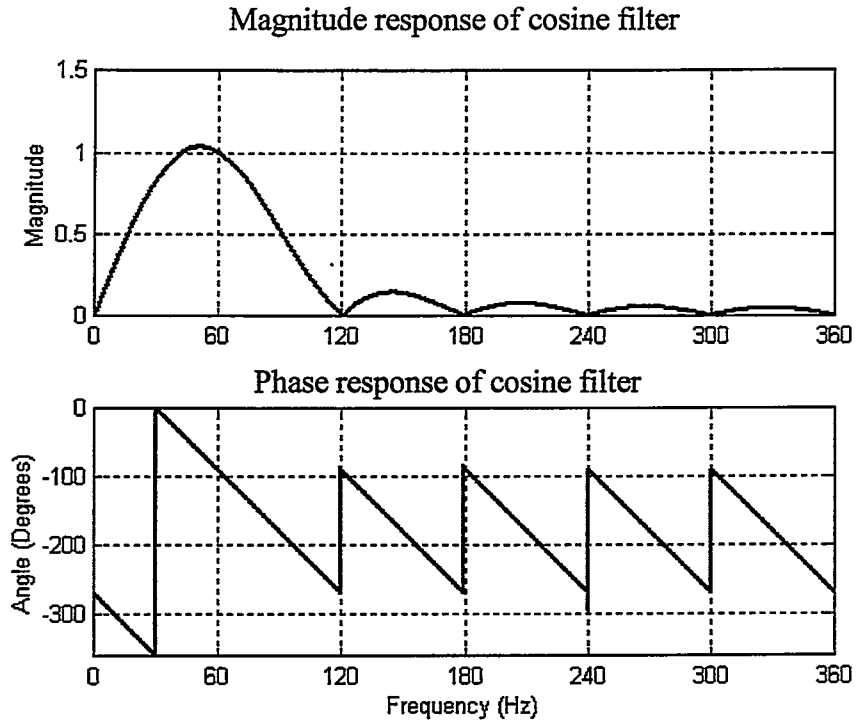

Figure 2.5: Frequency response of a DFT cosine filter

2.4.3 Least Error Square Algorithms

This class of algorithms use the least squares principle to minimize the error in the phasors estimated from the input samples [1,12]. This principle can be explained as follows:

Consider a set of measurements that satisfy Equation 2.16.

$$a + ct = m. \tag{2.16}$$

where,

m is the measurement
t is the time
a & c are parameters of the model.

'n' measurements can be represented by Equation 2.17.

$$\begin{aligned} a + ct_1 &= m_1 \\ a + ct_2 &= m_2 \\ &\cdots\cdots \\ a + ct_n &= m_n \end{aligned} \tag{2.17}$$

Assuming â and ĉ as the estimated values of the parameters, there is a difference between the estimates and measured values. The errors can be expressed as

$$\begin{aligned} &\hat{a}+\hat{c}t_1-m_1=\varepsilon_1,\\ &\hat{a}+\hat{c}t_2-m_2=\varepsilon_2,\\ &\cdots\cdots \qquad \textit{and}\\ &\hat{a}+\hat{c}t_n-m_n=\varepsilon_n\cdot \end{aligned} \tag{2.18}$$

In matrix form this equation can be written as

$$\begin{bmatrix} 1 & t_1\\ 1 & t_2\\ . & .\\ 1 & t_n \end{bmatrix}\begin{bmatrix}\hat{a}\\ \hat{c}\end{bmatrix}-\begin{bmatrix} m_1\\ m_2\\ .\\ m_n\end{bmatrix}=\begin{bmatrix}\varepsilon_1\\ \varepsilon_2\\ .\\ \varepsilon_n\end{bmatrix} \tag{2.19}$$

or

$$[A][x]-[m]=[e]$$

The sum of error squares is given by

$$[e]^T[e]=[[A][x]-[m]]^T[[A][x]-[m]]\cdot$$

Expanding the right hand side of this equation provides

$$[e]^T[e]=[[A][x]]^T[[A][x]]-[[A][x]]^T[m]-[m]^T[[A][x]]+[m]^T[m]$$

$$=\left[[x]^T[A]^T[A][x]\right]-2[x]^T[A]^T[m]+[m]^T[m]$$

For the sum of the error squares to be minimum, its derivative with respect to $[x]$ must be zero; this can be written as

$$\frac{d}{d[x]}\left\{\left[[x]^T[A]^T[A][x]\right]-2[x]^T[A]^T[m]+[m]^T[m]\right\}=0. \tag{2.20}$$

Taking the derivative provides

$$2\left[[A]^T[A][x]\right]-2[A]^T[m]=0. \tag{2.21}$$

Rearranging this equation provides

$$\left[[A]^T[A][x]\right]=[A]^T[m]. \tag{2.22}$$

The parameters of the model are now given by

$$[x] = \left[[A]^T[A]\right]^{-1}[A]^T[m] = [A]^{-1L}[m] \tag{2.23}$$

where,

$[A]^{-1L}$ is called the left pseudo-inverse of $[A]$ and is given by $\left[[A]^T[A]\right]^{-1}[A]^T$.

If the times, at which the measurements are taken, are known in advance, the left pseudo-inverse of $[A]$ can be calculated prior to sampling the data. This method can be used if the equations describing the waveforms of voltages and currents can be expressed in a linear form.

Consider a signal that can be represented by a combination of the fundamental frequency component and 2nd, 3rd, 4th and 5th harmonics and a decaying DC component. This waveform can be expressed as

$$v = Vp_1 \sin(\omega_0 t + \theta_1) + Vp_2 \sin(2\omega_0 t + \theta_2) + Vp_3 \sin(3\omega_0 t + \theta_3) + Vp_4 \sin(4\omega_0 t + \theta_4) + Vp_5 \sin(5\omega_0 t + \theta_5) + V_0 e^{-\frac{t}{\tau}} \tag{2.24}$$

The fundamental frequency term can be expanded as

$$Vp_1 \sin(\omega_0 t + \theta_1) = Vp_1 \sin(\theta_1)\cos(\omega_0 t) + Vp_1 \cos(\theta_1)\sin(\omega_0 t)$$

The terms representing the harmonics can also be expanded in a similar manner. The decaying dc component can be expanded using the Taylor series and can be approximated by the first two terms of the series as follows.

$$V_0 e^{-\frac{t}{\tau}} \approx V_0 - V_0 \frac{t}{\tau}$$

Using this approximation and expanding the sinusoids, Equation 2.24 can be written as,

$$v = Vp_1 \sin(\theta_1)\cos(\omega_0 t) + Vp_1 \cos(\theta_1)\sin(\omega_0 t) + Vp_2 \sin(\theta_2)\cos(2\omega_0 t) + Vp_2 \cos(\theta_2)\sin(2\omega_0 t) + Vp_3 \sin(\theta_3)\cos(3\omega_0 t) + Vp_3 \cos(\theta_3)\sin(3\omega_0 t) + Vp_4 \sin(\theta_4)\cos(4\omega_0 t) + Vp_4 \cos(\theta_4)\sin(4\omega_0 t) + Vp_5 \sin(\theta_5)\cos(5\omega_0 t) + Vp_5 \cos(\theta_5)\sin(5\omega_0 t) + V_0 - V_0 \frac{t}{\tau}$$

(2.25)

This equation has twelve unknowns namely, the real and imaginary parts of the phasors of the ac components, the constant part of the DC and the decaying part of the DC. Because there are twelve unknowns at least thirteen samples are needed to obtain a least squares solution.

Equation 2.25 can be rewritten as,

$$v = x_1 A_{n1} + x_2 A_{n2} + x_3 A_{n3} + x_4 A_{n4} + x_5 A_{n5} + x_6 A_{n6} + x_7 A_{n7} + x_8 A_{n8} + x_9 A_{n9} + x_{10} A_{n10} + x_{11} A_{n11} - x_{12} A_{n12}$$

(2.26)

where,

x_1	$Vp_1\sin(\theta_1)$	A_{n01}	$\cos(n\omega_0\Delta T)$
x_2	$Vp_1\cos(\theta_1)$	A_{n02}	$\sin(n\omega_0\Delta T)$
x_3	$Vp_2\sin(\theta_2)$	A_{n03}	$\cos(2n\omega_0\Delta T)$
x_4	$Vp_2\cos(\theta_2)$	A_{n04}	$\sin(2n\omega_0\Delta T)$
x_5	$Vp_3\sin(\theta_3)$	A_{n05}	$\cos(3n\omega_0\Delta T)$
x_6	$Vp_3\cos(\theta_3)$	A_{n06}	$\sin(3n\omega_0\Delta T)$
x_7	$Vp_4\sin(\theta_4)$	A_{n07}	$\cos(4n\omega_0\Delta T)$
x_8	$Vp_4\cos(\theta_4)$	A_{n08}	$\sin(4n\omega_0\Delta T)$
x_9	$Vp_5\sin(\theta_5)$	A_{n09}	$\cos(5n\omega_0\Delta T)$
x_{10}	$Vp_5\cos(\theta_5)$	A_{n10}	$\sin(5n\omega_0\Delta T)$
x_{11}	V_0	A_{n11}	1
x_{12}	V_0 / τ	A_{n12}	ΔT

The sample taken at time t = 0 can be expressed as

$$v = x_1 A_{01} + x_2 A_{02} + x_3 A_{03} + x_4 A_{04} + x_5 A_{05} + x_6 A_{06} + x_7 A_{07} + x_8 A_{08} + x_9 A_{09} + x_{10} A_{010} + x_{11} A_{011} - x_{12} A_{012}.$$

(2.27)

Similarly the sample taken at time t = -ΔT seconds can be expressed as

$$v = x_1 A_{-11} + x_2 A_{-12} + x_3 A_{-13} + x_4 A_{-14} + x_5 A_{-15} + x_6 A_{-16} + x_7 A_{-17} + x_8 A_{-18} + x_9 A_{-19} + x_{10} A_{-110} + x_{11} A_{-111} - x_{12} A_{-112}.$$

(2.28)

And the sample taken at time t = +ΔT seconds can be expressed as

$$v = x_1 A_{+11} + x_2 A_{+12} + x_3 A_{+13} + x_4 A_{+14} + x_5 A_{+15} + x_6 A_{+16} + x_7 A_{+17} + x_8 A_{+18} + x_9 A_{+19} + x_{10} A_{+110} + x_{11} A_{+111} - x_{12} A_{+112}.$$

(2.29)

Similarly, samples taken at t = -6ΔT, -5ΔT, -4ΔT, -3ΔT, -2ΔT, +2ΔT, +3ΔT, +4ΔT, +5ΔT and +6ΔT can be expressed by ten additional equations. Because the samples are taken at a predetermined sampling rate, cos($n\omega_0\Delta T$) and sin($n\omega_0\Delta T$) are known. For a nominal frequency of 60 Hz and a sampling frequency of 720 Hz,

$$\omega_0 \Delta T = \frac{2\pi 60}{720} = \frac{\pi}{6}.$$

Using this, the elements of the [A] matrix and its left pseudo can be calculated.

The phasors can be obtained by solving the equation,

$$\underset{12\times 1}{[x]} = \underset{12\times 13}{[A]^{-1L}} \underset{13\times 1}{[m]}.$$

(2.30)

The use of two rows of the left pseudo inverse of [A] provides the real and imaginary parts of the phasors representing a selected frequency included in the model of the signal.

Figures 2.6 and 2.7 show the frequency response of the LES 60 Hz filter. These figures show that these filters

- pass 60Hz component without any attenuation,
- removes the dc component, and
- removes all the harmonics.

LES algorithm removes the decaying DC component effectively.

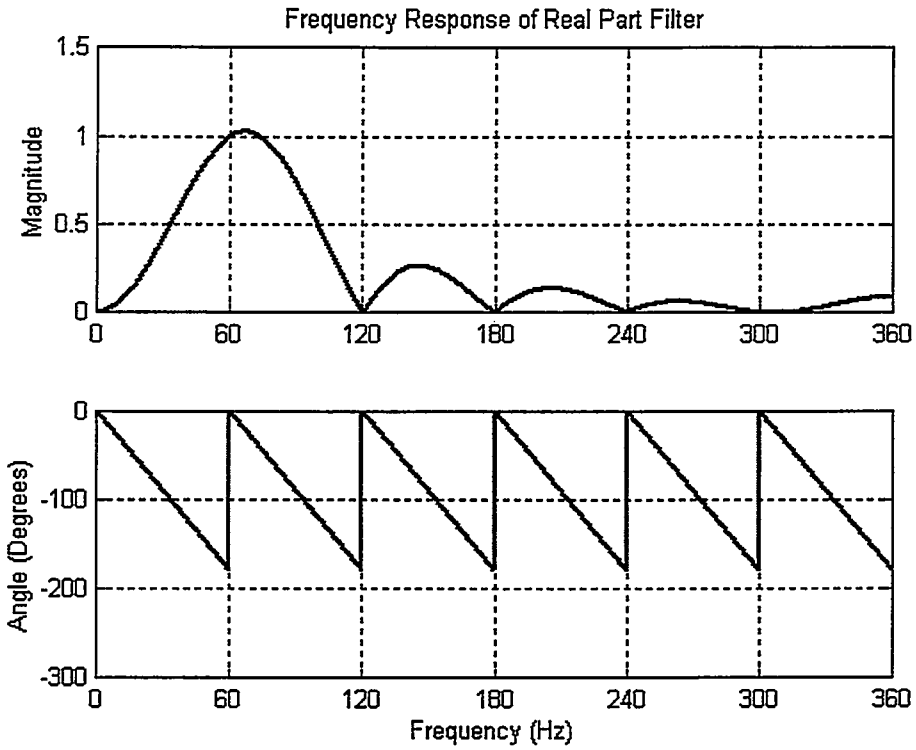

Figure 2.6: Frequency response of a 60 Hz real part LES filter

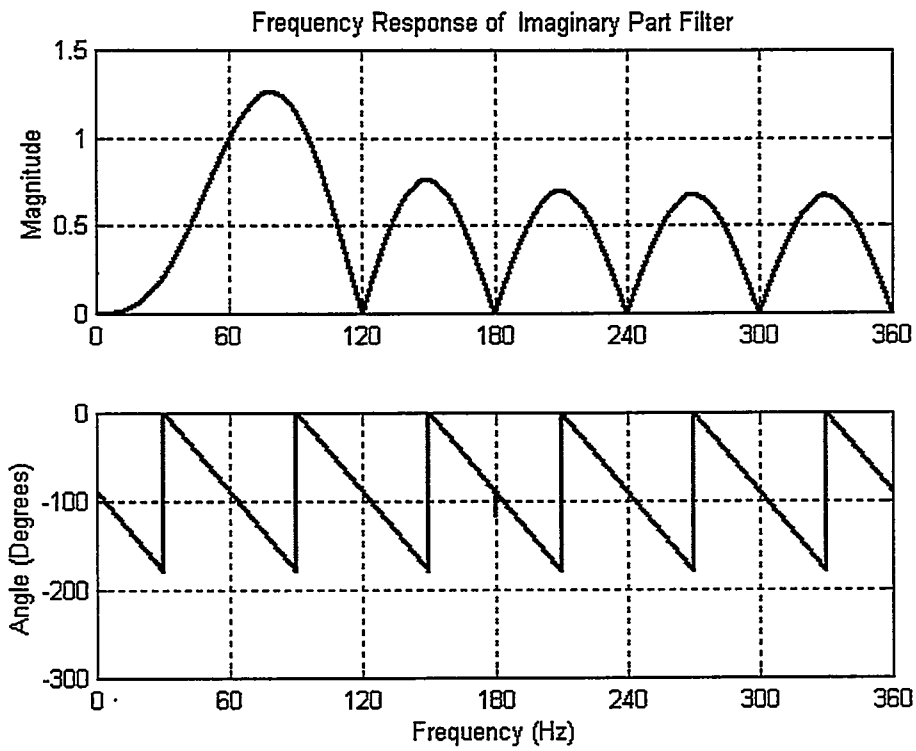

Figure 2.7: Frequency response of a 60 Hz imaginary part LES filter

2.5 Trip Algorithms

After the phasors are estimated, trip decisions, which depend on the application of the relay, are made. In an instantaneous over-current relay the peak value of current, computed from the quantized samples, is compared with a pre-specified threshold. If the current exceeds the threshold, the relay issues a trip command.

In a distance relay, the current and voltage phasors are computed from the quantized samples. The impedance seen by the relay is calculated from the phasors. When the seen impedance is in the pre-specified operating zone, it is concluded that the fault is in the protection zone and a trip command is issued.

In a transformer differential relay, the harmonic contents of the current are used for restraining the relay during magnetizing inrush. The phasors of the fundamental and harmonic components are estimated. The differential relay is blocked from operating when the magnitude of second harmonic component exceeds a threshold value. In some designs a combination of harmonics is used to restrain the relay.

The directional relays implement the following equation.

$$V_P I_P \cos(\theta_v - \theta_i - \tau) > 0 \tag{2.31}$$

where,

V_P is the voltage peak
I_P is the current peak
τ is the maximum sensitivity angle
θ_v is the voltage angle
θ_i is the current angle

V_P and I_P are estimated using the phasor estimating algorithms. Then Equation 2.31 is implemented. If the condition is satisfied, the protection system concludes that the fault is in the forward direction.

2.6 Disadvantages of Conventional Algorithms

Filters are essential parts of a relay and whenever filtering is done delays are introduced. There are two stages of filtering in a numerical relay, the low-pass analog filters in the input and the digital filters used to estimate phasors.

Low pass filters introduce a delay roughly proportional to the inverse of the cut-off frequency [1]. As the cut-off frequency approaches the power frequency, elimination of higher frequencies requires a longer delay. The sharpness of cut-off also affects the delay. The sharper the cut-off, longer is the delay required.

Reasonably accurate estimate of the phasors can be obtained only by using window sizes of one-cycle of the nominal frequency. For a nominal frequency of 60 Hz it takes atleast 16ms for an algorithm to respond to a fault. After the relay gives a trip command, the breaker takes time to operate. It, therefore, takes at least three cycles (≈ 50 ms) to isolate a faulted circuit. If a fault is not cleared in reasonable time, some components are likely to be damaged resulting in financial losses including those due to interruption of power.

These days load demands are increasing and construction of new transmission lines are not cost effective solutions. Power systems are, therefore, operated close to their design limits. It is essential that faults be identified as early as possible, and that the faulted components be isolated quickly.

2.7 Summary

This chapter has provided an overview of numerical relays. Block diagram of a typical numerical relay has been described and advantages of numerical relays have been discussed. Algorithms used in these relays have also been described and the disadvantages of the conventional algorithms have been outlined.

Chapter 3

Traveling Wave Theory

3.1 Introduction

This chapter provides an introduction to the origin and propagation of traveling waves in a transmission line. The behaviour of the traveling waves when they arrive at discontinuities is also discussed. The previously proposed traveling wave relays are presented as well.

An electric circuit can be usually considered as a circuit made of components of lumped parameters because the geometric dimensions of the elements are very small when compared with the wavelength of the voltage and current. The length of transmission lines is comparable with the wavelength of its voltage and current and, therefore, it is necessary to consider that its parameters are distributed throughout its length as shown in Figure 3.1. Each element of this network represents a small length of line, say Δx.

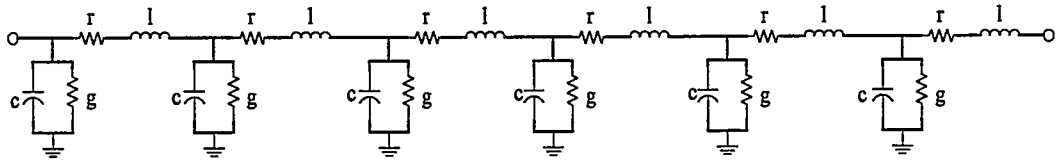

Figure 3.1: Distributed parameter network representing a transmission line; the terms r, l, c and g are defined in Page 33.

3.2 Transmission Line Equations

Modeling of transmission lines has been the subject of many textbooks. The transmission line equations, derived in this section, follow the procedure described in

"Electric Transmission Lines - Distributed Constants, Theory and Applications" by Hugh Hildreth Skilling [5].

Transmission lines can be represented by a pair of differential equations that are derived in this section. Voltage varies from point to point along a line and current also changes from one point to another. Voltage at the receiving end of the line is different from the voltage at the sending end due to the voltage drop across the line. Consider a Δx meters long section of a homogeneous transmission line at a distance x from the receiving end as shown in Figure 3.2.

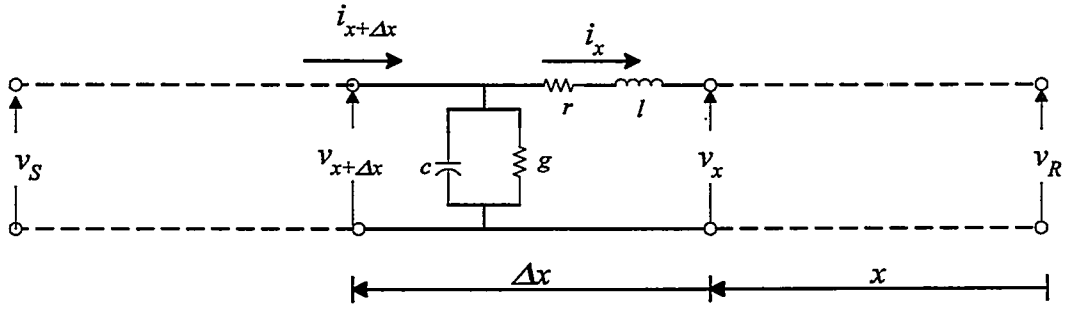

Figure 3.2: Distributed parameter network representing a section of transmission line

The line parameters are

- r the series resistance per unit length,
- l the series inductance per unit length,
- g the shunt conductance per unit length and
- c the shunt capacitance per unit length.

Let

- v_S be the sending end voltage,
- v_R be the receiving end voltage of the line,
- v_x be the voltage at the receiving end of the section under consideration,
- i_x be the current leaving the section under consideration,
- $v_{x+\Delta x}$ be the voltage at the sending end of the section under consideration,
- $i_{x+\Delta x}$ be the current entering the section under consideration.

The voltage $v_{x+\Delta x}$ can be expressed as

$$v_{x+\Delta x} = v_x + r\Delta x i_x + l\Delta x \frac{\partial i_x}{\partial t} \tag{3.1}$$

Rearranging Equation 3.1 and dividing both sides by Δx provides

$$\frac{v_{x+\Delta x} - v_x}{\Delta x} = r i_x + l \frac{\partial i_x}{\partial t} \tag{3.2}$$

As Δx approaches zero, this equation becomes

$$\frac{\partial v_x}{\partial x} = r i_x + l \frac{\partial i_x}{\partial t} \tag{3.3}$$

Rewriting this equation in terms of phasors gives

$$\frac{d\vec{V}}{dx} = r\vec{I} + j\omega l\vec{I}\,. \tag{3.4}$$

where,

ω is the frequency in radians per second and is equal to $2\pi f$ and

$\vec{I}$ is the phasor representation of current i.

Replacing $r + j\omega l$ by z provides

$$\frac{d\vec{V}}{dx} = z\vec{I}\,. \tag{3.5}$$

Proceeding in a similar manner, it can be shown that

$$\frac{d\vec{I}}{dx} = y\vec{V} \tag{3.6}$$

where,

y is a constant and is equal to $g + j\omega c$ and

$\vec{V}$ is the phasor representation of voltage v.

3.2.1 Solution of the Differential Equations

The solution of the Equations 3.5 and 3.6 provides voltage and current as functions of distance along the line. Differentiating Equation 3.5 with respect to x and substituting Equation 3.6 in the resulting equation, provides

$$\frac{d^2\vec{V}}{dx^2} = zy\vec{V}\,. \tag{3.7}$$

The auxiliary equation is

$$m^2 - zy = 0\,.$$

Solving this equation provides

$$m = \pm\sqrt{zy}\,.$$

The solution of Equation 3.7, therefore, is

$$\vec{V} = \vec{V}_1 e^{\sqrt{zy}x} + \vec{V}_2 e^{-\sqrt{zy}x} \tag{3.8}$$

where,

$\vec{V}_1$ and $\vec{V}_2$ are arbitrary constants.

Proceeding in the same manner, it can be shown that

$$\vec{I} = \vec{I}_1 e^{\sqrt{zy}x} + \vec{I}_2 e^{-\sqrt{zy}x} \tag{3.9}$$

Equations 3.8 and 3.9 describe the voltage and current along transmission line.

Differentiating Equation 3.8 with respect to x and substituting the result in Equation 3.5 provides

$$\sqrt{zy}\vec{V}_1 e^{\sqrt{zy}x} - \sqrt{zy}\vec{V}_2 e^{-\sqrt{zy}x} = z\vec{I}\,.$$

Substituting Equation 3.9 in this equation provides

$$\sqrt{zy}\vec{V}_1 e^{\sqrt{zy}x} - \sqrt{zy}\vec{V}_2 e^{-\sqrt{zy}x} = z\vec{I}_1 e^{\sqrt{zy}x} + z\vec{I}_2 e^{-\sqrt{zy}x}\,. \tag{3.10}$$

Dividing Equation 3.10 by $\sqrt{zy}$ provides

$$\vec{V}_1 e^{\sqrt{zy}x} - \vec{V}_2 e^{-\sqrt{zy}x} = \sqrt{\frac{z}{y}}\vec{I}_1 e^{\sqrt{zy}x} + \sqrt{\frac{z}{y}}\vec{I}_2 e^{-\sqrt{zy}x}\,. \tag{3.11}$$

Differentiating Equation 3.9, substituting the result in Equation 3.6 and substituting Equation 3.8 in that equation provides the following equation that is similar to Equation 3.10.

$$\sqrt{zy}\,\vec{I}_1 e^{\sqrt{zy}x} - \sqrt{zy}\,I_2 e^{-\sqrt{zy}x} = y\vec{V}_1 e^{\sqrt{zy}x} + y\vec{V}_2 e^{-\sqrt{zy}x}\,. \tag{3.12}$$

Dividing Equation 3.12 by y and rearranging provides

$$\vec{V}_1 e^{\sqrt{zy}x} + \vec{V}_2 e^{-\sqrt{zy}x} = \sqrt{\frac{z}{y}}\vec{I}_1 e^{\sqrt{zy}x} - \sqrt{\frac{z}{y}}\vec{I}_2 e^{-\sqrt{zy}x}\,. \tag{3.13}$$

Adding Equations 3.11 and 3.13 and eliminating $e^{\sqrt{zy}x}$ that is present in both sides of the equation provides

$$\vec{V}_1 = \sqrt{\frac{z}{y}}\vec{I}_1\,. \tag{3.14}$$

Subtracting Equation 3.11 from 3.13 and eliminating $e^{-\sqrt{zy}x}$ that is present in both sides of the equation provides

$$\vec{V}_2 = -\sqrt{\frac{z}{y}}\vec{I}_2 \ . \tag{3.15}$$

$\sqrt{\frac{z}{y}}$ is called the characteristic impedance or surge impedance of the line and is denoted by Z_0. Equations 3.14 and 3.15 can now be rewritten as

$$\vec{V}_1 = Z_0\vec{I}_1 \qquad \text{and} \tag{3.16}$$

$$\vec{V}_2 = -Z_0\vec{I}_2 . \tag{3.17}$$

$\sqrt{zy}$ is called the propagation constant and is often represented by γ, which is a complex quantity, and can be expressed as

$$\gamma = \sqrt{zy} = \alpha + j\beta .$$

where,

α is the real part and is called the attenuation constant, and
β is the imaginary part and is called the phase constant.

Equations 3.8 and 3.9 can be written in terms of these constants as

$$\vec{V} = \vec{V}_1 e^{\alpha x} e^{j\beta x} + \vec{V}_2 e^{-\alpha x} e^{-j\beta x} \tag{3.18}$$

$$\vec{I} = \vec{I}_1 e^{\alpha x} e^{j\beta x} + \vec{I}_2 e^{-\alpha x} e^{-j\beta x} \tag{3.19}$$

3.2.2 Interpretation of the Solutions

The behaviour of traveling waves can be explained by assuming $\vec{V}_2 = 0$ and $\vec{V} = \vec{V}_1 e^{\alpha x} e^{j\beta x}$. This term represents a sinusoidal voltage at a location x meters from the receiving end. When $x = 0$, $\vec{V}\,(= \vec{V}_1)$ is the voltage at the receiving end of the line. At a location x meters from the receiving end

- the magnitude of the voltage is $\vec{V}_1 e^{\alpha x}$ that is larger than $\vec{V}_1$, and
- the phase angle of the voltage is advanced by an angle βx.

This indicates that $\vec{V}_1 e^{\alpha x} e^{j\beta x}$ is a wave traveling from the source end to the receiving end.

If $\vec{V}_1 = 0$, $\vec{V}$ will equal $\vec{V}_2 e^{-\alpha x} e^{-j\beta x}$. This term also represents a sinusoidal voltage at a location x meters from the receiving end. When $x = 0$, $\vec{V}\ (= \vec{V}_2)$ is the voltage at the receiving end of the line. At a location x meters from the receiving end

- the magnitude of the voltage is $\vec{V}_2 e^{-\alpha x}$ that is smaller than $\vec{V}_2$, and
- the phase angle of the voltage is retarded by an angle βx.

This indicates that $\vec{V}_2 e^{-\alpha x} e^{-j\beta x}$ is a wave traveling from the receiving end to the source end.

The total voltage on a transmission line can be described as the sum of two traveling waves, one traveling from the sending end to the receiving end, called the incident wave, and the other traveling from the receiving end to the sending end, called the reflected wave.

Velocity and Wavelength

The traveling waves have a velocity of propagation and a wavelength. The wavelength, λ, which is the value of x when βx equals 2π in $\vec{V}_1 e^{\alpha x} e^{j\beta x}$ is given by $\lambda = 2\pi/\beta$. The velocity of propagation of the wave is

$$\upsilon = \lambda f \tag{3.20}$$

Substituting for wavelength in this equation provides

$$\begin{aligned} \upsilon &= \frac{2\pi}{\beta} f \\ &= \frac{\omega}{\beta}. \end{aligned} \tag{3.21}$$

On overhead lines, the velocity of traveling waves is close to the velocity of light.

3.3 Points of Discontinuity

When voltage and current waves travel on a line, they encounter discontinuities where reflections take place. The relation between the reflected wave and the incident wave depends on the nature of the discontinuity. The behaviour of the traveling waves at the discontinuities is described in this section. The ratio of the incident wave and

reflected wave at a discontinuity is called the reflection factor. If a transmission line is terminated in a load of impedance Z_r,

$$\frac{\vec{V}_r}{\vec{I}_r} = Z_r. \tag{3.22}$$

The receiving end voltage and current are given by

$$\vec{V}_r = \vec{V}_1 + \vec{V}_2 \quad \text{and} \tag{3.23a}$$

$$\vec{I}_r = \vec{I}_1 + \vec{I}_2 \tag{3.23b}$$

Substituting Equations 3.23(a) and 3.23(b) in Equation 3.22 gives

$$\frac{\vec{V}_1 + \vec{V}_2}{\vec{I}_1 + \vec{I}_2} = Z_r \tag{3.24}$$

Substituting for $\vec{I}_1$ and $\vec{I}_2$ from Equations 3.16 and 3.17 and rearranging provides

$$Z_0 \frac{\vec{V}_1 + \vec{V}_2}{\vec{V}_1 - \vec{V}_2} = Z_r$$

Rearranging this equation provides

$$\frac{\vec{V}_2}{\vec{V}_1} = \frac{Z_r - Z_0}{Z_r + Z_0} \tag{3.25}$$

This is the voltage reflection factor, ρ_v, that can be written as

$$\rho_v = \frac{1 - \frac{Z_0}{Z_r}}{1 + \frac{Z_0}{Z_r}} \tag{3.26a}$$

$$= \frac{\frac{Z_r}{Z_0} - 1}{\frac{Z_r}{Z_0} + 1} \tag{3.26b}$$

Similarly the current reflection factor, ρ_i, is given by

$$\rho_i = -\frac{1 - \frac{Z_0}{Z_r}}{1 + \frac{Z_0}{Z_r}} \tag{3.27a}$$

$$= -\frac{\frac{Z_r}{Z_0} - 1}{\frac{Z_r}{Z_0} + 1} \qquad (3.27b)$$

Because Z_0 is predominantly resistive and if Z_r is also predominantly resistive, the reflection factor is not numerically greater than one. The reflected wave, therefore, is not greater than the incident wave in power systems

Open-Circuited Line

When a line is open circuited at the receiving end, Z_r is equal to infinity. Substituting $\propto$ for Z_r in Equations 3.26(a) and 3.27(a)

$$\rho_v = 1$$

$$\rho_i = -1.$$

The voltage phasors of the incident and reflected waves at the receiving end of an open-circuited line are equal and, therefore, the instantaneous values are equal. The current phasors of the incident and reflected waves are equal in magnitude but 180^0 out of phase. The instantaneous value of the reflected current wave is, therefore, equal to the instantaneous value of the incident wave but is opposite in sign.

Short-Circuited Line

When a line is short circuited, Z_r is equal to zero. Substituting 0 for Z_r in Equations 3.26(b) and 3.27(b)

$$\rho_v = -1$$

$$\rho_i = 1.$$

The voltage phasors of the incident and reflected waves are equal in magnitude but 180^0 out of phase. The instantaneous value of the reflected voltage wave is, therefore, equal to the instantaneous value of the incident wave but is opposite in sign. The current phasors of the incident and reflected waves at the receiving end of a short-circuited line are equal and, therefore, the instantaneous values are equal.

Line Terminated in Z_0

When a line is terminated in an impedance equal to the surge impedance of the line, Equations 3.26(a) and 3.27(a) provide

$$\rho_v = 0$$

$$\rho_i = 0.$$

There are no reflections and, therefore, no reflected waves are produced.

3.3.1 Junction of Three Lines

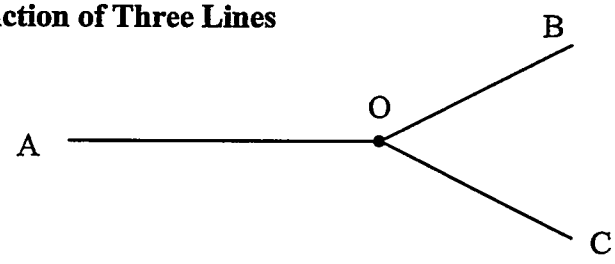

Figure 3.3: Junction of three lines

Consider a junction of three lines A, B and C as shown in Figure 3.3. Let the surge impedances of lines A, B and C be Z_{A0}, Z_{B0} and Z_{C0} respectively. Consider that the voltage and current waves, V_{1A} and I_{1A}, on line A are traveling towards the junction O. On arriving at the junction O, the traveling waves encounter a load that is equal to the parallel combination of the surge impedances of the lines OB and OC. Let the parallel combination of the two surge impedances be Z_{P0}.

The reflected voltage and current waves, V_{2A} and I_{2A}, on line A are given by

$$\begin{aligned} V_{2A} &= V_{1A}\rho_v \\ &= V_{1A}\frac{Z_{P0} - Z_{A0}}{Z_{P0} + Z_{A0}} \\ I_{2A} &= I_{1A}\rho_i \\ &= -I_{1A}\frac{Z_{P0} - Z_{A0}}{Z_{P0} + Z_{A0}}. \end{aligned}$$

The voltage at O on the arrival of the traveling wave becomes

$$V = V_{1A} + \rho_v V_{1A}$$

The transmitted voltages waves on the lines OB and OC are of a magnitude equal to V. The current traveling wave on line OB is given by

$$I_{OB} = \frac{V}{Z_{B0}}$$
$$= \frac{V_{1A} + \rho_v V_{1A}}{Z_{B0}}.$$

Similarly, the current traveling wave on line OC is given by

$$I_{OC} = \frac{V}{Z_{C0}}$$
$$= \frac{V_{1A} + \rho_v V_{1A}}{Z_{C0}}.$$

Consider the system shown in Figure 3.4 that includes two transmission lines T_{r1} and T_{r2} terminating at Bus-C and a line, T_{r3} connecting Bus-C to Bus-D. The surge impedance of line T_{r1} is Z_{01} and it is connected to a source whose impedance is equal to the surge impedance of line T_{r1}. The surge impedance of line T_{r2} is Z_{02} and it terminates at an impedance of Z_{g2}. Consider that a fault occurs at location F at time t_0.

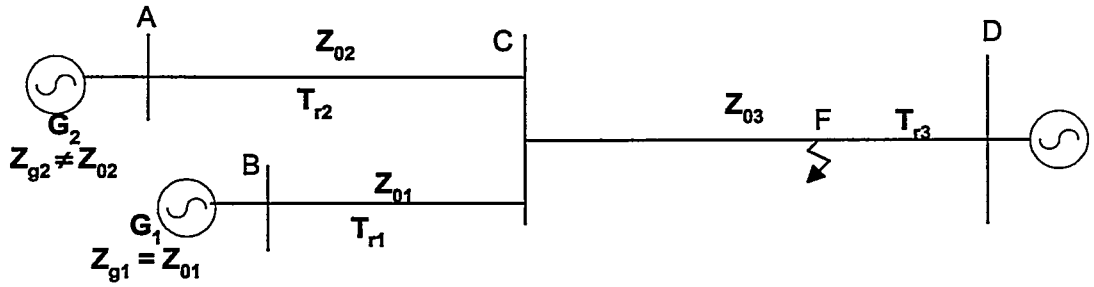

Figure 3.4: Junction of three lines

The following incidents occur on the inception of the fault

- Traveling wave V_2 originates at location F at time t_0.
- The wave travels from F to C and reaches Bus-C at time t_1.
- At Bus-C, part of the wave is transmitted to lines T_{r1} and T_{r2} and a part is reflected towards the fault location F.

- The reflected wave reaches the fault at time t_3 and is reflected back from there.
- The waves transmitted to line T_{r1} reach Bus-B at time t_2. No reflection is produced because the line is terminated in its surge impedance.
- The wave transmitted on line T_{r2} reaches Bus-A at time t_4; part of this wave is reflected.
- The wave reflected from Bus-A travels on line T_{r2} and reaches Bus-C at time t_7.
- These processes continues until the traveling waves attenuates to zero

The phenomenon of traveling waves is usually described by a lattice diagram [19]. The lattice diagram for the system shown in Figure 3.4 is displayed in Figure 3.5.

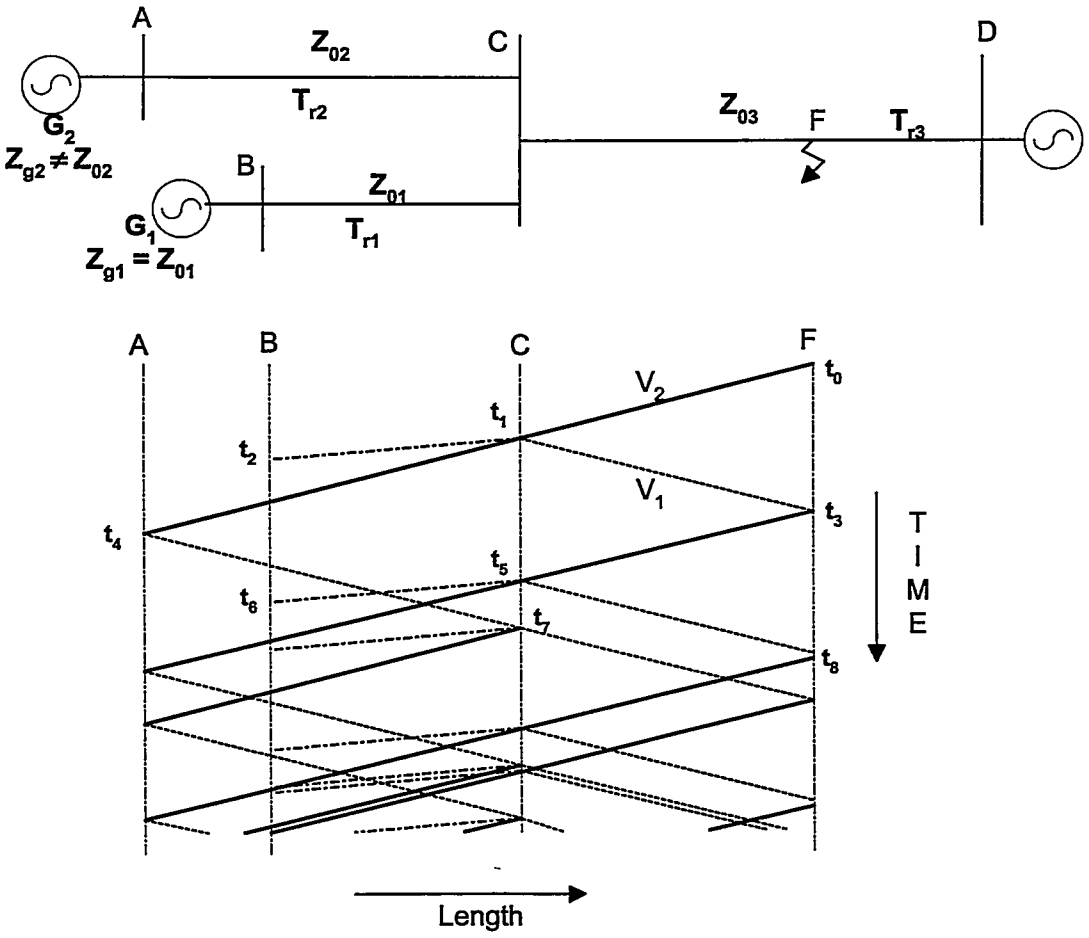

Figure 3.5: Lattice diagram showing traveling waves

In this lattice diagram, the horizontal distance represents length along the line and the vertical distance represents time. The magnitude of the slope of the lines is the inverse of the velocity. While this is a useful technique for studying traveling waves on a line, it is not practical for analysing traveling waves on complex networks.

3.4 Physical Interpretation of Traveling Waves

Each element of length Δx shown in Figure 3.2 consists of a shunt capacitance, a shunt conductance, a series inductance and a series resistance. When a voltage is applied to one end of the line, the capacitor of the first element gets charged to the applied voltage [6]. The first inductor causes a delay and the second capacitor is charged after a small time delay. Similarly the second inductor delays the charging of the third capacitor. The farther away the capacitor is from the line terminal more is the delay in charging of the capacitor. If the applied voltage is an impulse function, the voltages on the intermediate capacitors are also impulse functions occurring with delays. This can be interpreted as the applied impulse propagating on the line in the form of a traveling wave.

In a power system a sinusoidal voltage produced by an ac generator is applied at the sending end of the transmission line. This voltage propagates on the line toward the receiving end as a traveling wave. This wave reaches various points along the line after some delays, which are proportional to the distance from the generator. The consequence is that the amplitude of the wave becomes smaller as it arrives at locations that are farther from the source. The traveling wave phenomenon in this manner, manifests in the voltage reducing and phase angle becoming more lagging as the wave arrives at locations that are farther from the source end.

3.5 Traveling Wave Relays

No numerical traveling wave relay has been proposed in the past. All the traveling wave relays proposed in the past use analog technologies. Some of the previously proposed traveling wave relays are described in this section. Some basic equations, which are common to all the relays, are first presented.

The wave equations for voltage $v(x,t)$ and current $i(x,t)$, are given by [2]

$$v(x,t) = F_1(x - \upsilon t) + F_2(x + \upsilon t)$$

$$i(x,t) = [F_1(x - \upsilon t) - F_2(x + \upsilon t)] / Z_0 \qquad (3.27)$$

where,

F_1 and F_2 are functions of distance and time.

If the voltage and current are measured at location x, then F_1 and F_2 can be determined by

$$v(x,t) + Z_0\, i(x,t) = 2F_1(x - \upsilon t)$$

$$v(x,t) - Z_0\, i(x,t) = 2F_2(x + \upsilon t) \qquad (3.28)$$

If measurements are taken at $x = 0$, traveling waves can be determined by

$$S_1 = v(0,t) + Z_0\, i(0,t) = 2F_1(0 - \upsilon t) \qquad (3.29a)$$

$$S_2 = v(0,t) - Z_0\, i(0,t) = 2F_2(0 + \upsilon t) \qquad (3.29b)$$

S_1 represents the signal changes at the relaying point due to the forward traveling waves and S_2 represents signal changes due to backward traveling waves.

Let

v and i be the post fault voltage and current, and
v' and i' be the pre fault voltage and current.

Then the changes in voltage and current Δv and Δi are given by

$$\Delta v = v - v'$$

$$\Delta i = i - i' \qquad (3.30)$$

Since v' and i' represent the pre fault quantities, they are only power frequency components and therefore Δv and Δi contain the transient components like traveling waves and the difference between the pre-fault and the post-fault power frequency components.

The incremental signals Δv and Δi are measured by subtracting the instantaneous values observed during the previous cycle from the instantaneous values observed during the present cycle. Figure 3.6 gives the block diagram for the method used to derive the incremental signal. Traveling wave relays use the incremental signal to identify faults.

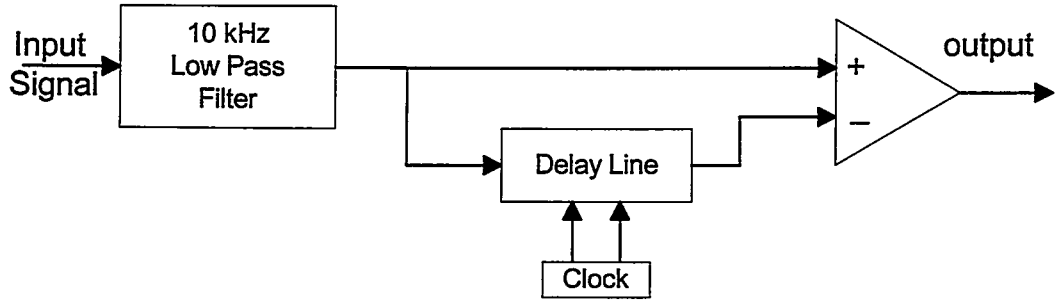

Figure 3.6: Derivation of incremental voltage

Two traveling wave relays, previously proposed in literature are briefly described in this section.

3.5.1 The Chamia, Liberman Algorithm

Chamia and Liberman [13] proposed an algorithm that achieves directional discrimination by comparing the polarity of Δi and Δv directly after fault inception. Consider the system in Figure 3.9.

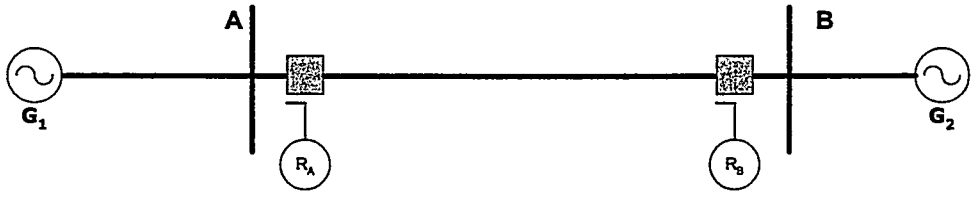

Figure 3.7: A simple power system model

If the pre-fault voltage is positive and a fault occurs on the line, Δi is positive and Δv is negative, at the relays R_A and R_B, when the traveling waves arrive at the relays. If the pre-fault voltage is negative, Δi is negative and Δv is positive at the relays R_A and R_B, when the traveling waves arrive at the relays.

If a fault is on the bus-side of R_A and the pre-fault voltage is positive, Δi and Δv are negative at relay R_A, when the traveling waves arrive at the relay. At relay R_B, Δv is negative but Δi is positive when the traveling waves arrive at the relay. If a fault is on the bus-side of R_A and the pre-fault voltage is negative, Δi and Δv are positive at relay R_A, when the traveling waves arrive at the relay. At relay R_B, Δv is positive but Δi is negative when the traveling waves arrive at the relay.

It can be concluded that, for an internal fault, the current and voltage at both terminals are of opposite signs but, for external faults, the current and voltage changes are of the same sign at one of the terminals.

3.5.2. Crossley and McLaren Algorithm

The relay proposed by Crossley and McLaren [14] estimates the distance of the fault from the line terminal. If the estimated distance is less than the setting of the relay, a trip signal is produced.

This algorithm uses the time taken by a wave to travel from the line terminal to the fault and back. The time T between similar changes in the signals S_2 and S_1, defined in Equation 3.29, provide the distance to the fault, X_F, as follows.

$$X_F = \frac{T}{2}\upsilon .$$

The signals defined in Equations 3.29(a) and 3.29(b) are correlated to recognise the wave returning from the fault and distinguish it from other traveling waves present on the system. The following cross-correlation function, which gives the correlation between a signal x and a delayed signal y, is used.

$$\Phi xy(\tau) = \frac{1}{N}\sum_{k=1}^{N} x(k\Delta t + \tau)\cdot y(k\Delta t)$$

where,

τ is the delay.

The correlator output is maximum when the two signals are similar.

3.6 Summary

The theory of propagation of traveling waves on transmission lines has been introduced in this chapter. Equations describing the traveling waves have been derived. The behaviours of traveling waves for different line terminations have been outlined. The traveling wave relays proposed in the past have been reviewed in this chapter.

Chapter 4

Proposed High-Speed Relays

4.1 Introduction

The concept of traveling waves has been introduced in the previous chapter. These waves start immediately after the inception of a fault and last for a few milliseconds only.

Two techniques for extracting information from these waves are proposed. The first technique extracts information at a terminal of the protected line and determines if the fault, which caused the traveling waves, is on the protected line. One relay of this design would be required at each terminal of the line. The second technique extracts information from both terminals of the line and uses a communication channel, between the two terminals, to determine if the fault is on the line or not. The techniques are used in designing high-speed relays.

4.2 First Differences

The proposed techniques use the first differences for extracting information on traveling waves from voltages and currents observed at the line terminals. A brief description of first differences [11] is, therefore, provided in this section.

The first difference of a signal v is defined by

$$\Delta v_k = v_{k+\frac{1}{2}} - v_{k-\frac{1}{2}} \qquad (4.1)$$

where,

$v_{k+\frac{1}{2}}$ is the value of v at $\left(k+\frac{1}{2}\right)\Delta T$ seconds, and

$v_{k-\frac{1}{2}}$ is the value of v at $\left(k-\frac{1}{2}\right)\Delta T$ seconds.

4.2.1 Extraction of Traveling Waves using First Differences

The arrival of traveling waves at the relay location is indicated by a step change in a voltage as shown in Figure 4.1. The first differences obtained by using Equation 4.1 are shown in Figure 4.2. A perusal of this figure shows that sharp spikes are produced at the instants when there are step changes in the voltages shown in Figure 4.1.

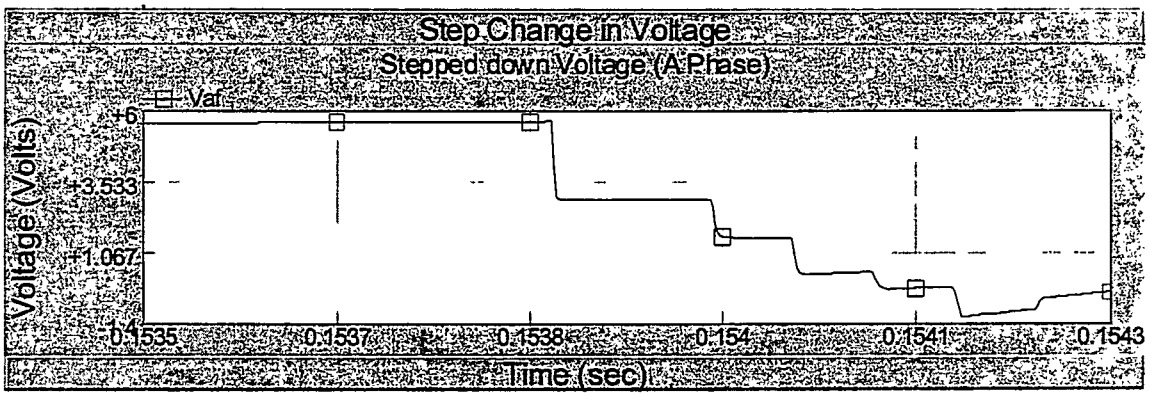

Figure 4.1: Step change in the input voltage signal

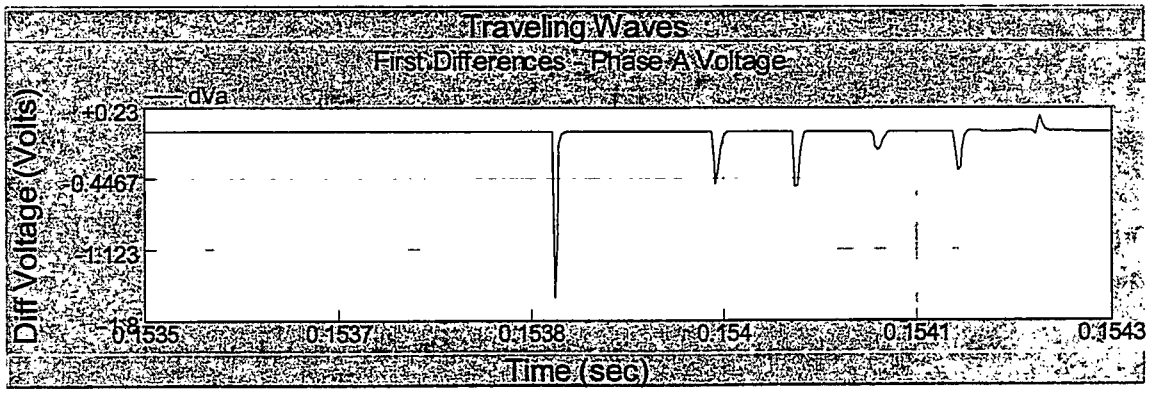

Figure 4.2: The difference equation output showing the spikes

4.2.2 Frequency Response of the First Differences

The frequency response of the first differences can be determined as follows.

Taking the z-transform of Equation 4.1 provides

$$H(z) = z^{\frac{1}{2}} - z^{-\frac{1}{2}} \tag{4.2}$$

where,

$H(z)$ is the transfer function representing the first differences.

Replacing z by $e^{j\omega\Delta T}$ provides the following transfer function in the radian-frequency domain.

$$\begin{aligned} H(\omega) &= e^{\frac{j\omega\Delta T}{2}} - e^{-\frac{j\omega\Delta T}{2}} \\ &= j2\sin\left(\omega\frac{\Delta T}{2}\right). \end{aligned} \tag{4.3}$$

For a given sampling frequency, ΔT is known. The frequency response can be obtained by assigning different values to ω. Figure 4.3 shows the frequency response of the first differences for a sampling frequency of 500 kHz. The figure shows that the first differences suppress the power frequencies but pass the high frequencies through.

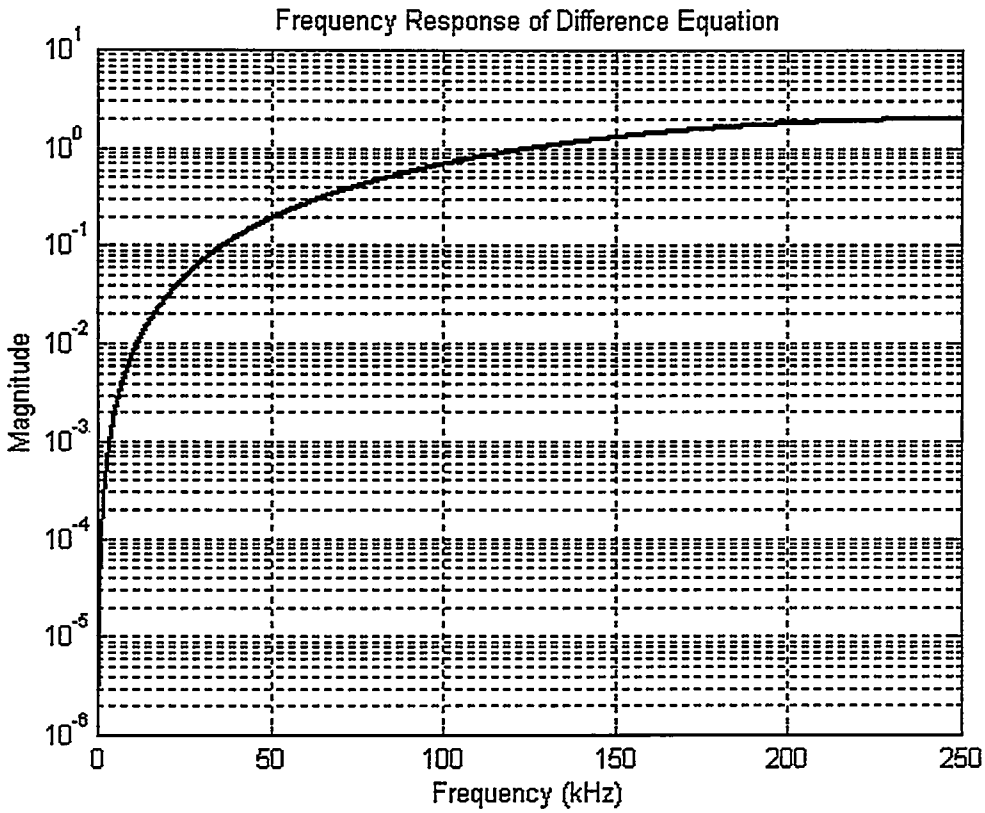

Figure 4.3: Frequency response of the first order difference equation filter

4.3 Line Protection Requirements

Consider the system shown in Figure 4.4 in which line A-B is to be protected. Also consider that a relay is provided at each terminal as shown in the figure. A fault on the bus side of relay R_A, at location F_1 is outside the protected zone. Similarly, a fault on the bus-side of relay R_B, at location F_2, is outside the protected zone. A fault on the line A-B is in the line-protection zone and both relays, R_A and R_B, should operate.

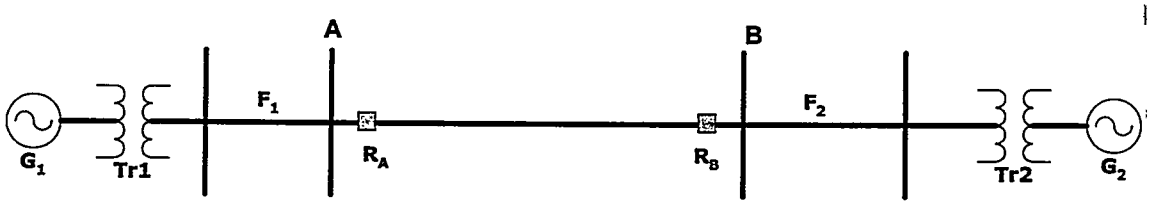

Figure 4.4: A system to be protected

Two techniques for detecting line faults from information on traveling waves are presented in Sections 4.4 and 4.5.

4.4 Single-ended Technique

This technique uses currents and voltages from the local terminal of the line only. Consider a fault at F on the protected line A-B as shown in Figure 4.5.

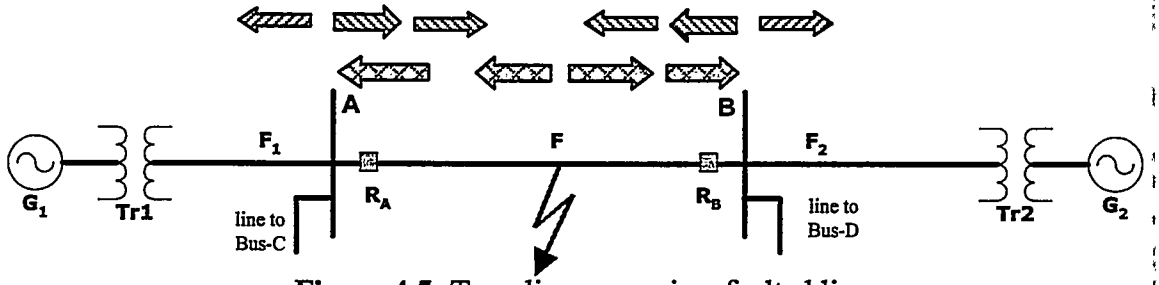

Figure 4.5: Traveling waves in a faulted line

The incidence of the fault starts voltage and current traveling waves. A voltage traveling wave, and its associated current wave start from F and travel toward the line terminal A. A few microseconds after inception, the waves arrive at Bus-A (and relay R_A). A fraction of the voltage wave and a fraction of the current wave are reflected from Bus-A. These reflected waves travel to the fault from where they are again reflected. A few microseconds later these waves arrive at Bus-A (and Relay R_A). The time (T_A μs)

between the instants at which the first and the second set of waves arrive at Bus-A is proportional to twice the distance between the fault and Bus-A. Hence the distance between the Bus-A and the fault can be calculated by,

$$x_A = \frac{\upsilon T_A}{2} \tag{4.4}$$

where,

υ is the velocity of the traveling wave in m/μs, and
x_A is the distance between the fault and the relay in m.

The faults on the line can be detected by comparing the calculated value of x and the line length.

Another voltage traveling wave, and its associated current wave start from F and travel toward the line terminal B. A few microseconds after inception, the waves arrive at Bus-B (and relay R_B). A fraction of the voltage wave and a fraction of the current wave are reflected from Bus-B. These reflected waves travel to the fault from where they are again reflected. A few microseconds later these waves arrive at Bus-B (and Relay R_B). The time (T_B μs) between the instants at which the first and the second set of waves arrive at Bus-B is proportional to twice the distance between the fault and Bus-B. Hence the distance between the Bus-B and the fault can be calculated by,

$$x_B = \frac{\upsilon T_B}{2} \tag{4.4}$$

where,

υ is the velocity of the traveling wave in m/μs, and
x_B is the distance between the fault and the relay in m.

When the fault is on the protected zone, or beyond the remote bus, the voltage and current traveling waves arriving at the line terminal are of opposite polarities as shown in Figure 4.6. When a fault is on the bus-side of the relay, the voltage and current traveling waves are of the same polarities as shown in Figure 4.7. This fact is used to differentiate between the bus-side faults and the line-side faults.

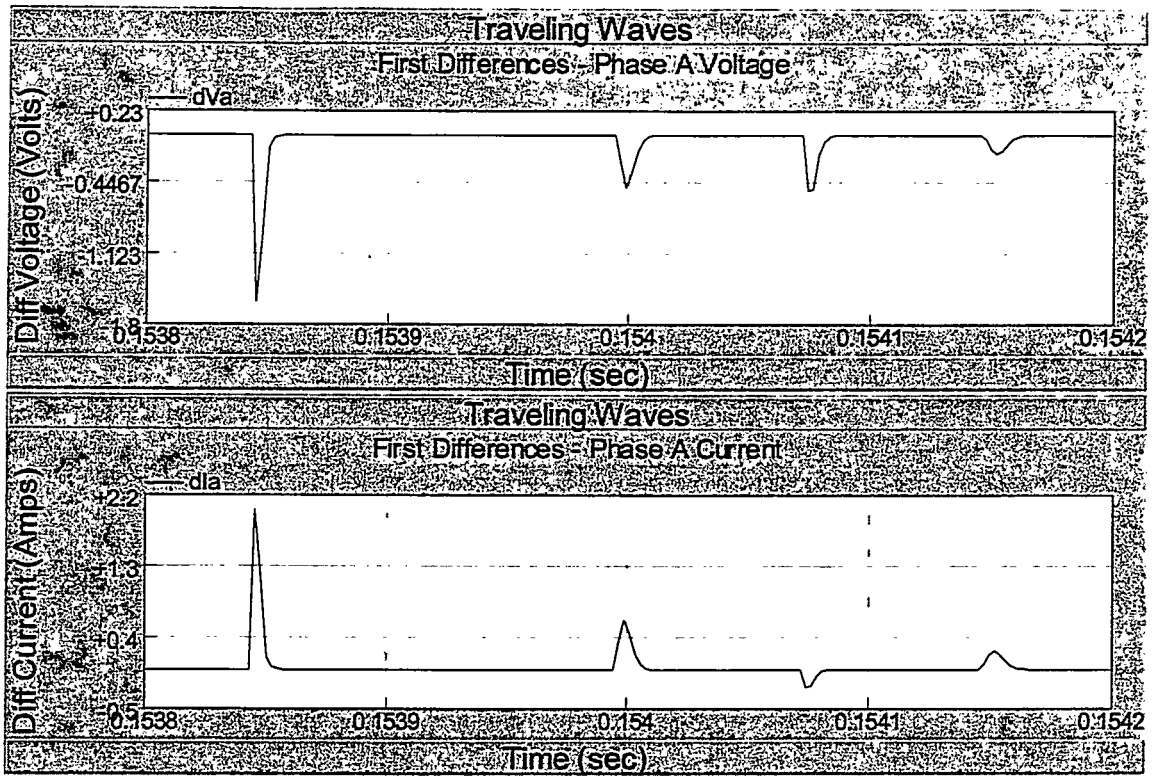

Figure 4.6: Fault in the protected zone; the spikes have opposite signs

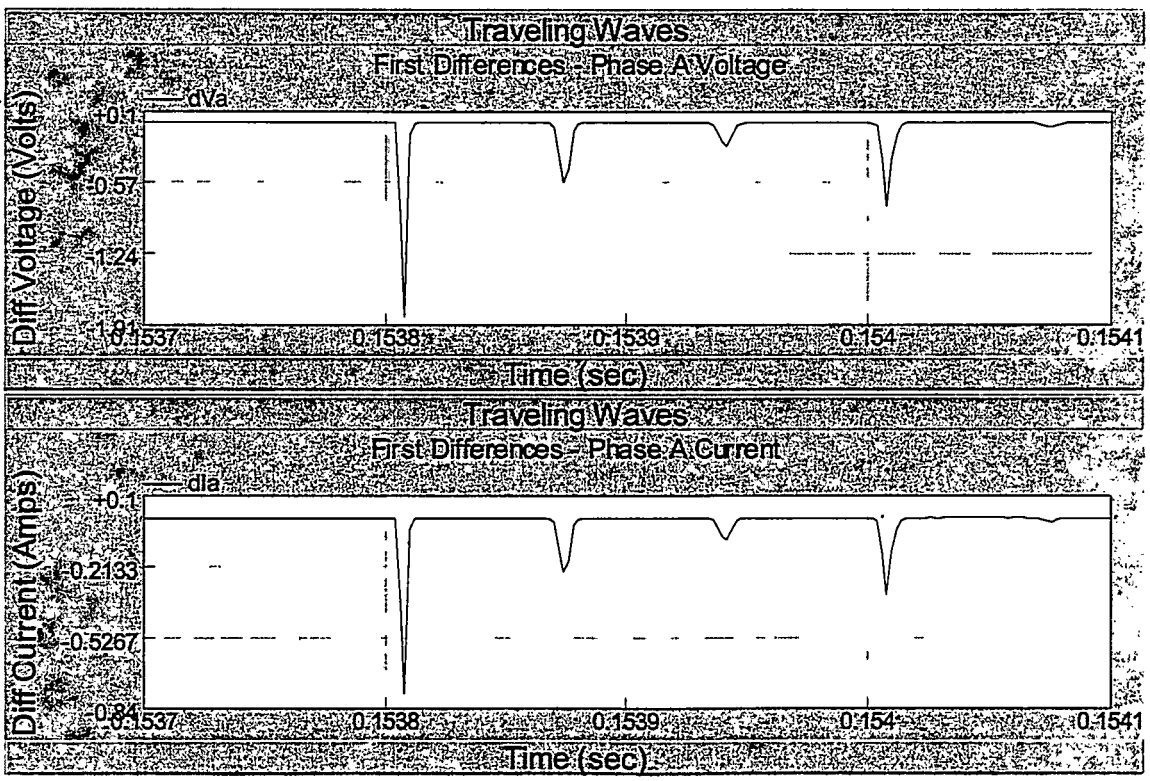

Figure 4.7: Fault on the bus-side; the spikes have same sign

4.4.1 The Algorithm

The relay algorithm consists of the following steps.

1. Apply the difference equation on the input current and voltage waveforms. The difference equation gives "spike" outputs when there are step changes in the input.
2. Detect the spikes.
3. When the spikes appear, compare the direction of the current and the voltage spikes.
4. If the signs are the same, then ignore it since it is a bus-side fault.
5. If the signs are opposite, then start a counter.
6. Detect the reflected waveform. These are the set of spikes with the same signs as the incident spikes.
7. Stop the counter when the reflected spikes are detected.
8. From value of the counter (time) calculate the distance.
9. If the distance is less than the relay setting then it is an internal fault.
10. Else it is an external fault.

The implementation of this algorithm is illustrated in the flowchart given in Figure 4.8.

4.4.2 Features of the Single-ended Technique

This technique can differentiate between the bus-side and internal faults as well as between the remote-end and internal faults. Very few calculations are required and the time taken to detect a fault is minimal. If the velocity of propagation is 3×10^8 m/s (the velocity of light in free-space), on a 100 km over-head line, the time, T_{2L}, taken by the waves for traveling from one terminal to the other and back is given by

$$T_{2L} = \frac{200 \times 10^3}{3 \times 10^8} = 0.67 \quad ms.$$

Assuming a 2 ms overhead, the operating time of the relay would be less than 3 ms. No communication channel is required between the two terminals when this technique is used.

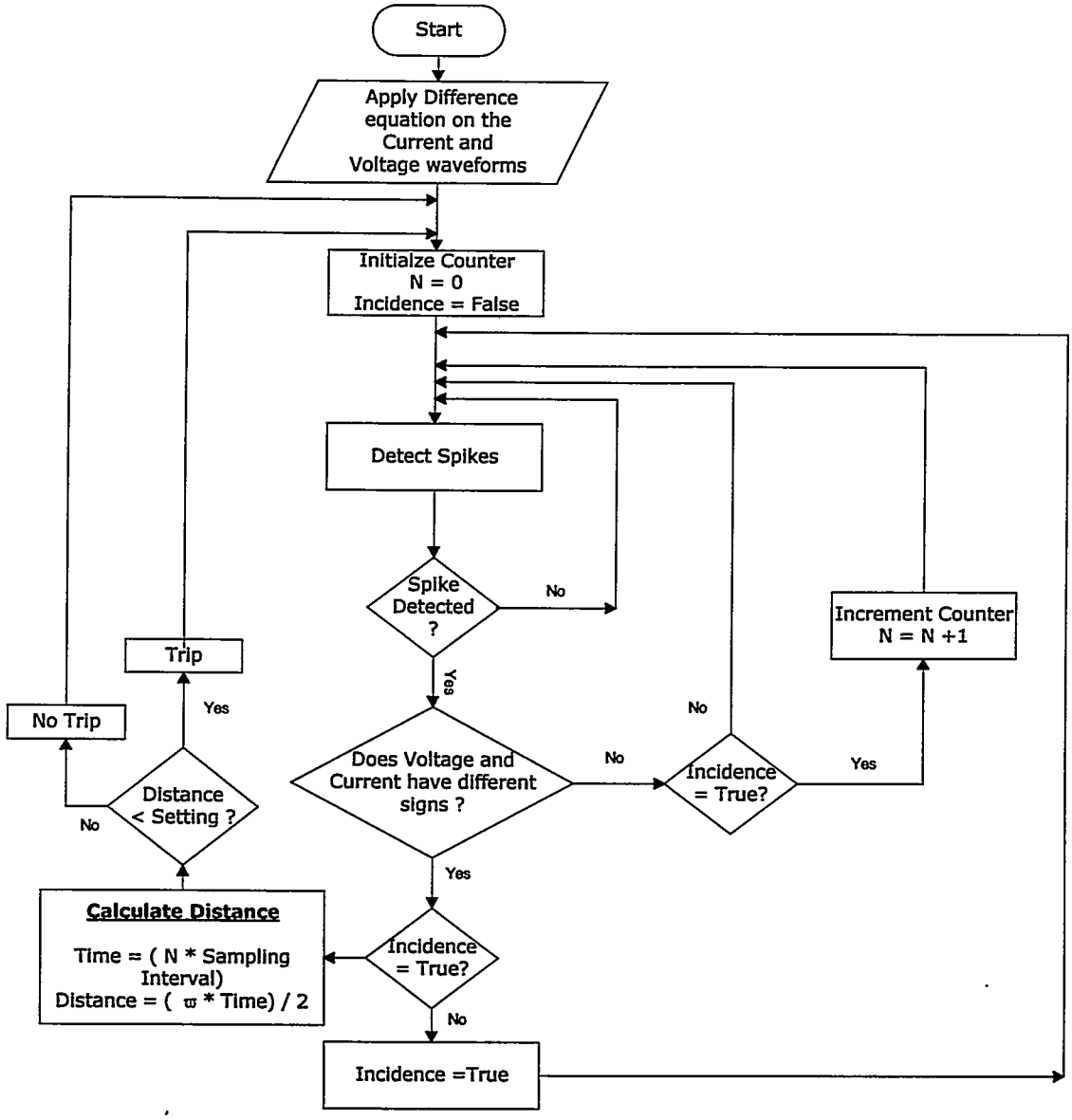

Figure 4.8: Flowchart for the single-ended technique

4.5 Double-ended Technique

This technique uses the currents and voltages from the local terminal of the line and information from the remote terminal of the line. For the relay to receive information from the remote terminal, a communication channel between the two terminals of the line is required. Figure 4.9 shows a typical arrangement for implementing this technique.

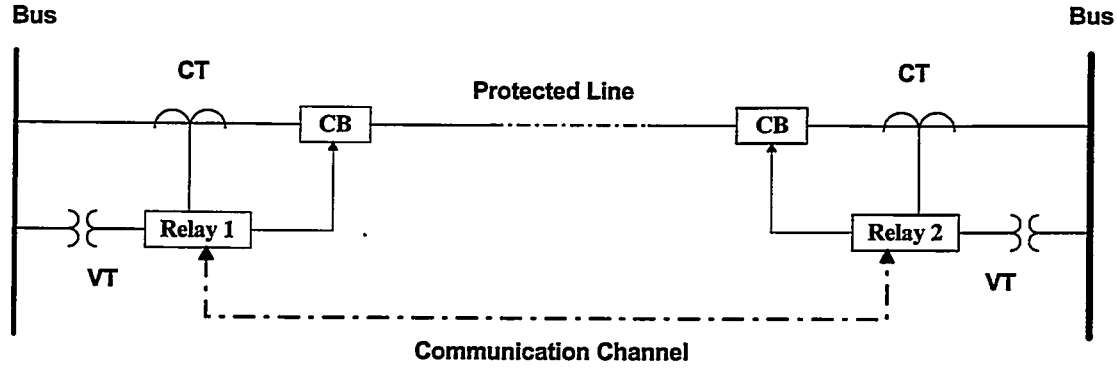

CT - Current Transformer
VT - Voltage Transformer
CB - Circuit Breaker

Figure 4.9: A typical arrangement of two-ended relays for implementing the technique

Consider the system shown in Figure 4.10 in which

T is the time taken by a wave to travel from one end of the line to the other,
T_1 is the time at which the wave is detected by relay R_A, and
T_2 is the time at which the wave is detected by relay R_B.

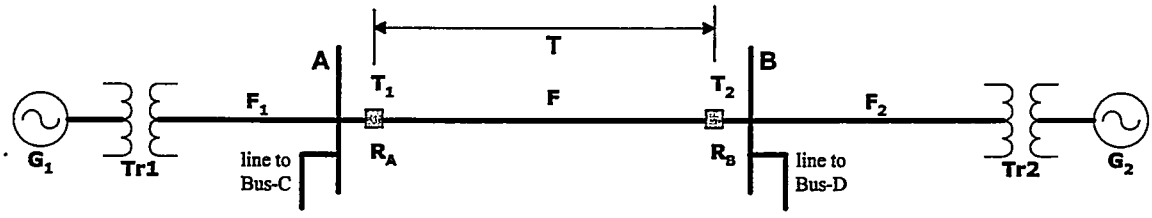

Figure 4.10: A two machine and interconnecting line model of a power system

When a fault occurs at location F on line AB, the difference between the instants of time at which the traveling waves are detected by relays R_A and R_B, is less than or equal to T.

$$|T_1 - T_2| \leq T \tag{4.5}$$

When a fault is outside the line AB, at location F_1 or F_2, the difference between the instants of time at which the traveling waves are detected by relays R_A and R_B, is equal to T.

$$|T_1 - T_2| = T \tag{4.6}$$

This fact is used to differentiate between the internal faults and the external faults.

4.5.1 Time Stamping

It is essential that the data acquired by relays provided at the two line terminals should be time-stamped using synchronized clocks. This can be achieved by using the Global Positioning System (GPS) that consists of 24 satellites, with four satellites in each of the six orbits at an altitude of 17,538 km [3]. The satellites provide 1 pulse-per-second (1 pps) that can be received at any location in the world with an accuracy of about 1 μs when decoded with appropriate receivers. The format proposed in the IEEE standard 1344 can be used for time-stamping the voltage and current samples acquired by the relays [17].

4.5.2 The Algorithm

The relay algorithm consists of the following steps.

1. Both the ends of the line are continuously time stamped.
2. Apply the difference equation on the input current and voltage waveforms. The difference equation gives "spike" outputs when there are step changes in the input.
3. Detect the spikes.
4. When the spikes appear, note the time and send it to the other end.
5. Wait for time from the other end.
6. Find the difference of the two time-stamps.
7. Check if it is less then the maximum time T.
8. If yes, give trip signal. Else no trip.

The implementation of this algorithm is illustrated in the flowchart given in Figure 4.11.

4.5.3 Features of the Double-ended Technique

This technique can differentiate between the bus-side faults and internal faults as well as between the remote-end and internal faults. Very few calculations are required and the time taken to detect a fault is minimal. If the velocity of propagation is 3×10^8 m/s, on a 100 km line, the time, T_{1L}, taken by the waves for traveling from one terminal to the other is given by

$$T_{1L} = \frac{100 \times 10^3}{3 \times 10^8} = 0.33 \quad ms$$

Assuming a 2 ms communication delay and a 2 ms overhead, the operating time of the relay would be less than 5 ms.

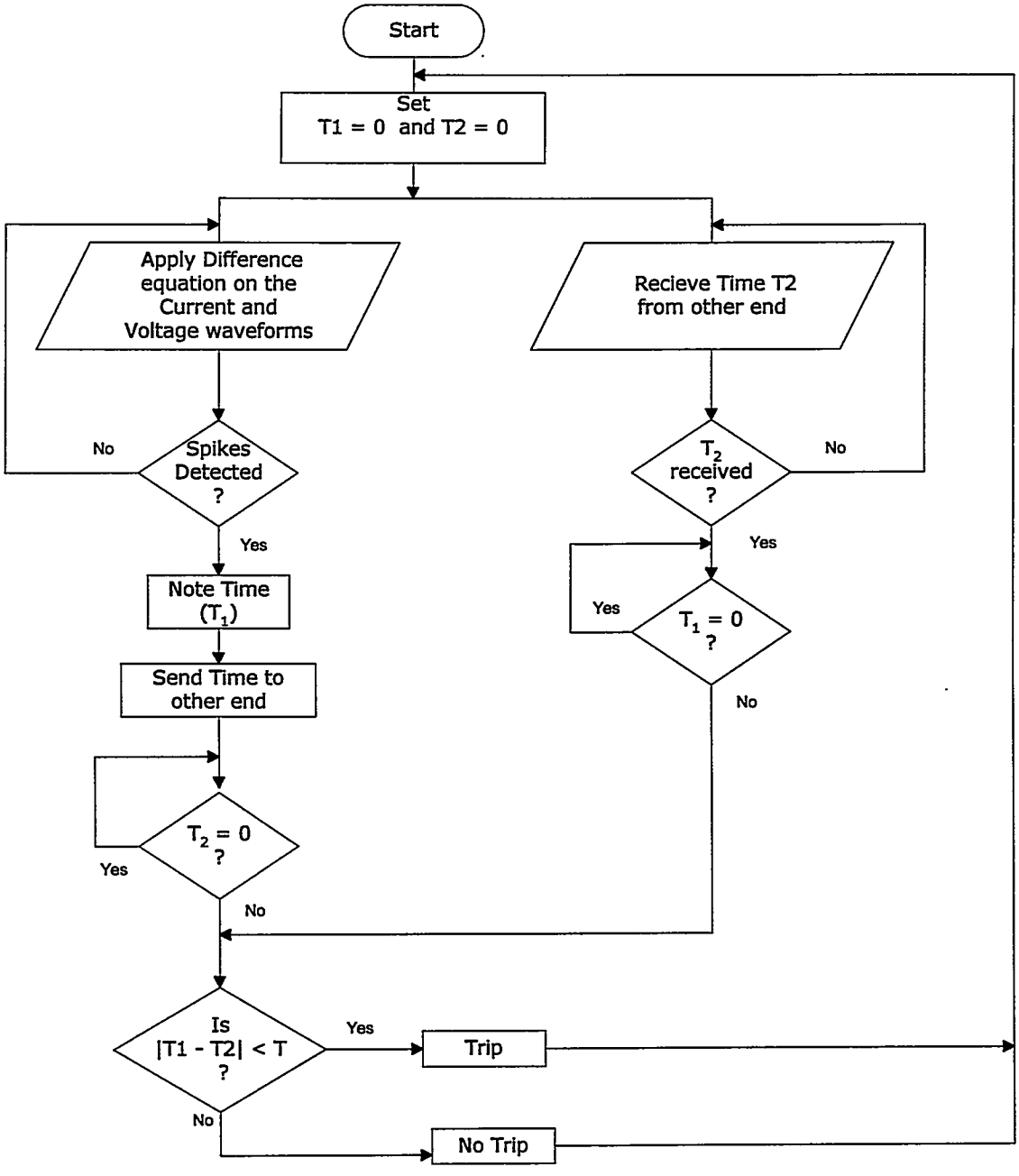

Figure 4.11: Flowchart for the double-ended technique

4.6 Summary

Two high-speed relaying techniques have been explained in this chapter. Both techniques acquire the voltages and currents from the power system, apply the first differences to the data, extract the traveling waves and make trip decisions based on the information contained in the waves. Both relays have operating times of less than 5 ms.

Chapter 5

Simulation Studies

5.1 Introduction

Two high-speed relaying techniques for detecting transmission line faults have been proposed in Chapter 4. The basis of fault-detection has also been presented in that chapter.

The two techniques were tested using data generated by simulating an eight-bus power system using EMTDC, an electromagnetic transient analysis program. The fault-resistance, fault-inception-angle and the presence of wave traps were included in some simulations. The hardware constraints were also modelled. Data representing different types of faults at different locations were obtained from the simulations. The data was then used to test the performance of the techniques during system disturbances. Some details of the simulations and results from the performance-tests are presented in this chapter.

5.2 System Modeling and Data Processing

Data were generated on a PC using the EMTDC; an overview of the EMTDC is given in Appendix A. Details on modeling components, such as resistors, inductors, generators are available in Reference 18. The eight-bus power system, shown in Figure 5.1, was modeled for generating the fault data. The proposed relaying techniques were also modelled.

5.2.1 Eight-Bus Power System

This system consists of eight buses connected by seven 500 kV transmission lines. The protected line, T_{rl}, is 160 km long and connects Bus-1 to Bus-2; Relay1 is provided at the Bus1 terminal of the line and Relay2 is provided at the Bus2 terminal of the line. The transmission line, T_{r2}, connects Bus-1 to Bus-3 to which generator S_2 is connected. The line T_{r3} connects Bus-1 to Bus-4 to which generator S_1 is connected. The load L_1 is connected to Bus-5, which is connected to Bus-1 through line T_{r4}. The three transmission lines, T_{r5}, T_{r6} and T_{r7}, connect Bus-2 to Buses 6, 7 and 8 respectively. The load L_2 is connected to Bus-6 and load L_3 is connected to Bus-8. The motor M is connected to Bus-7. The parameters of all the components are given in Appendix B. The models of different parts of the system developed in the EMTDC are shown in Figures 5.2 to 5.8. Models of VTs of ratio $288.7kV:63.5V$ reduced the levels of the three phase-voltages. Models of CTs of ratio $1500:5A$ reduced the levels of the three phase-currents. The outputs of the VTs and CTs were used by the relay models.

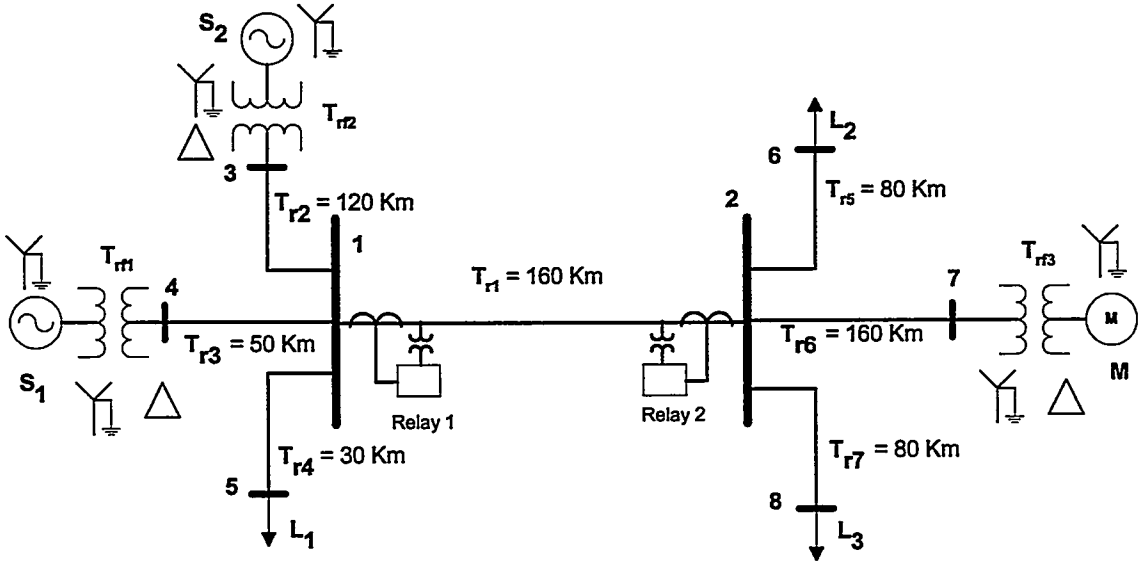

Figure 5.1: Single line diagram of the system-model used for generating fault data

5.2.2 Relay Model

The relay model used in this project includes the data acquisition system (DAS) that consists of auxiliary transformers and analog to digital (A/D) converters. It also includes models of the protection techniques.

5.2.2.1 Data Acquisition System Model

The DAS model is shown in Figure 5.9. The auxiliary VTs step down the voltages by a factor of 8.98. The auxiliary CTs of ratio 20 : 1 and their outputs applied to one-ohm resistors convert the currents to equivalent voltages.

The A/D converter model samples the outputs of VTs and current to voltage converters. In the EMTDC, these samples are floating-point numbers that are converted by the A/D converter model to equivalent integers. The conversion formulae that were used are

$$V_{Dig} = Round\left[2^{n-1} + \frac{Vin\ (2^{n-1}-1)}{V_{AD}}\right] \quad \text{For } Vin \geq 0 \tag{5.1a}$$

$$V_{Dig} = Round\left[\frac{(V_{AD} - |Vin|)2^{n-1}}{V_{AD}}\right] \quad \text{For } Vin < 0 \tag{5.1b}$$

where,

V_{in} is the input floating point value,
V_{AD} is the input range (from $-V_{AD}$ to $+V_{AD}$),
n is the number of bits, and
V_{Dig} is the integer output.

The negative values are converted to integers from 0 to 2^{n-1} and the positive values are converted to integers from $(2^{n-1}+1)$ to (2^n-1). The outputs of the A/D converter-model range from zero to (2^n-1). To extract the AC signals from the outputs of the A/D converter model, 2^{n-1} was subtracted from the numbers provided by the formulae given in Equation 5.1.

5.2.2.2 Protection Techniques Model

The flowcharts shown in Figures 4.8 and 4.11 were implemented in the model shown in Figure 5.10.

5.2.3 Communication Channel

The communication channel required for the second technique was not modelled.

5.2.4 Additional Information

Detailed descriptions of the parameters of the DAS and protection-technique models are given in Appendix C. The FORTRAN code for implementing the algorithms is also given in that Appendix.

5.3 Test Studies

Faults were simulated on all the seven transmission lines of the system shown in Figure 5.1. Two hundred and eighty nine studies, listed in Tables 5.1 to 5.3, were conducted. The parameters that were varied are the fault-type, fault-location, fault-resistance, fault-inception-angle, sampling-frequency and A/D converter resolution. The impacts of these changes on both the techniques were evaluated. All distances to the faults, referred in this chapter, are from Relay1.

The cases listed in Table 5.1 were simulated using the calculation steps of 2 μs. The fault resistance was 1 Ω and the A/D converter resolution was 16 bits. Fault types and fault locations were varied in these cases.

Single-phase to ground faults listed in Table 5.2 were also simulated. The fault-locations, fault-resistance, fault-inception-angle, sampling-frequency and A/D converter resolution were varied in these cases.

The single-phase to ground faults listed in Table 5.3 were simulated by using the calculation steps of 2 μs. The fault resistance was 1 Ω and the A/D converter resolution was 16 bits. The configuration of the transmission-line T_{r1} was varied in these cases by adding the following features.

1. Wave traps
2. A parallel line on a separate right-of-way
3. A parallel line on the same right-of-way

5.4 Case Studies

The following cases are discussed in this section.

Case Study No	Case Description	Comments
1	Single-phase to ground fault at 15 km on the line T_{r1}	
2	Single-phase to ground fault at 30 km on the line T_{r1}	Blind spots for faults at a distance equal to the length of a bus-side transmission line
3	Single-phase to ground fault on the bus-side line T_{r2}	Bus-side faults
4	Two-phase fault on the line T_{r1}	A two-phase fault
5	Three-phase fault on the line T_{r1}	A three-phase fault
6	Single-phase to ground fault at 0.5 km on the line T_{r1}	A close-in fault
7	Single-phase to ground fault on the line T_{r1} (Two cases)	Different sampling frequencies
8	Single-phase to ground fault on the line T_{r1} (Four cases)	Impact of A/D converter resolution
9	Single-phase to ground fault on the line T_{r1} (Two cases)	Impact of fault resistance
10	Single-phase to ground fault on the line T_{r1} (Four cases)	Impact of fault inception angle
11	Single-phase to ground fault on the line T_{r1}	Impact of wave traps
12	Single-phase to ground fault on the line T_{r1}	Impact of parallel lines
13	Single-phase to ground fault on the line T_{r1}	Impact of double-circuit lines

5.4.1 Single Phase to Ground Fault at 15 km on the Protected Line, T_{r1} (Case 1)

A single phase to ground fault was simulated on line T_{r1} at a location 15 km from Relay 1. As already stated, the following parameters were used.

1. Calculation steps of 2 μs
2. A/D converter of 16 bits
3. Fault resistance of 1 Ω
4. Fault incidence angle of 90° (peak value of voltage)

The voltage and current waveforms of phases A, B and C, as observed by Relay 1, are shown in Figures 5.11a, 5.11b and 5.11c respectively. The waveforms of the outputs provided by the first differences technique are shown in Figures 5.12 to 5.15. Figures 5.12 to 5.14 show the outputs seen by Relay 1 from phases A, B and C respectively, whereas Figure 5.15 shows the outputs seen by Relay 2 from phase-A.

The first technique implemented in Relay 1 detected the first set of voltage and current waves on phase-A at 154.034 ms, as shown in Figure 5.12, and started a counter that was incremented after every sampling interval. The second-set of traveling waves were detected on phase-A at 154.132 ms, as shown in Figure 5.12. The counter was stopped at this instant. The value of the counter was multiplied by 2 to get the time between the arrivals of the two sets of waves. In this case, the counter was 50. The time, T_{2L}, was, therefore, 100 μs. The distance of the fault, x, was calculated as follows by using T_{2L} and the velocity of propagation on the line.

$$x = 2.94117647 \times 10^{8} \times \frac{100}{2} \times 10^{-6} m = 14.7\ km.$$

Because the calculated distance was less than the length of the line, Relay 1 issued a trip command.

The first technique implemented in Relay 2 detected the first set of voltage and current waves at 154.468 ms, as shown in Figure 5.15, and started a counter that was incremented every sampling interval. The second-set of traveling waves were detected on phase-A at 155.440 ms. The counter was stopped at this instant. The value of the counter was multiplied by 2 to get the time between the arrivals of the two sets of waves. In this case, the counter was 486. The time, T_{2L}, was, therefore, 972 μs. The distance of the fault was, therefore, calculated as,

$$x = 2.94117647 \times 10^{8} \times \frac{972}{2} \times 10^{-6} m = 142.941\ km.$$

Because the calculated distance was less than the length of the line, Relay 2 issued a trip command as well.

The second technique implemented in Relay 1 detected the first-set of voltage and current waves on phase-A at 154.034 ms, as shown in Figure 5.12. The time, t_1, of this instant was noted and also transmitted to the relay at the remote end. Similarly the second technique implemented in Relay 2 detected the first-set of voltage and current waves at 154.468 ms, as shown in Figure 5.15. The time, t_2, of this instant was transmitted to Relay 1. When the Relay 1 received the time t_2 from Relay 2, it calculated the difference, t, between t_2 and t_1 as follows.

$$t = 154.468 - 154.034$$
$$= 0.434 \text{ ms.}$$

The time taken by the traveling waves to go from one terminal of the line to the other is,

$$T = \frac{160000}{2.94117647 \times 10^8} = 0.544\ ms$$

Since t was less than T, Relay 1 concluded that the fault was on the protected line and, therefore, issued a trip command.

When Relay 2 detected the first-set of waves at 154.468 ms, it had already received the time t_1 from Relay 1; Relay 2 calculated the following time difference.

$$t = 154.468 - 154.034$$
$$= 0.434 \text{ ms.}$$

Since t was less than T, Relay 2 also concluded that the fault was on the protected line and, therefore, issued a trip command.

5.4.2 Single Phase to Ground Fault at 30 km on the Protected Line, T_{r1} (Case 3)

A single phase to ground fault was simulated on the line, T_{r1}, at a location 30 km from Relay 1. The waveforms of the outputs provided by the first-differences technique are shown in Figures 5.16 and 5.17.

The length of the transmission line T_{r4} is also 30 km. When the traveling waves arrived at Bus 1, parts of the waves were reflected back towards the load and parts of the waves were transmitted through on line T_{r4}. The waves transmitted on this line were reflected from Bus 5 and the waves reflected towards the fault were reflected back from

the fault. The waves from Bus 5 and the fault arrived at the relay location at the same time. The polarities of the voltage waves from line T_{r4} and the protected line, T_{r1}, were alike but the polarities of the current waves were opposite. Because of this phenomenon, the magnitude of the voltage wave, observed by the relay, was large and the magnitude of the current waves, observed by the relay, was small. Figure 5.16 displays the outputs of the first-differences technique calculated by Relay 1. The first technique implemented in this relay, therefore, was not able to detect the current wave. The presence of voltage wave only could be used as an indication of a fault at a location 30 km from the relay. The first technique implemented in Relay 2 was, however, able to detect both the voltage and the current waves. Based on its observations, Relay 2 concluded that the fault was on the protected line and, therefore, issued a trip command.

The second technique implemented in Relay 1 detected the first-set of voltage and current waves, at 153.876 ms, as shown in Figure 5.16. The instant of time at which the second technique implemented in Relay 2 detected the first-set of waves was 154.418 ms. The time-differences calculated by Relay 1 and Relay 2 were, therefore, 0.334 ms. Since t was less than T = 0.544 ms, both relays concluded that the fault was on the protected line and, therefore, issued trip commands.

5.4.3 Single Phase to Ground Fault at 1 km on Bus-side Line, T_{r2} (Case 16)

A single phase to ground fault was simulated on the bus-side line, T_{r2}, at a location one km from Relay 1. The waveforms of the outputs provided by the first differences technique, seen by Relay 1 and Relay 2, are shown in Figures 5.18 and 5.19 respectively.

In this case, the first-set of current and voltage waves have the same polarities. The first technique implemented in Relay 1 identified this as an external fault and did not issue a trip command. The first technique implemented in Relay 2 detected the first and second set of voltage and current waves, calculated the distance from the fault and determined that the fault was beyond the protected line. Therefore, Relay 2 did not issue a trip command either.

The second technique implemented in Relay 1 detected the first-set of voltage and current waves at time t_1 = 153.986 ms. The second technique implemented in Relay 2 detected the first set of voltage and current waves at time t_2 = 154.530 ms. The difference, t was 0.544 ms. Because t was equal to T, Relay 1 as well as Relay 2 concluded that the fault was outside the protected line and did not issue trip commands.

5.4.4 Two Phase Fault at 20 km on the Protected Line, T_{rl} (Case 31)

A phase A to phase B fault was simulated on line T_{rl} at a location 20 km from Relay 1. The waveforms of the outputs provided by the first differences technique are shown in Figures 5.20 to 5.23. Figures 5.20 to 5.22 show the outputs seen by Relay 1 from phases A, B and C respectively, whereas Figure 5.23 shows the output seen by Relay 2 from phase-A.

The first technique implemented in Relay 1 and Relay 2 concluded that there was a fault between phases A and B and, therefore, issued trip commands. The second technique implemented in Relay 1 and Relay 2 also concluded that there was a fault between phases A and B and, therefore, issued trip commands.

5.4.5 Three Phase Fault at 20 km on the Protected Line, T_{rl} (Case 79)

A three-phase fault was simulated on line T_{rl} at a location 20 km from Relay 1. The output waveforms from the first differences technique are shown in Figures 5.24 to 5.27. Figures 5.24 to 5.26 show the outputs from the first-differences technique for phases A, B and C respectively as seen by Relay 1. Figure 5.27 shows the output of the first differences technique for phase-A voltage and current as seen by Relay2.

The first technique implemented in Relay 1 as well as Relay 2 concluded that the fault was on phases A, B and C and issued trip commands. The second technique implemented in both relays, Relay 1 and Relay 2, also concluded that the fault was on phases A, B and C in the protection zone and, therefore, issued trip commands.

5.4.6 Single Phase to Ground Fault at 0.5 km on the Protected Line, T_{r1} (Case 2)

A single phase to ground fault was simulated on line T_{r1} at a location 0.5 km from Relay 1. The waveforms of the outputs provided by the first differences technique are shown in Figures 5.28 to 5.31. Figures 5.28 to 5.30 show the outputs from the first-differences technique from phases A, B and C respectively as seen by Relay 1, whereas Figure 5.31 shows the output from the first differences technique from phase-A as seen by Relay 2.

Figure 5.28 shows that the second-set of waves overlap with the first-set of waves and, therefore, are not clearly defined. Because of this problem, this close-in fault was not detected by the first technique when the selected sampling rate was used.

The second technique implemented in Relay 1 detected the first-set of voltage and current waves at 153.986 ms, as shown in Figure 5.28. The time, t_1, of this instant was noted and was transmitted to the remote end. Similarly the second technique implemented in Relay 2 detected the first-set of voltage and current waves at 154.514 ms, as shown in Figure 5.31. The time, t_2, of this instant was transmitted to Relay 1. When Relay 1 received the time from Relay 2, it calculated the difference between the time t_1 and t_2 as follows.

$$t = 154.514 - 153.986$$
$$= 0.528 \text{ ms.}$$

The time taken by traveling waves to go from one terminal to the other is T = 0.544 ms. Since t is less than T, Relay 1 concluded that the fault was on the protected line and, therefore, issued a trip command.

When Relay 2 detected the first-set of waves at 154.514 ms, it had already received the time t_1 from Relay 1 and it calculated the following time difference.

$$t = 154.514 - 153.986$$
$$= 0.528 \text{ ms.}$$

Since t was less than T, Relay 2 also concluded that the fault was on the protected line and, therefore, issued a trip command.

5.4.7 Effect of Sampling Frequency (Cases 125 and 131)

Single-phase to ground faults were simulated on the line, T_{rl}, at a location 24 km from Relay 1. Sampling frequencies of 1 MHz and 500 kHz were used in cases 125 and 131 respectively. Fault-resistance of 1 Ω, fault-inception-angle of 90° and A/D converter resolution of 16 bits were used in this case. The voltage waveforms, provided by the first differences technique, are shown in Figure 5.32.

When the sampling rate of 1 MHz was used, the first technique implemented in Relay 1 detected the first set of voltage and current traveling waves on phase-A at 154.061 ms and started a counter that was incremented after every sampling interval. The second-set of traveling waves were detected on phase-A at 154.224 ms and the counter was stopped at this instant. In this case, the counter was 163. The time, T_{2L}, was, therefore, 163 μs. The distance of the fault, x, was calculated as follows by using T_{2L} and the velocity of propagation on the line.

$$x = 2.94117647 \times 10^{8} \times \frac{163}{2} \times 10^{-6} m = 23.97\ km.$$

The calculated distance of the fault was 23.97 km whereas the fault was at 24 km. The error, therefore, was 30 m in this case.

When the sampling rate of 500 kHz was used, the first technique implemented in Relay 1 detected the first set of traveling waves on phase-A at 154.050 ms and started a counter that was incremented after every sampling interval. The second-set of traveling waves were detected on phase-A at 154.186 ms. when the counter was stopped. The value of the counter was 81. This value was multiplied by 2 to get the time between the arrivals of the two sets of traveling waves. The time T_{2L} was, therefore, 162 μs. The distance of the fault, x, was calculated as follows by using T_{2L} and the velocity of propagation on the line.

$$x = 2.94117647 \times 10^{8} \times \frac{162}{2} \times 10^{-6} m = 23.823\ km.$$

The calculated distance of the fault was 23.823 km whereas the fault was at 24 km. The error, therefore, was 177 m in this case.

This case shows that the error in the calculated distance to the fault increases as the sampling frequency decreases.

5.4.8 Effect of Resolution of A/D Converters (Cases 141 to 145)

Single-phase faults were simulated on line T_{rl} at a location 15 km from Relay 1. A/D converters of 8-bits, 12-bits, 16-bits, 20-bits and 24-bits sizes were simulated in cases 141, 142, 143, 144 and 145 respectively. The calculation step of 2 μs, fault-resistance of 1 Ω and fault-inception-angle of 90° were used. The waveforms of the outputs from the first differences technique, when 8, 12 and 16 bit A/D converters were used, are shown in Figure 5.33. The output waveforms from the first differences technique, when 20 and 24 bit A/D converters were used, are shown in Figure 5.34.

These figures show that when low-resolution A/D converters are used, the waveforms of the outputs are not smooth and include small step changes in addition to the traveling waves. The proposed first difference technique interprets the step changes as traveling waves. The figure also shows that as the resolution of the A/D converters increases, the waveforms become smoother. Also, there is very little difference between the outputs when 16-bit and 20-bit A/D converters are used.

It is reasonable to conclude from these cases that A/D converters with 16 bit or higher resolutions should be used when the proposed techniques are implemented.

5.4.9 Effect of Fault Resistance (Cases 148 and 248)

Single-phase faults with fault resistances of 0.01 and 100 Ω were simulated on line T_{rl} at a location 20 km from Relay 1. Calculation step of 2 μs, fault-inception angle of 90° and A/D converter resolution of 16 bits were used. The waveforms of the outputs provided by the first-difference technique are shown in Figure 5.35.

This figure shows that the magnitude of the second set of traveling waves become smaller as the fault resistance increases. Also, the wave fronts become less steep because the high fault resistances distort the waves. The first technique proposed in Chapter 4

does not work well when the fault resistance is high. However, high fault resistances did not affect the performance of the second technique because the first-set of waves were properly detected.

It can, therefore, be concluded that the single ended technique will not detect high resistance faults and, therefore, backup relays using conventional algorithms should be provided as well.

5.4.10 Effect of Fault Inception Angle (Cases 267, 272, 277 and 282)

Single-phase faults were simulated on line T_{rl} at a location 15 km from Relay 1. Fault inception angles of 90°, 60°, 30° and 0° were used in these cases. Calculation step of 2 μs, fault-resistance of 1 Ω and A/D converter resolution of 16 bits were used. The waveforms of the outputs provided by the first differences technique for fault inception angles of 90° and 60° are shown in Figures 5.36. The waveforms of the outputs provided by the first differences technique for fault inception angles of 30° and 0° are shown in Figures 5.37.

These figures show that the magnitude of the traveling waves becomes smaller as the fault inception angle approaches the zero crossings. Particularly, there are no traveling waves when the fault inception angle is 0°.

The proposed techniques will, therefore, not detect faults when the inception angles are close to the zero crossings. It is, therefore, necessary that backup protection using other conventional techniques be provided in addition to the traveling wave relays.

5.4.11 Impact of Wave traps (Case 286)

A wave trap is a parallel resonant circuit, which is tuned to offer high impedance at a specific carrier frequency that is inserted in series with one of the phases of a transmission line. The impedance of a wave trap is negligible at power frequencies and large at high frequencies. Wave traps were included in the configuration of Figure 5.1

that provided the configuration shown in Figure 5.38. The parallel resonant circuit is shown in Figure 5.39.

A single-phase to ground fault was simulated on line T_{rl} of the system shown in Figure 5.38 at a location 20 km from Relay 1. Figure 5.40 shows the traveling waves seen by the relay when wave traps were included in the simulations. Figure 5.41 shows the traveling waves seen by the relay when wave traps were not included in the simulation. A study of these figures shows that high frequency oscillations are introduced on the trailing edges of the traveling waves. The fronts of the traveling waves are not affected by the presence of the wave traps.

The first technique implemented in Relay 1 detected the first set of voltage and current waves on phase-A at 154.050 ms, as shown in Figure 5.40, and started a counter that was incremented after every sampling interval. The second-set of traveling waves were detected on phase-A at 154.186 ms, as shown in Figure 5.40. The counter was stopped at this instant. The value of the counter was multiplied by 2 to get the time between the arrivals of the two sets of waves. In this case, the counter was 68. The time, T_{2L}, was, therefore, 136 μs. The distance of the fault, x, was calculated as follows by using the time, T_{2L}, and the velocity of propagation on the line.

$$x = 2.94117647 \times 10^{8} \times \frac{136}{2} \times 10^{-6} m = 20\ km\ .$$

Because the calculated distance was less than the length of the line, Relay 1 concluded that the fault was on the protected line and, therefore, issued a trip command.

The first technique implemented in Relay 2 detected the first set of voltage and current waves at 154.450 ms and started a counter that was incremented every sampling interval. The second-set of traveling waves were detected on phase-A at 155.398 ms. The counter was stopped at this instant. The value of the counter was multiplied by 2 to get the time between the arrivals of the two sets of waves. In this case, the counter was 474. The time T_{2L} was, therefore, 948 μs. The distance of the fault was therefore calculated as,

$$x = 2.94117647 \times 10^{8} \times \frac{948}{2} \times 10^{-6}\, m = 139.412\, km.$$

Because the calculated distance was less than the length of the line, Relay 2 concluded that the fault was on the protected line and issued a trip command as well.

The second technique implemented in Relay 1 detected the first-set of voltage and current waves on phase-A at 154.050 ms. The time, t_1, of this instant was noted and also transmitted to the relay at the remote end. Similarly, the second technique implemented in Relay 2 detected the first-set of voltage and current waves at 154.450 ms. The time, t_2, of this instant was transmitted to Relay 1. When Relay 1 received the time from Relay 2, it calculated the time-difference, t, between t_2 and t_1 as follows.

$$t = 154.450 - 154.050$$
$$= 0.400 \text{ ms.}$$

Because t was less than T = 0.544 ms, Relay 1 concluded that the fault was on the protected line and, therefore, issued a trip command.

When Relay 2 detected the first-set of waves at 154.450 ms, it had already received the time t_1 from Relay 1; it calculated the following time difference.

$$t = 154.450 - 154.050$$
$$= 0.400 \text{ ms.}$$

Because t was less than T, Relay 2 also concluded that the fault was on the protected line and, therefore, issued a trip command.

This study demonstrates that the presence of wave traps does not affect adversely the performance of the proposed protection techniques.

5.4.12 Impact of Parallel Lines (Cases 287 and 288)

The effect of parallel lines on the relay performance was investigated. A line in parallel to T_{r1} but on a separate right-of-way was added. The changed configuration is shown in Figure 5.42.

A single-phase to ground fault was simulated on line T_{rl} at a location 15 km from Relay 1. Figure 5.42 shows the outputs of the first differences technique for the voltage and current of phase A as seen by the Relay 1. Figure 5.43 shows the outputs of the first differences technique for the voltage and current of phase A as seen by the Relay 2.

The first technique implemented in Relay 1 detected the first set of voltage and current waves on phase-A at 154.034 ms and at 154.132 ms while the counter ramped-up to 50. The value of the counter was multiplied by 2 to get T_{2L} of 100 μs. The distance of the fault, x, was calculated as follows by using T_{2L} and the velocity of propagation on the line.

$$x = 2.94117647 \times 10^8 \times \frac{100}{2} \times 10^{-6} m = 14.7\ km.$$

Because the distance was less than the line length, Relay 1 concluded that the fault was on the protected line and, therefore, issued a trip command.

The first technique implemented in Relay 2 detected the voltage and current waves on phase-A at 154.468 ms and at 155.440 ms while the counter ramped-up to 486. The value of the counter was multiplied by 2 to get T_{2L} of 972 μs. The distance of the fault, x, was calculated as follows by using T_{2L} and the velocity of propagation on the line.

$$x = 2.94117647 \times 10^8 \times \frac{972}{2} \times 10^{-6} m = 142.941\ km.$$

Because the calculated distance was less than the length of the line, Relay 2 concluded that the fault was on the protected line and, therefore, issued a trip command as well.

The second technique implemented in Relays 1 and 2 detected the first-set of voltage and current waves on phase-A at 154.034 ms and 154.468 ms respectively. Each relay forwarded the arrival-time of traveling waves to the other relay. Both relays calculated the difference, t, between the arrival-times of the traveling waves at the two terminals as follows.

$$t = 154.468 - 154.034$$

= 0.434 ms.

Because the time t was less than T = 0.544 ms, both relays concluded that the fault was on the protected line and, therefore, issued trip commands.

Single-phase faults were simulated on the parallel line also. In those cases, no traveling waves were observed on line T_{rl}.

Therefore, parallel lines on a separate right-of-way do not affect adversely the performance of the proposed traveling wave techniques.

5.4.13 Impact of Mutually Coupled Lines (Case 289)

The impact of mutual coupling between parallel circuits on the performance of the proposed techniques was investigated. A line in parallel to T_{rl} on the same right-of-way was added for this purpose. Figure 4.45 shows the conductor arrangement for the double-circuit line.

A single-phase to ground fault was simulated on line, T_{rl} at a location 15 km from Relay 1. Figure 5.46 shows the outputs of the first-differences technique for voltage and current of phase A as seen by the Relay 1. Figure 5.47 shows the outputs of the first-differences technique for voltage and current of phase A as seen by the Relay 2.

The first technique implemented in Relay 1 detected the first set of voltage and current waves on phase-A at 154.034 ms and at 154.132 ms while the counter ramped-up to 50. The value of the counter was multiplied by 2 to get T_{2L} of 100 μs. The distance of the fault, x, was calculated as follows by using T_{2L} and the velocity of propagation on the line.

$$x = 2.94117647 \times 10^{8} \times \frac{100}{2} \times 10^{-6} m = 14.7\ km.$$

Because the calculated distance was less than the length of the line, Relay 1 concluded that the fault was on the protected line and, therefore issued a trip command.

The first technique implemented in Relay 1 detected the first set of voltage and current waves on phase-A at 154.468 ms and at 155.440 ms while the counter ramped-up to 486. The value of the counter was multiplied by 2 to get T_{2L} of 972 μs. The distance of the fault, x, was calculated as follows by using T_{2L} and the velocity of propagation on the line.

$$x = 2.94117647 \times 10^8 \times \frac{972}{2} \times 10^{-6} m = 142.941\ km.$$

Because the calculated distance was less than the length of the line, Relay 2 concluded that the fault was on the protected line and, therefore issued a trip command as well.

The second technique implemented in Relays 1 and 2 detected the first-set of voltage and current waves on phase-A at 154.034 ms and 154.468 ms respectively. Each relay forwarded the arrival-time of traveling waves to the other relay. Both relays calculated the difference, t, between the arrival-times of the traveling waves at the two terminals as follows.

$$t = 154.468 - 154.034$$
$$= 0.434 \text{ ms.}$$

Because the time t was less than T = 0.544 ms, both relays concluded that the fault was on the protected line and, therefore, issued trip commands.

This study shows that mutually coupled lines do not adversely affect the proposed traveling wave protection techniques.

5.5 Summary

The simulation procedure used for studying the performance of the proposed high-speed relays has been described in this chapter. Different types of faults were simulated and data from the simulations were used to evaluate the techniques. The impacts of sampling frequency, resolution of A/D converters, fault inception angle and fault-resistance on the performance of the techniques were studied and have been examined in this chapter. The impacts of wave traps, parallel lines and coupled lines were also studied and are outlined in this chapter. These studies have shown that the

proposed technique distinguishes correctly between internal and external faults. The time needed for making the decisions ranges from four to five ms. The studies, however, reveal that the techniques do not detect faults when the fault inception angles are close to the zero crossings. The traveling wave relays should, therefore be used in conjunction with relays that make decisions based on the fundamental frequency components of voltages and currents.

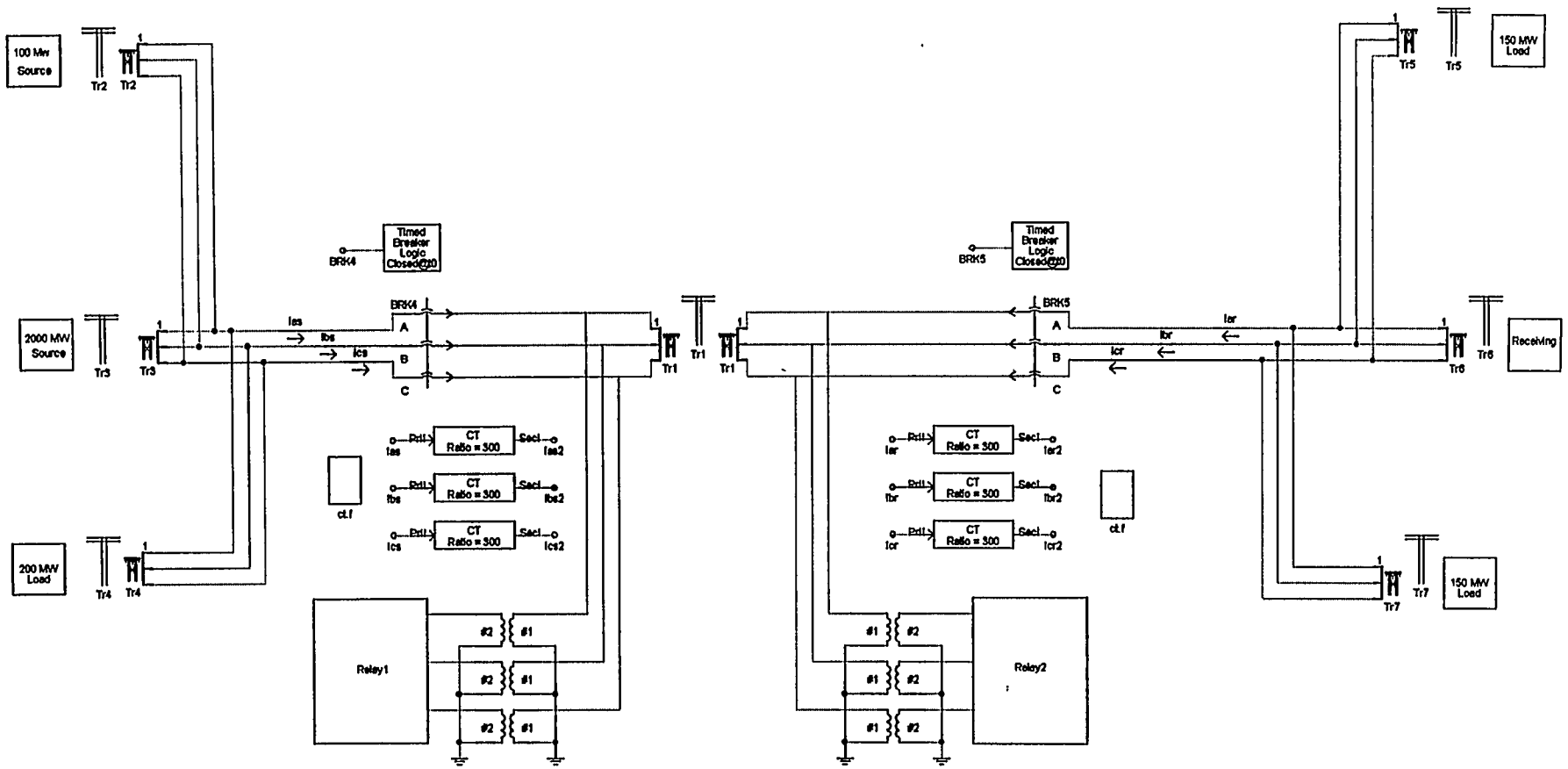

Figure 5.2: System model in EMTDC

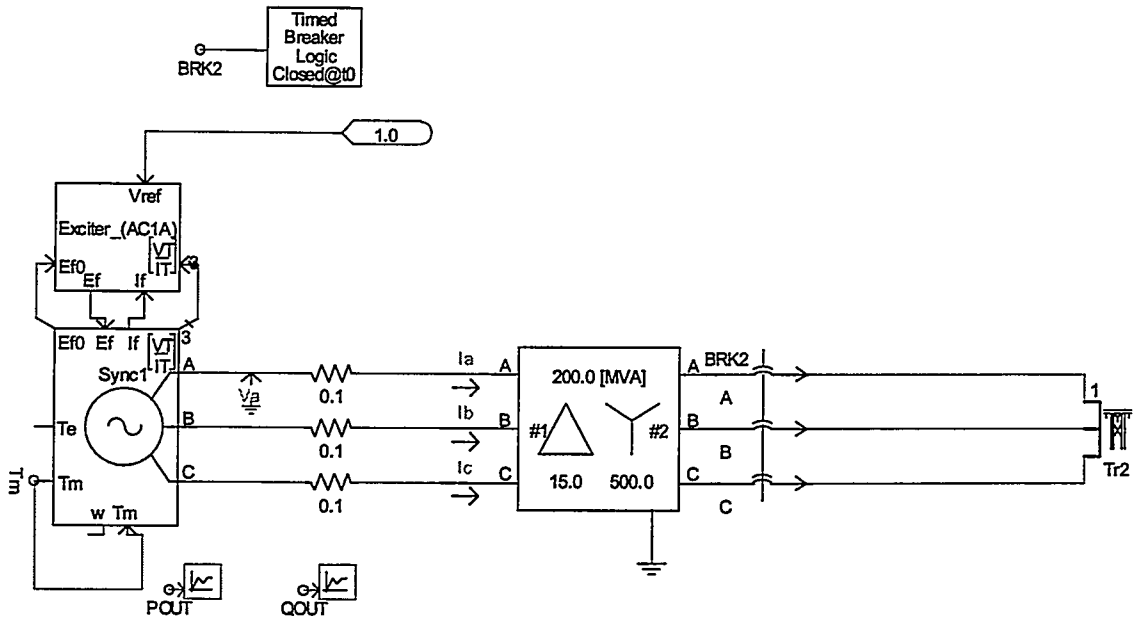

Figure 5.3: Source 1 model in EMTDC

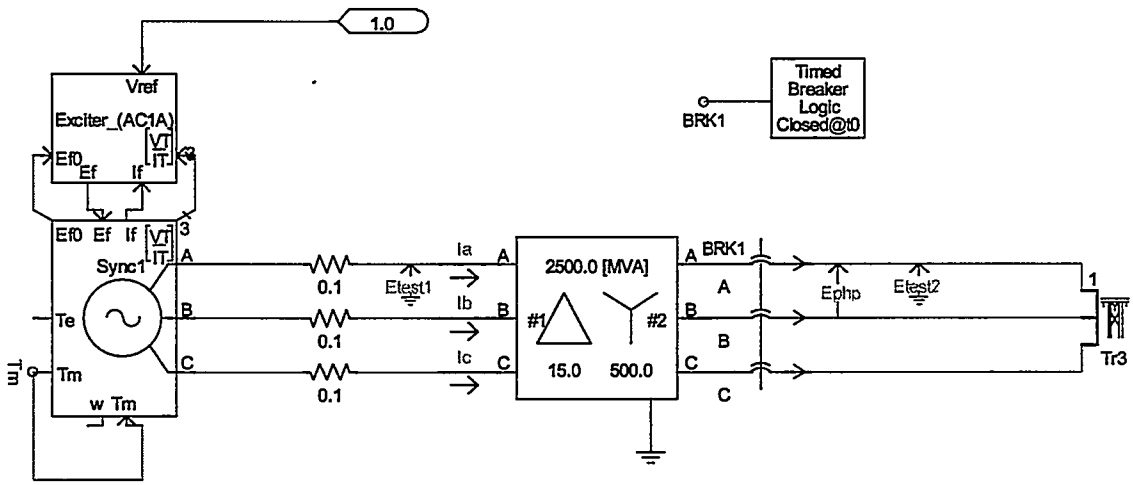

Figure 5.4: Source 2 model in EMTDC

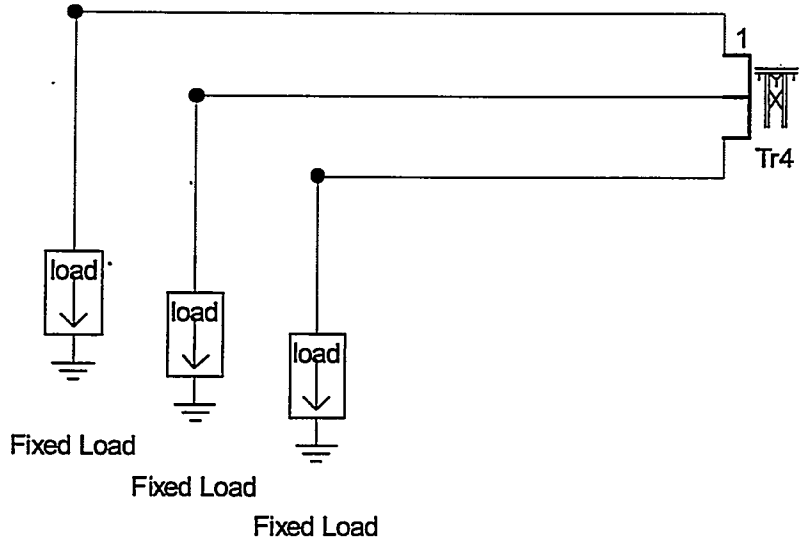

Figure 5.5: Load 1 model in EMTDC

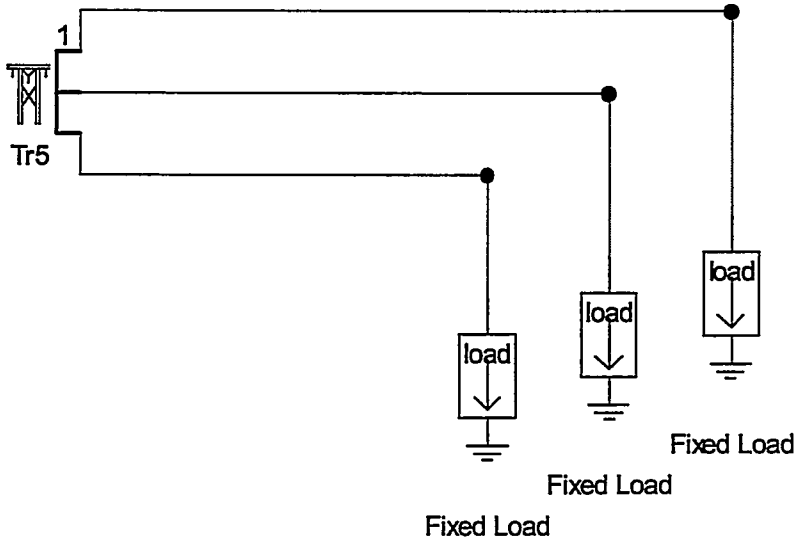

Figure 5.6: Load 2 model in EMTDC

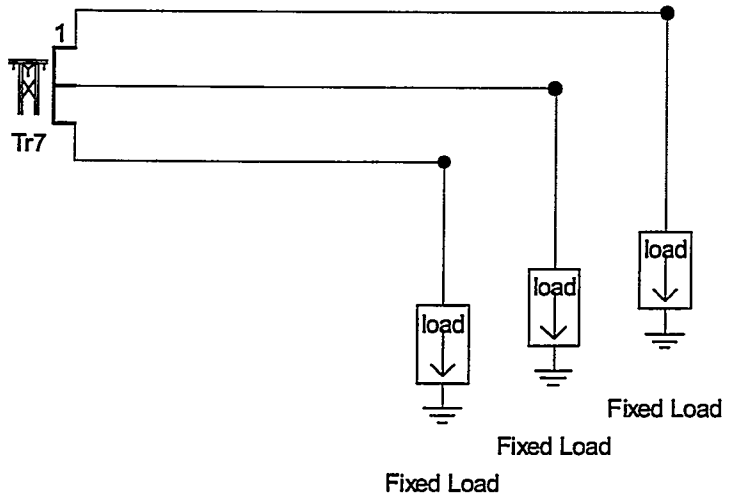

Figure 5.7: Load 3 model in EMTDC

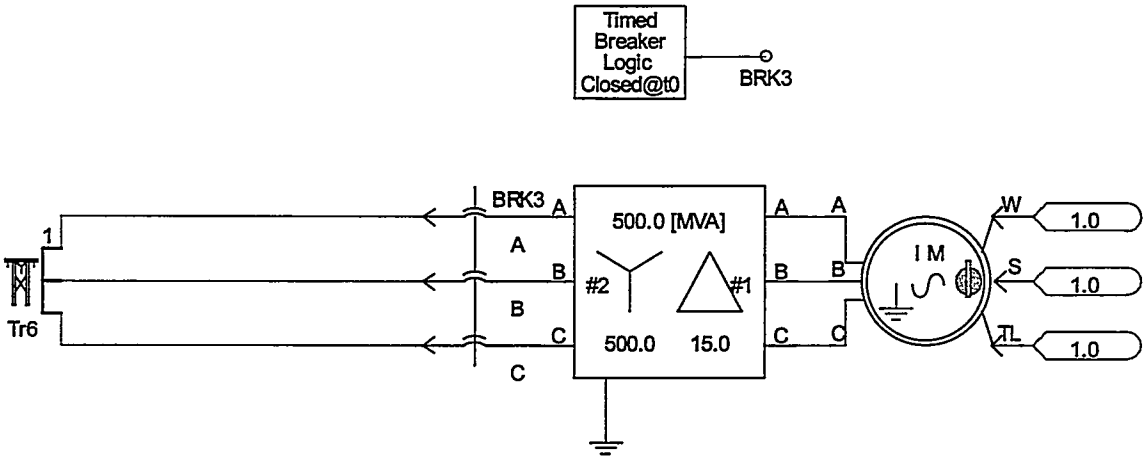

Figure 5.8: Motor model in EMTDC

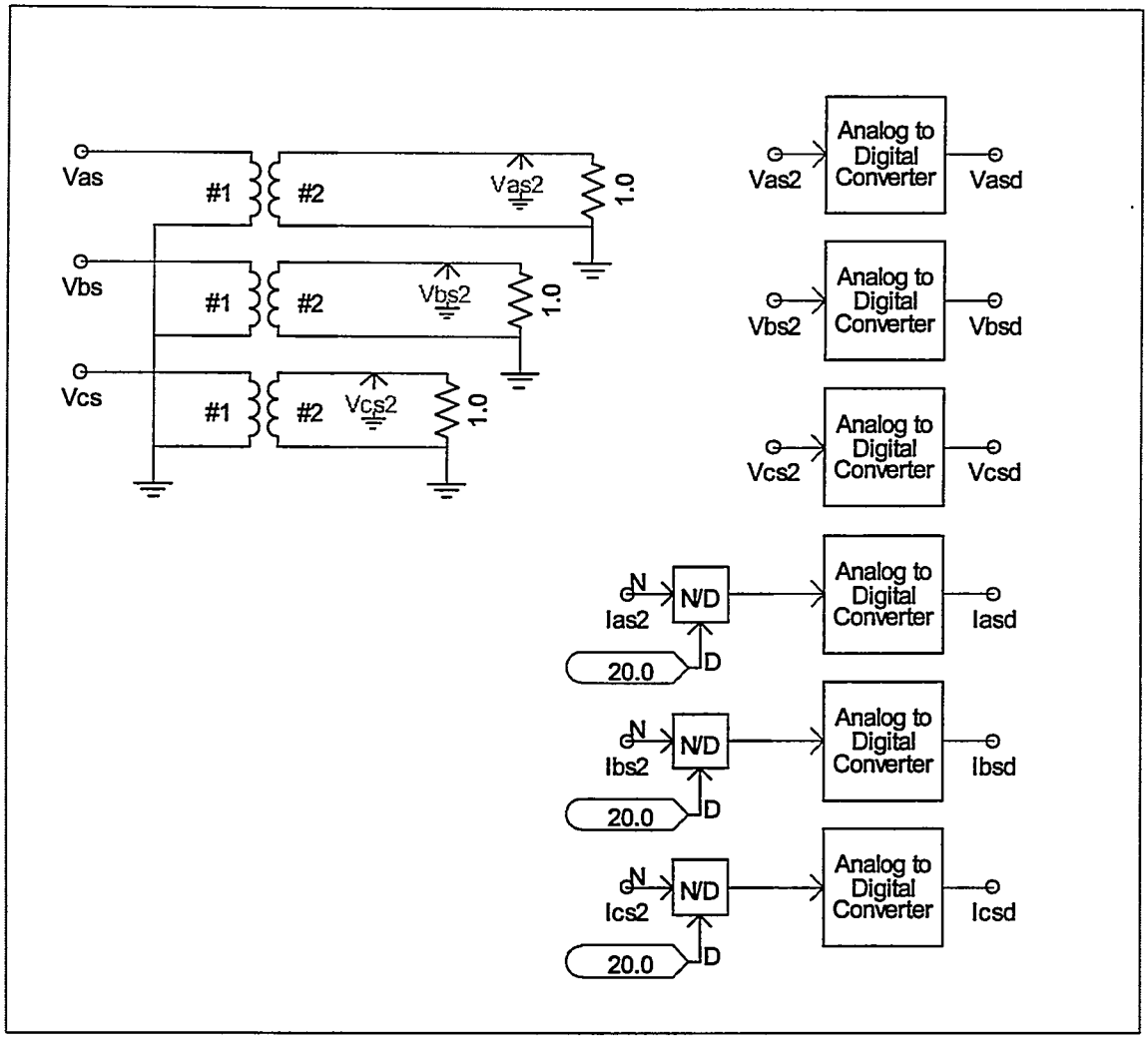

Figure 5.9: EMTDC data acquisition system model

N is the input and D is the ratio of the auxiliary CTs.

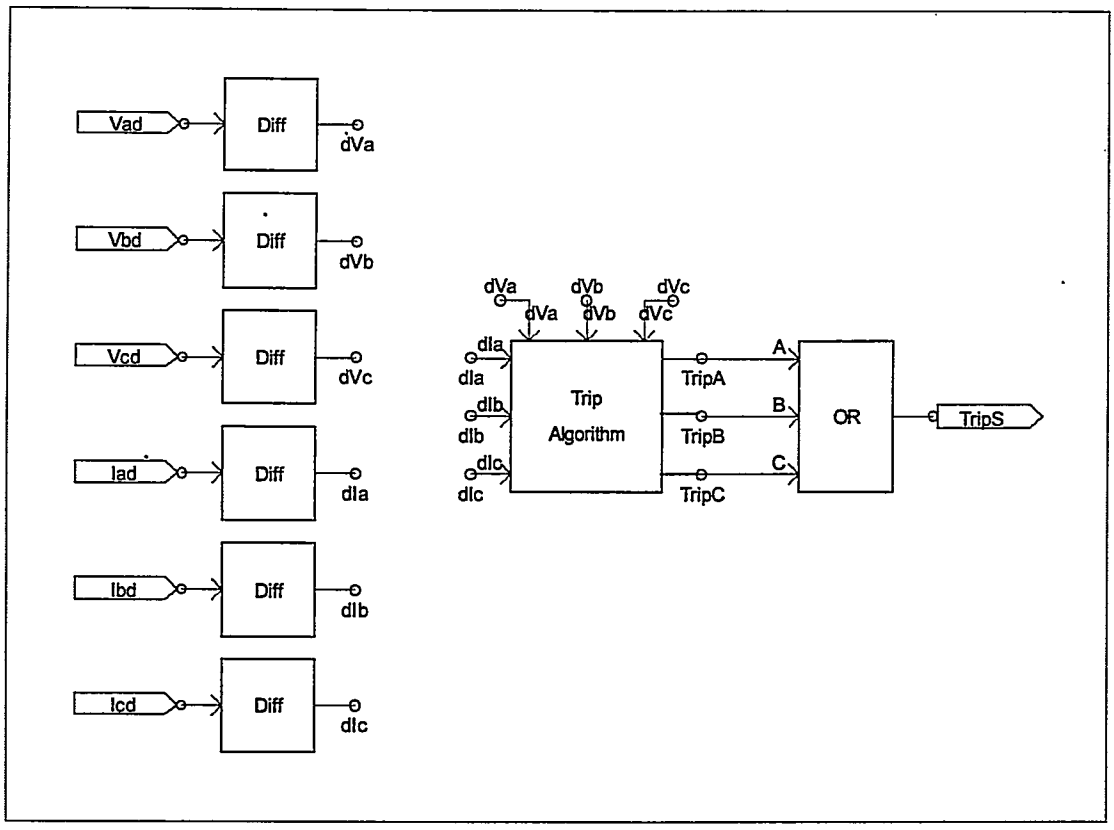

Figure 5.10: Protection technique model in EMTDC

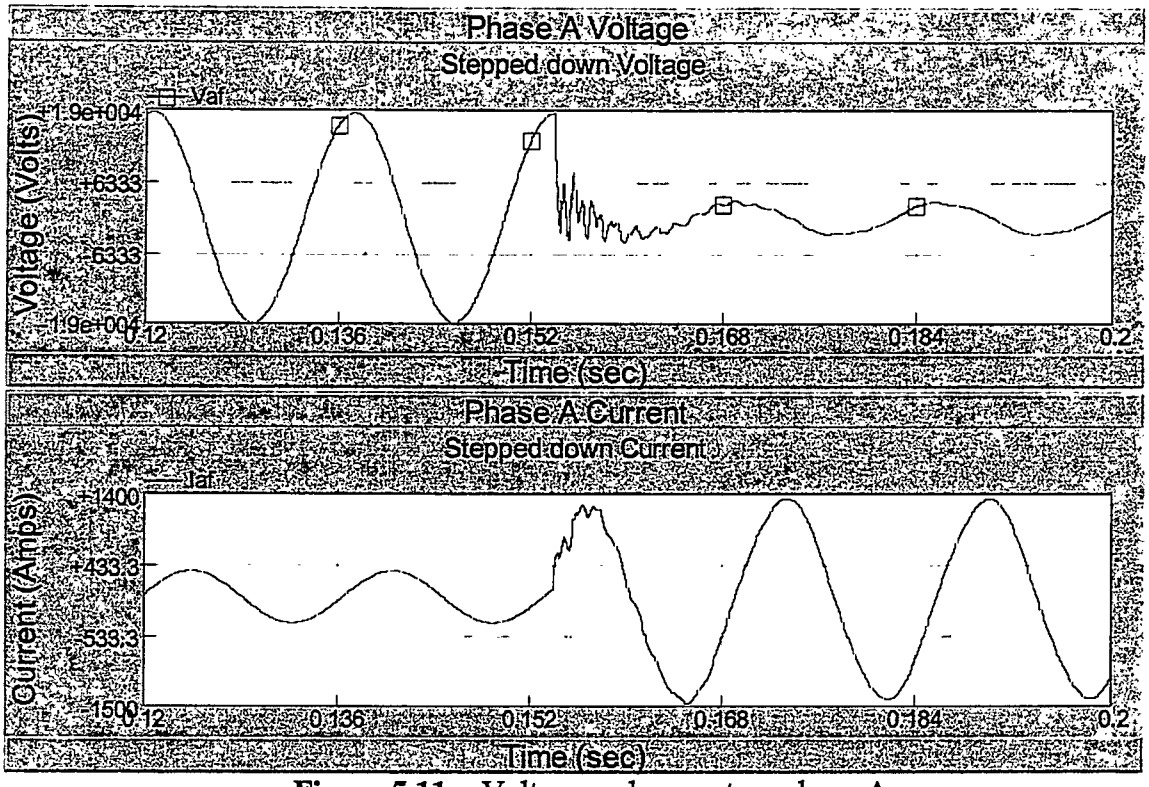

Figure 5.11a: Voltage and current on phase-A

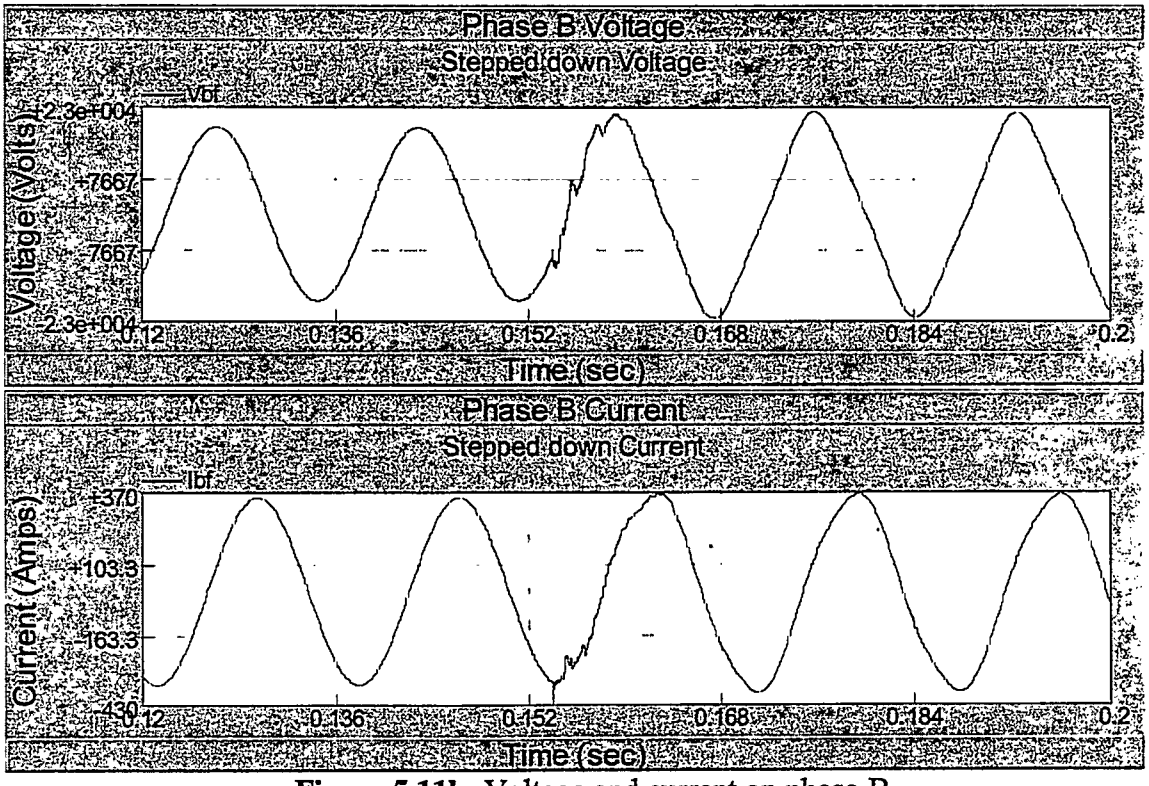

Figure 5.11b: Voltage and current on phase-B

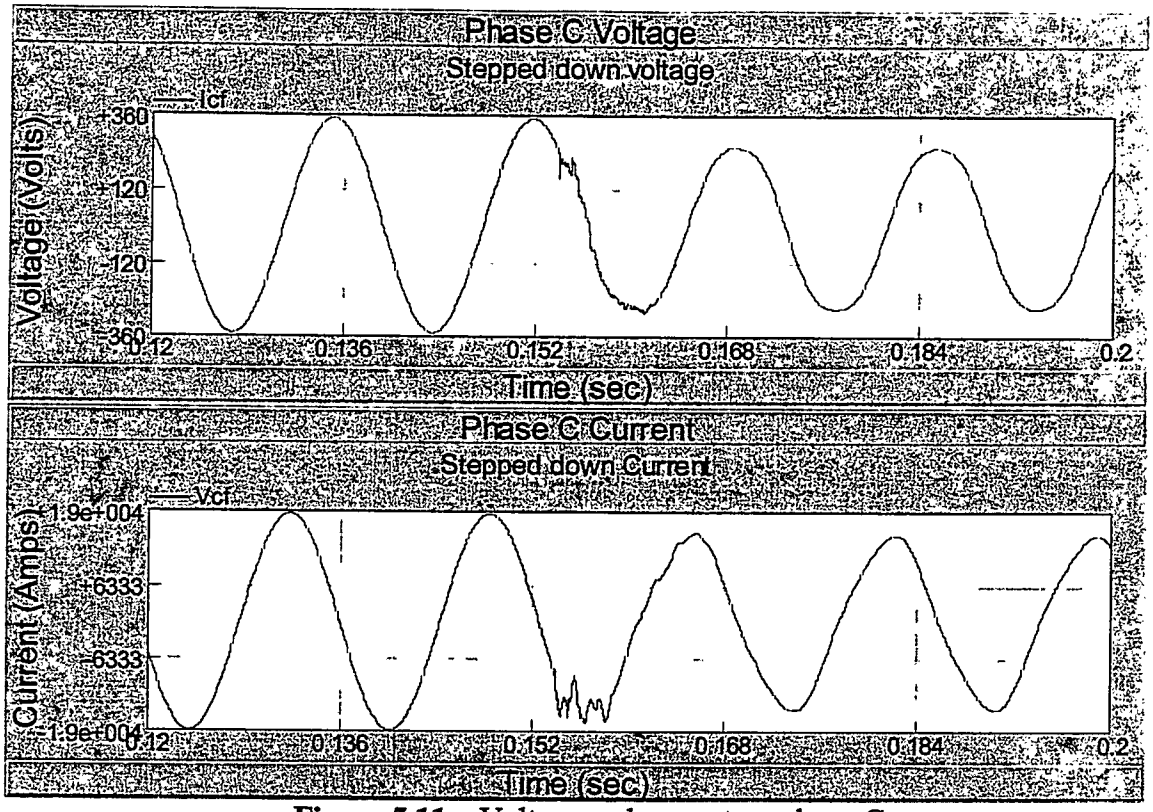

Figure 5.11c: Voltage and current on phase-C

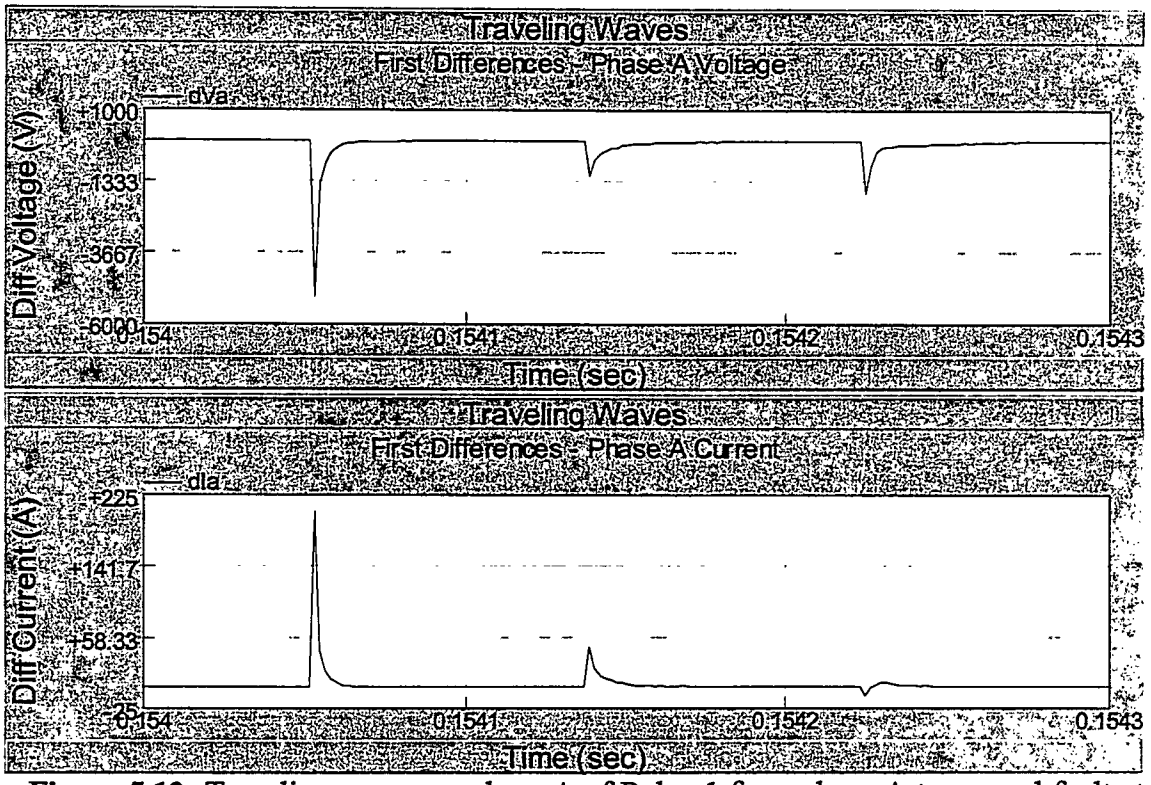

Figure 5.12: Traveling waves on phase A of Relay 1 for a phase-A to ground fault at 15 km

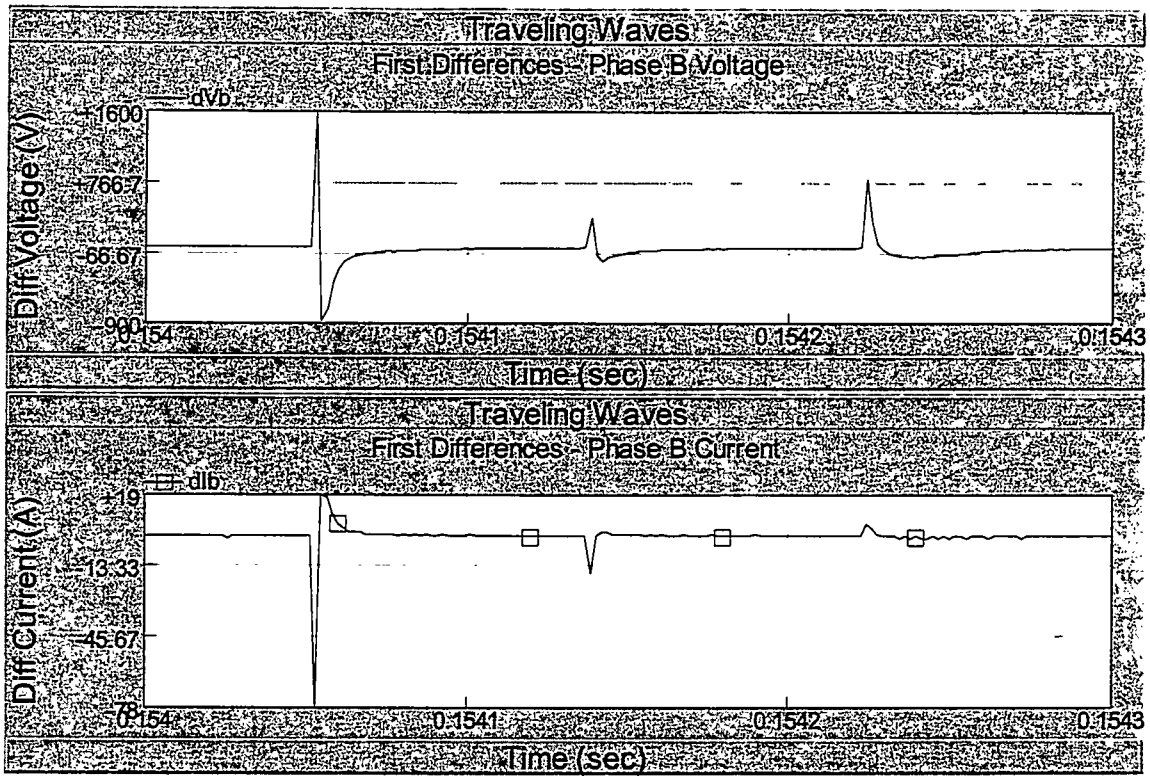

Figure 5.13: Traveling waves on phase B of Relay 1 for a phase-A to ground fault at 15 km

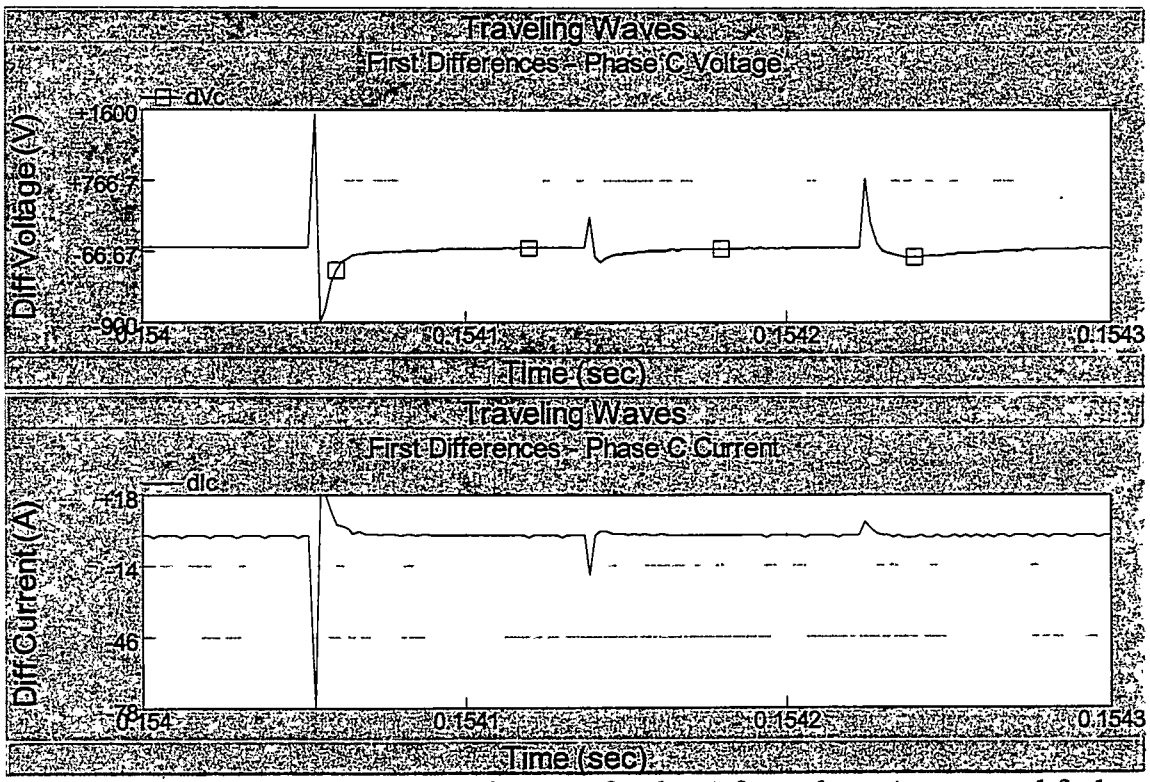

Figure 5.14: Traveling waves on phase C of Relay 1 for a phase-A to ground fault at 15 km

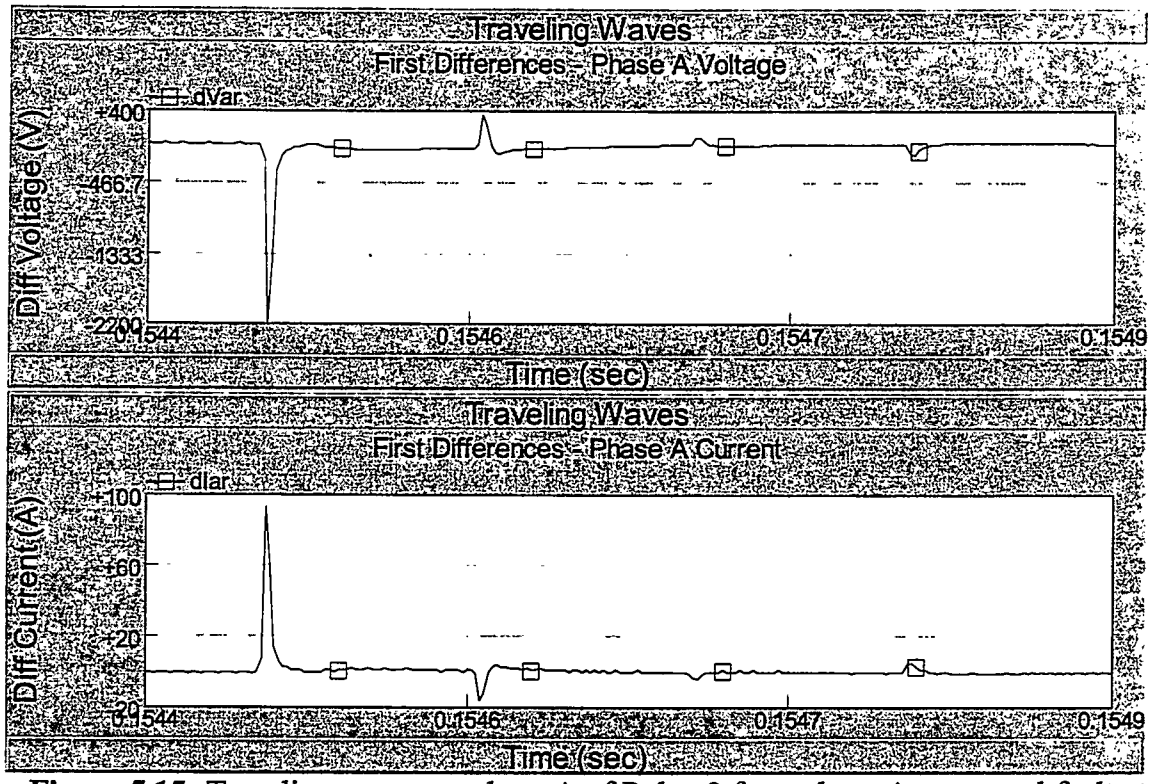

Figure 5.15: Traveling waves on phase A of Relay 2 for a phase-A to ground fault at 15 km

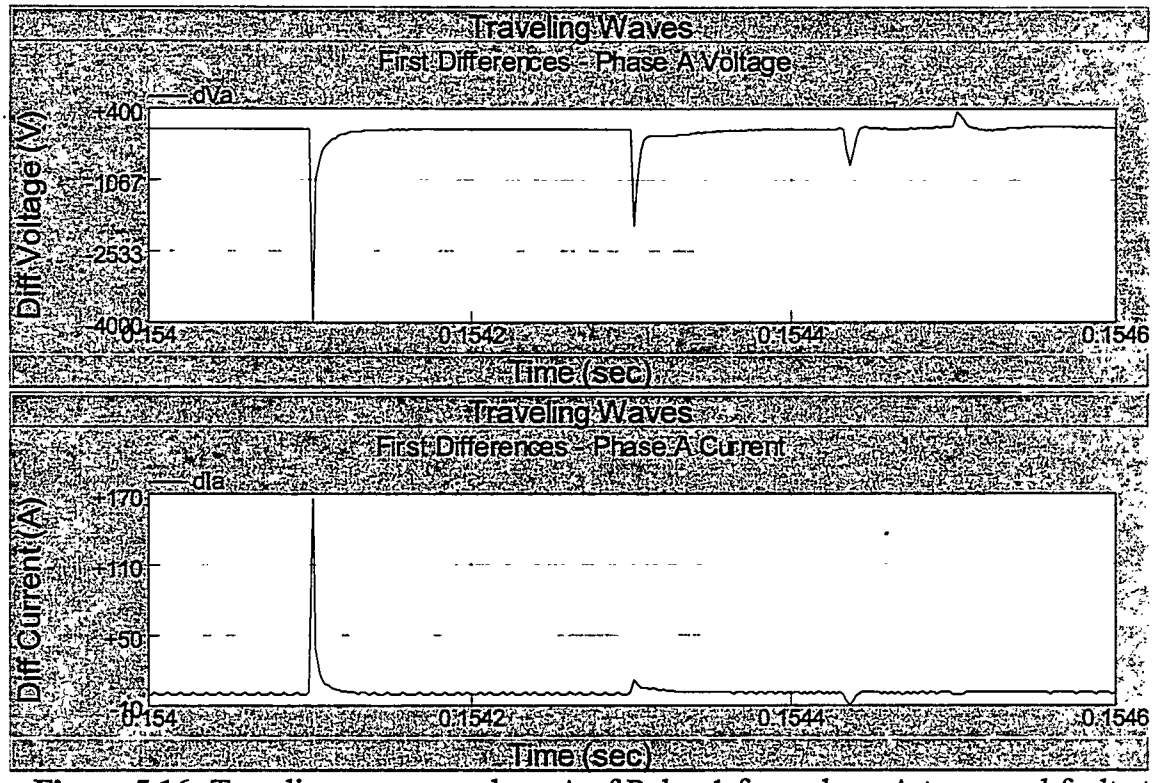

Figure 5.16: Traveling waves on phase A of Relay 1 for a phase-A to ground fault at 30 km

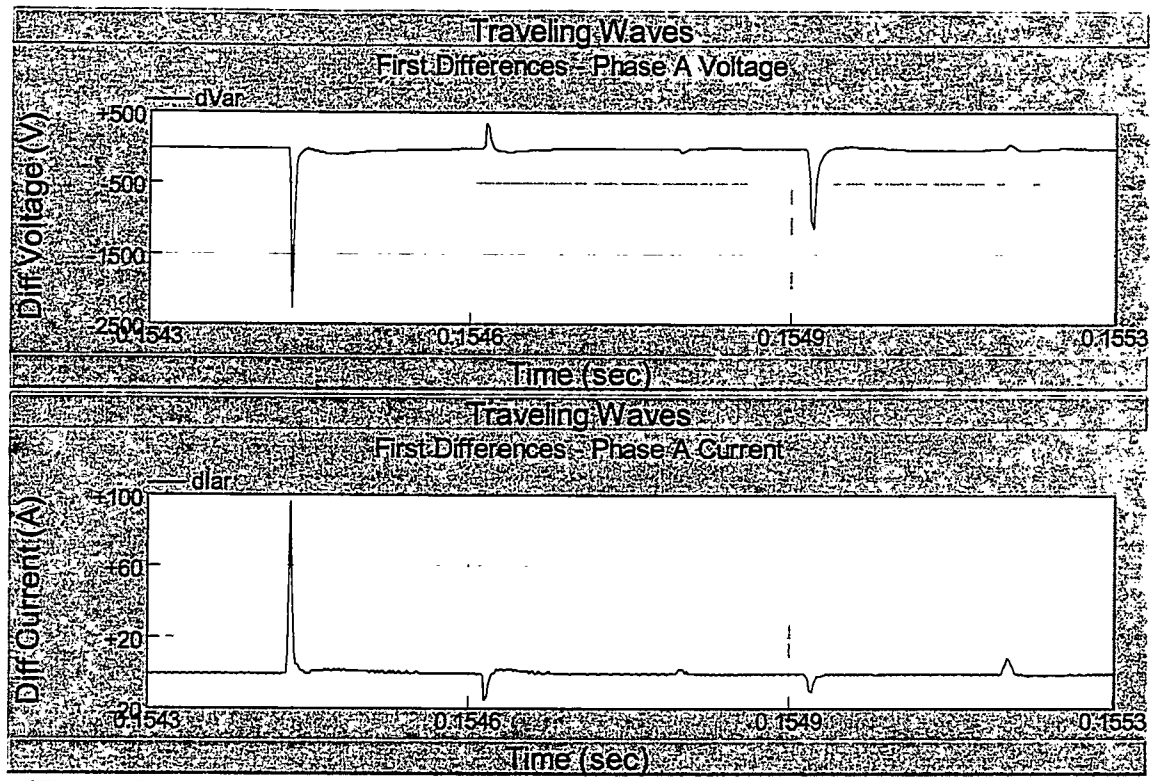

Figure 5.17: Traveling waves on phase A of Relay 2 for a phase-A to ground fault at 30 km

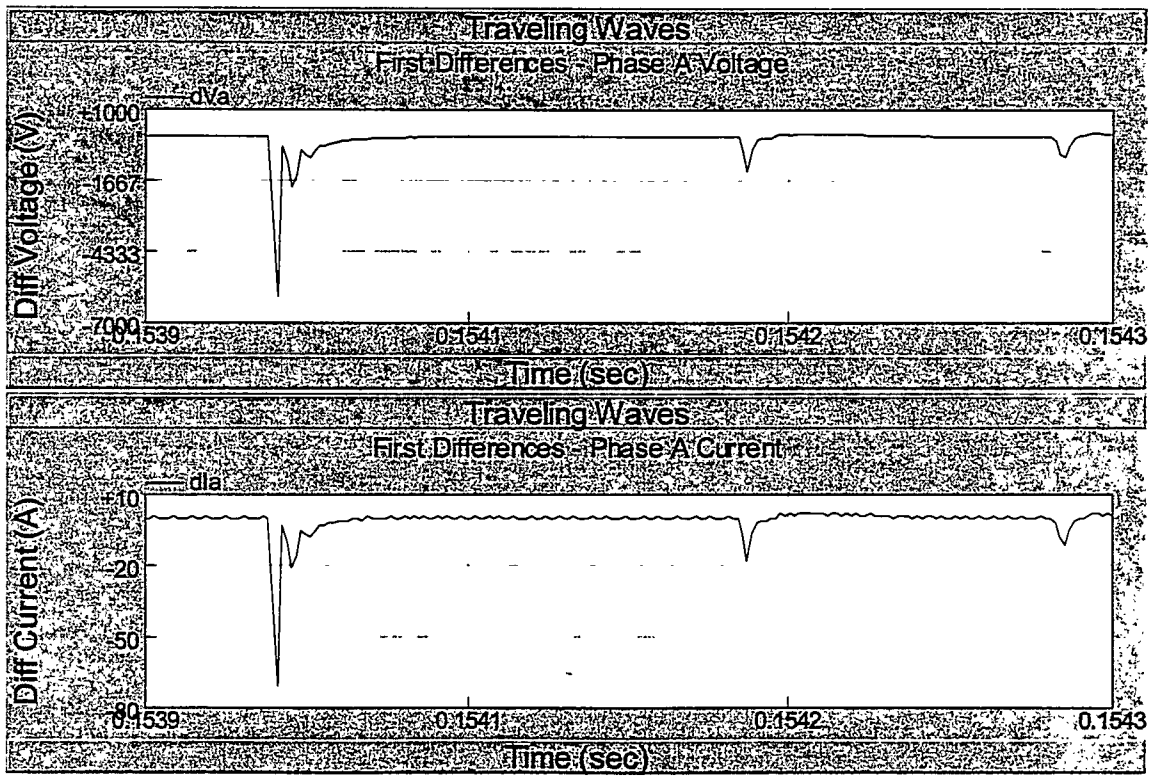

Figure 5.18: Traveling waves on phase A of Relay 1 for a phase-A to ground fault at 1 km on line T_{r2}

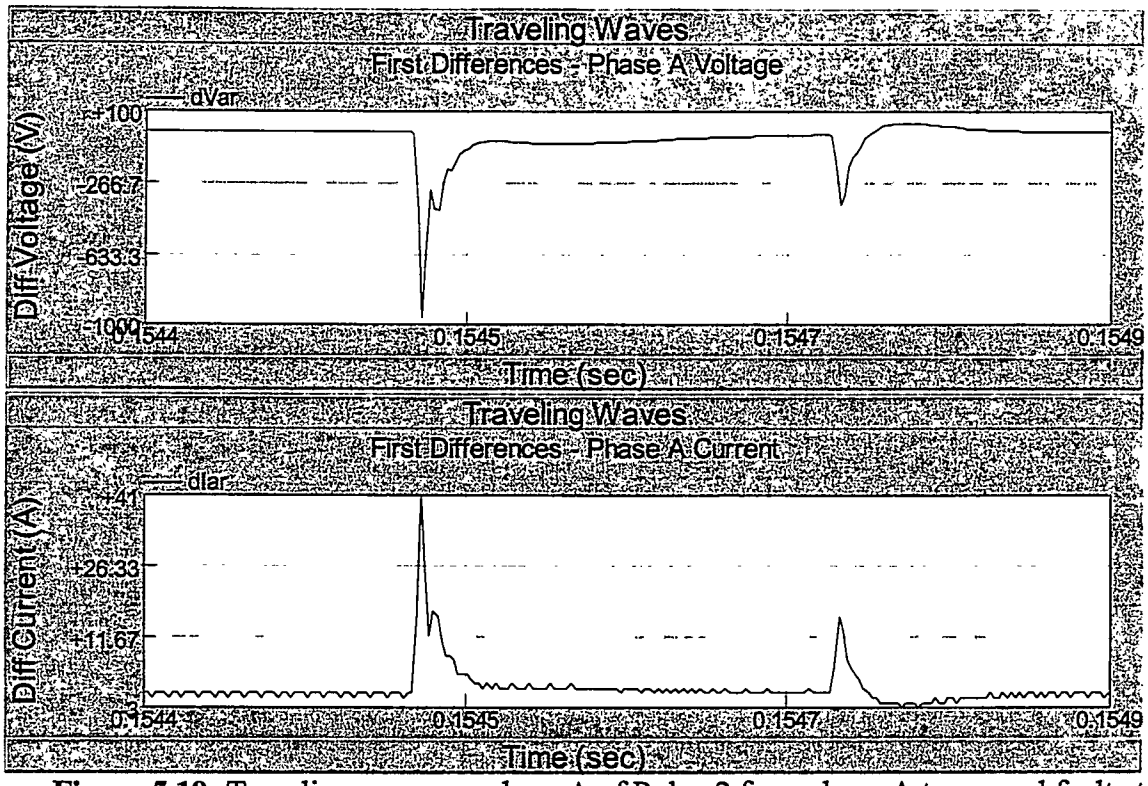

Figure 5.19: Traveling waves on phase A of Relay 2 for a phase-A to ground fault at 1 km on line T_{r2}

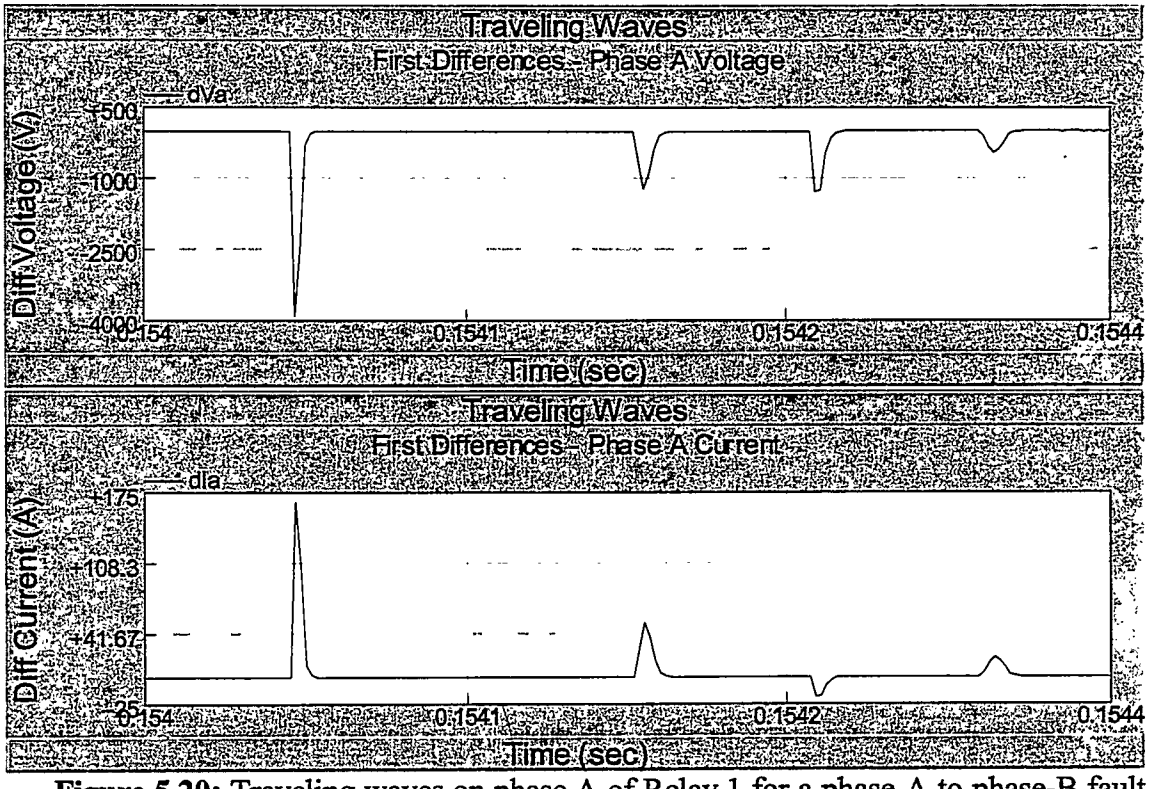

Figure 5.20: Traveling waves on phase A of Relay 1 for a phase-A to phase-B fault at 20 km